

Aus dem Institut für Radiologie
der Medizinischen Fakultät Charité – Universitätsmedizin Berlin

DISSERTATION

**Assessment of the choline metabolism
in human breast cancer by
High Resolution Magic Angle Spinning
¹H Magnetic Resonance Spectroscopy
and quantitative Polymerase Chain Reaction**

zur Erlangung des akademischen Grades
Doctor medicinae (Dr. med.)

vorgelegt der Medizinischen Fakultät
Charité – Universitätsmedizin Berlin

von

Hannah Maria Schäfer

aus Berlin

Gutachter/in: 1. Prof. Dr. med. M. Taupitz
 2. Prof. Dr. med. T. Albrecht
 3. Priv.-Doz. Dr. H. Bruhn

Datum der Promotion: 09.09.2011

Für Rolf und Julie Schäfer

1 Table of contents

1	Table of contents	4
2	List of figures	6
3	List of tables	8
4	List of pictures	9
5	Abbreviations.....	10
6	Introduction.....	12
6.1	Aim of this study	13
6.2	The hypotheses.....	13
7	Background	15
7.1	Metabolic changes in cancerous tissue	15
7.2	Change in the choline metabolites' concentration in malignant cells.....	15
7.3	Relevance of choline	16
7.4	Phosphoglycerid synthesis.....	18
7.5	The Kennedy cycle.....	19
7.5.1	Selected enzymes of the Kennedy cycle.....	21
7.6	Regulation of the choline metabolism.....	28
7.6.1	The Kennedy cycle and the rise in choline concentration	28
7.7	Nuclear magnetic resonance.....	29
7.7.1	High resolution magic angle spinning.....	30
7.8	Choline metabolites and MRS.....	33
8	Materials and methodologies.....	35
8.1	Design of the study.....	35
8.2	Tissue samples	36
8.3	HRMAS ¹ H MR Spectroscopy	38
8.3.1	Spectroscopic procedures.....	38
8.3.2	Spectral analysis	38
8.3.3	Transfer of MRS data to JMP.....	38
8.4	Histopathological analysis	40
8.4.1	Handling of samples.....	42
8.5	Laser Capturing Microdissection	42
8.6	RNA techniques	44
8.6.1	Real-time quantitative PCR.....	45
8.6.2	Relative quantification	45
8.6.3	Housekeeping gene	45
8.6.4	Process of PCR.....	46
8.6.5	Correlation of MRS data and PCR results.....	50
9	Preliminary measures.....	51
9.1	Serial dilutions	51
9.2	Amplification efficiency.....	52
9.3	C _t -value	54
9.4	Calculation of amplification efficiency.....	55
9.4.1	Assumption	56
9.4.2	Method	56
9.4.3	Adjusting C _t -values for differences in amplification efficiency	57
9.4.4	Amplification efficiency adjustment tool.....	58
9.5	Use of $\Delta\Delta C_t$ versus use of $2^{-\Delta\Delta C_t}$	61
10	Results.....	61
10.1	Exclusion of samples.....	62
10.2	Statistic procedures.....	63

10.2.1	Handling of outliers	63
10.2.2	Use of ANOVA	64
10.2.3	Statistical power	65
10.3	Choline kinase.....	65
10.3.1	PCR results without MRS-correlation.....	65
10.3.2	PCR results in correlation to MRS data.....	71
10.4	Phospholipase D	77
10.4.1	PCR results without MRS-correlation.....	77
10.4.2	PCR results for PLD with correlation to MRS data.....	78
10.5	PCYT1.....	82
10.5.1	PCR results without MRS-correlation.....	82
10.5.2	PCR results with MRS-correlation.....	82
10.6	SLC22A.....	87
10.6.1	PCR results without MRS-correlation.....	87
10.6.2	PCR results with MRS-correlation.....	87
10.7	GPC to PC switch.....	92
10.8	General development of genes of interest.....	94
11	Discussion of results	97
11.1	Existing study approaches and theories on metabolite increase.....	97
11.2	Main findings of the study.....	97
11.2.1	ChoK.....	98
11.2.2	PCYT	100
11.3	Additional findings	102
11.3.1	PLD.....	102
11.3.2	SLC22A.....	102
11.3.3	GPC to PC switch	104
11.3.4	Enzymatic changes between tumour grades.....	105
11.4	Correlation of the histological grade with MRS.....	106
11.5	Discrepancies to other studies	106
11.6	Results of this study in context with current research.....	107
11.7	Possible confounders of the study.....	107
11.7.1	Unknown interdependencies of enzymes.....	107
11.7.2	Limitations of MRS	108
11.7.3	Implications of the Kennedy pathway.....	108
11.7.4	Challenges of the rt-q-PCR technique.....	109
11.7.5	Limitations of statistical analysis	109
11.7.6	Posttranslational regulation.....	110
11.8	Alternative experimental approaches	110
11.9	Conclusion	110
11.9.1	Possible clinical use of the findings.....	112
12	Summary	113
13	Selbständigkeitserklärung.....	114
14	Acknowledgements.....	115
15	Bibliography	116

2 List of figures

Figure 1 PtdCho biosynthesis pathway.....	17
Figure 2 The salvage pathway from serine to PtdCho.....	18
Figure 3 Schematic overview of the Kennedy cycle.....	19
Figure 4 Use of choline in different metabolic pathways.....	20
Figure 5 Configuration of the active ChoK enzyme.....	22
Figure 6 Screenshot of JMP program.....	39
Figure 7 Theoretical plot of PCR.....	48
Figure 8 Concentration and C_t relation.....	51
Figure 9 Amplification efficiency for different concentrations.....	52
Figure 10 Amplification efficiency for different C_t -values.....	53
Figure 11 Comparison of $2^{-\Delta C_t (adj)}$ of ChoK α and ChoK β in grades 2 and 3.....	66
Figure 12 ΔC_t ChoK β and TGrade.....	67
Figure 13 $2^{\Delta C_t}$ ChoK β and TGrade.....	67
Figure 14 ChoK β grade 2.....	69
Figure 15 ChoK β grade w/o.....	69
Figure 16 ChoK β and ChoK α	70
Figure 17 PC+GPC and ChoK α w/o.....	72
Figure 18 PC+GPC and ChoK α and β w/o.....	72
Figure 19 GPC and ChoK α w/o.....	73
Figure 20 GPC and ChoK α grade 2 w/o.....	74
Figure 21 GPC and ChoK α grade 3.....	74
Figure 22 Chol and ChoK α w/o.....	75
Figure 23 PLD 1 and 2; $2^{-\Delta C_t (adj)}$ in grades 2 and 3.....	77
Figure 24 PLD and TGrade w/o.....	78
Figure 25 PC+GPC and PLD2.....	79
Figure 26 PC+GPC and PLD2 w/o.....	79
Figure 27 PC+GPC and PLD2.....	80
Figure 28 PC+GPC and PLD2 w/o.....	80
Figure 29 PC+GPC and PLD1/2.....	81
Figure 30 PC+GPC and PLD1/2 w/o.....	81
Figure 31 PCYT1A/B ($2^{-dC_t (adj)}$) in grade 2 and 3.....	82
Figure 32 PC+GPC and PCYT1A/B.....	83
Figure 33 PC+GPC and PCYT1A/B w/o.....	83
Figure 34 GPC and PCYT1A grade 3.....	84
Figure 35 GPC and PCYT1A grade 3 w/o.....	84
Figure 36 GPC and PCYT1B grade 2.....	85
Figure 37 GPC and PCYT1B grade 2 w/o.....	85
Figure 38 PC+GPC and PCYT1B grade 3.....	86
Figure 39 PC+GPC and PCYT1B grade 3 w/o.....	86
Figure 40 Comparison of SLC22A1/2 expression ($2^{-\Delta C_t (adj)}$) in grade 2 and 3.....	87
Figure 41 GPC and SLC22A1 grade 2.....	88
Figure 42 GPC and SLC22A1 grade w/o.....	88
Figure 43 PC+GPC and SLC22A1 grade 2.....	89
Figure 44 PC+GPC and SLC22A1 grade 2 w/o.....	89
Figure 45 PC+GPC and SLC22A2 grade 3.....	90
Figure 46 PC+GPC and SLC22A2 grade 3 w/o.....	90
Figure 47 GPC to PC switch.....	92
Figure 48 Average concentration ratios measured by MRS (y-axis=MRS concentration results).....	93

Figure 49 Average concentration ratios measured by MRS (y-axis=MRS concentration results).	93
Figure 50 Choline and TGrade.	94
Figure 51 PC+GPC and TGrade.....	94
Figure 52 Comparison of GOI concentrations.	95
Figure 53 GOI average 2^{-dCt} (adj) in grade 2 and 3 w/o PLD2.	96

|

3 List of tables

Table 1 Comparative studies of detection techniques.	12
Table 2 Exemplary metabolic changes in malignant tissue.	15
Table 3 Enzymes and corresponding genes of the choline metabolism.	21
Table 4 Two primary choline transport mechanisms.	25
Table 5 Comparison of different choline transport mechanisms.	26
Table 6 Comparison of MRS and mass spectroscopy.	29
Table 7 An overview of choline phospholipid metabolite levels.	32
Table 8 An overview of choline phospholipid metabolite levels in cell lines.	33
Table 9 Comparison of related studies by Eliyahu and Glunde.	35
Table 10 Complete sample list including TNM staging and patient age.	37
Table 11 Overview of samples.	37
Table 12 Variables used for MRS data presentation in JMP.	39
Table 13 Material used for cryostat work and preparation of serial slides.	40
Table 14 H/E staining protocol.	41
Table 15 Staining protocol for LCM.	43
Table 16 Material used for PCR.	46
Table 17 Overview of primer provenance.	47
Table 18 Sample overview.	62
Table 19 Excluded enzymes.	62
Table 20 Summary of outliers.	64
Table 21 Concentration differences between enzymes and grades.	65
Table 22 Concentration differences of ChoK α and ChoK β between grades 2 and 3.	65
Table 23 Mann-Whitney-U test: TGrade and ChoK β	68
Table 24 Comparison of GPC and PC concentration across grades 2 and 3.	93
Table 25 Overview of sample size and outliers per enzyme.	95
Table 26 Concentration differences per enzyme and tumour grade w/o outliers.	96

4 List of pictures

Picture 1 Invasive ductal carcinoma in breast tissue x20.....	42
Picture 2 Invasive ductal carcinoma in breast tissue x60.....	44
Picture 3 Sample amplification plot 7000 System SDS Software.	49
Picture 4 Adjustment tool instructions page.....	59
Picture 5 Adjustment tool hypothesis page.....	60

5 Abbreviations

Abbreviations	
A°	Angstroem
Adj	adjusted
ADP	adenosine diphosphate
AE	amplification efficiency
ANOVA	analysis of variance
app	approximately
ATP	adenosine triphosphate
Ave	average
bFGF	basic fibroblast growth factor
BrCA	breast cancer
C. total	total sum of square distances to the mean of the sample
CCl4	carbon tetrachloride
CCT	CTP:PC cytidyltransferase
CDP-Cho	cytidyldiphosphate choline
cGMP	cyclic guanosine monophosphate
ChoK	choline kinase
CHT	choline high affinity transporter
CI	confidence limit
Cr	creatine
C _t	cycle threshold
CTL	choline transporter-like protein
CTP	cytidyltriphosphate
DCIS	ductal carcinoma in situ
dd	double distilled
δ	chemical shift
DF	degree of freedom
DNTP	desoxynucleosid triphosphate
DTT	dithiothreitol
EtOH	ethanol
x exp	to the x power (e.g. 2exp x=2 ^x)
fCho	free choline
FNAB	fine needle aspiration biopsy
G6PDH	glucose-6-phosphat-dehydrogenase
Gd	Gadolinium
GOI	gene of interest
GPC	glycerophosphocholine
GTPase	guanosine triphosphatase
H0	Null hypothesis
HRMAS- ¹ H MRS	High Resolution Magic Angle Spinning ¹ H Magnetic Resonance Spectroscopy
Hz	Hertz
IDC	invasive ductal carcinoma
i.e.	id est
IQR	interquartile range
IRB	institutional review board
JMP	software by SAS Institute Inc., data analysis statistic programme
Km	Michaelis-Menten constant
kDa	kilo Dalton
LCIS	lobular carcinoma in situ
LCM	laser capturing microdissection
MRI	magnetic resonance imaging
MRS	magnetic resonance spectroscopy
MS	mass spectroscopy
MW	megawatt

n	number of samples
NMR	nuclear magnetic resonance
PAE	percentile amplification efficiency
PAH	polycyclic aromatic hydrocarbon
PC	phosphocholine
PCR	polymerase chain reaction
PDGF	platelet-derived growth factor
PEMT	phosphatidylethanolamine N-methyltransferase
PETN	phosphoethanolamine
PKA	protein kinase A
PKC	protein kinase C
PLA	phospholipase A
PLC	phospholipase C
PLD	phospholipase D
ppm	parts per million
PtdCho	phosphatidylcholine
q-rt-PCR	quantitative real-time polymerase chain reaction
ras	rat sarcoma (a proto-oncogene)
RNA	ribonucleic acid
Rpm	rounds per minute
RT	reverse transcriptase
SAM	S-adenosyl methionine
SD	standard deviation
shRNA	small/short hairpin RNA
Si	Silicium
siRNA	small interfering RNA
Std	standard
T	Tesla
tCho	total choline
TGrade	tumour grade
TM	registered trademark
US	ultrasound
Vmax	maximum velocity
w/o	without

6 Introduction

Breast cancer is a significant health issue in industrialized countries. It is the most common cancer among women and the second most common cancer worldwide (an estimated 1.152.161 new cases per year), trailing only lung cancer. In 2009, it accounted for 15% of deaths from cancer among women in the United States [1].

The current medical approach to this disease involves early detection and treatment. This strategy yields an 85% 10-year survival rate in the United States. Survival is directly related to stage at diagnosis, as illustrated by a 98% 10-year survival rate for patients diagnosed at stages 0 and I disease compared to a 65% 10-year survival rate for patients diagnosed at stage III disease [2]. To improve survival in this disease, more patients need to be identified at an early stage.

Nowadays routine screening is the gold standard for early detection. The commonly applied technologies like self-examination, mammography and sonography (ultra sound, US) still lack reliability. One way of increasing sensitivity is the introduction of advanced MRI. Not only does it enable the examination of breast tissue from younger patients (age < 40 years), where glands and connective tissue are dense and hinder high-resolution mammography, but it also improves the follow-up in patients after surgery, where MRI can help to distinguish tumour recurrence from scar tissue. The sensitivity of MRI in visualizing invasive cancer is nearly 100%, yet specificity values vary [3].

Study	Value	Mammography (%)	US (%)	MRI (%)
Preoperative evaluation [4]	Detection rate	84,6	97,3	93,7
	Sensitivity	22,2	20,6	66,7
	Specificity	85,7	85,2	64,2
	Accuracy of intraductal spread	50,0	50,0	65,6
Screening in women with familial or genetic predisposition [5]	Sensitivity	33,3	-	79,5
	Specificity	95	-	89,8

Table 1 Comparative studies of detection techniques.

A study investigating preoperative imaging techniques found that MRI had a detection rate comparable to that of US and a sensitivity rate higher than that of both mammography and US (see table 1) [3]. Also, MRI is superior to both US and mammography in detecting intraductal spread [4, 6]. It also shows promise in screening women with familial or genetic predispositions to breast cancer [7]. On the downside, MRI is prone to detect lesions that are benign [8]. More advanced

diagnostic technologies include tomosynthesis, sono- / MR elastography, Raman spectroscopy and diffraction techniques, but none of them has yet been introduced into routine clinical use. However, not even with an intensification of MRI use maximum diagnostic reliability can be provided.

As 14-53% of non-invasive lesions (i.e. LCIS/DCIS) progress to invasive forms of cancer [10], early detection is crucial. The introduction of new parameters into the diagnostic process is thus essential to increase survival rates. One of those parameters could be found on the molecular level. Here, typical changes observed in breast cancer tissue (for intraductal, intralobular and in situ forms) include the elevation of certain metabolites, among others those of the Kennedy pathway, namely phosphocholine (PC) and total choline containing metabolites. Proton magnetic resonance spectroscopy (^1H MRS) consistently detects significant differences in choline phospholipid metabolite levels of malignant versus benign breast lesions [11]. High-resolution nuclear magnetic resonance (HRNMR) studies of breast cancer cell extracts also found that PC levels increase with malignancy [12-14]. Studies have been performed on cell lines to explain the aberrant choline metabolism in breast cancer. However, the results of those studies differ and have mostly been performed on cell lines [11, 15], not on tissue samples.

It is critically important to understand the molecular causes underlying these metabolic changes: the evaluation of total choline (tCho) may not only improve diagnostic results, but could also identify novel targets for therapy in cancer cells [16, 17] and could be used as a biomarker [15], for treatment planning [18] and treatment response control [19] in breast cancer patients.

6.1 Aim of this study

The aim of this study is to histopathologically grade breast cancer tissue, perform ex vivo measurements of the expression of key enzymes of the Kennedy pathway within the tissue and relate their concentration to the magnetic resonance spectra gained using ^1H MRS.

6.2 The hypotheses

H0 = There is no statistically significant correlation between histological grade, the concentration of certain enzymes of the Kennedy pathway and metabolites measured

by ^1H MRS in malignant breast cancer tissue.

H1 = There is a statistically significant correlation between histological grade, the concentration of certain enzymes of the Kennedy pathway and metabolites measured by ^1H HMRS in malignant breast cancer tissue.

To test these hypotheses:

- the histologic grade of the samples is determined by a pathologist
- the expression levels of enzymatic mRNA involved in the choline metabolic pathways in these areas are quantified using quantitative real-time PCR
- ^1H MRS is used to measure choline and its phosphate metabolites in intact tissue samples and
- ^1H MRS and q-rt-PCR results are matched and monitored for specific patterns.

This was done during a research project in the laboratory of Prof. Leo Cheng, Radiology and Pathology Department, Harvard Medical School, Boston (USA) as part of a transatlantic cooperation with Charité Universitätsmedizin Berlin. Statistical analysis, discussion of results and potential scientific implications were performed at Charité Universitätsmedizin under the supervision of PD Dr. Matthias Taupitz, Institut für Radiologie.

7 Background

7.1 Metabolic changes in cancerous tissue

In cancerous tissue, numerous metabolic changes take place, such as an increase in lactate (known as the Warburg effect), taurine or unsaturated lipids, or a decrease in creatine and citrate (see table 2).

Increase	Decrease
- lactate [20]	- N-acetyl aspartate (in brain cancer) [21]
- unsaturated lipids (in breast and brain cancer) [21]	- creatine [21]
- choline	- alanine (in meningiomas)
- UDP-hexose [22]	- citrate (in prostate cancer)
- taurine (in breast cancer)	

Table 2 Exemplary metabolic changes in malignant tissue.

As one of the first to conduct a study on phosphorous-containing metabolites in different types of breast tissue (malignant, benign and non-involved human breast tissue) Merchant et al. found characteristic changes in malign tissue in 1988. Working with ^{31}P MRS, he suggested that an elevation in phosphocreatine “*permits a differentiation between malignancy and benignancy in breast disease*” [23].

7.2 Change in the choline metabolites' concentration in malignant cells

Based on Merchant's work, Ackerstaff et al. [24] tried to describe a metabolic pattern common to epithelial cell lines undergoing carcinogenesis. They found an early switch in the major choline phospholipid from glycerophosphocholine (GPC) to phosphocholine (PC). Apart from this switch, total choline-containing metabolites were not significantly elevated in the cell lines that had been immortalized (through benzo- α -pyrene), thus had undergone the first stage of carcinogenesis [24]. Bolan measured total choline levels and found these to be elevated in malignancies compared to benign lesions [25].

Despite the acknowledgement of this common feature of significant changes in the choline metabolism of malign tissue, the reason for the increase in choline metabolites remains unclear. Several theories have been put forward:

- increase in choline metabolism as a crucial component of membrane proliferation necessary for accelerated tumour cell growth

- since anti-inflammatory agents such as indomethacin decrease the level of choline metabolites in malignant cells [26], their elevated concentration may – in part – be attributed to the inflammatory state of cancer cells
- increased expression and activity of choline kinase (ChoK) [27], a higher rate of choline transport [28] and increased phospholipase D (PLD) [29], phospholipase A2 (PLA2) [30] and cytidyltriphosphate:phosphocholine cytidyltransferase (CCT) activity for so far unknown reasons.

All of the enzymes mentioned in the latter theory contribute substrates to or are part of a metabolic process called the Kennedy (CDP-choline) pathway. ChoK activation has been associated with variable indicators of greater malignancy in breast tumours [15, 27], PLD has been found to be overexpressed in human breast cancer tissue, transmembraneous choline transporter organic cation transporter (OCT) is a major source of extra-cellular choline and CCT is considered to be one of the main regulatory steps within the Kennedy pathway.

Before explaining more thoroughly the mechanisms of the Kennedy pathway, more details on one of its major components – choline – will be given.

7.3 Relevance of choline

Choline is a quaternary amine alcohol (trimethyl- β -hydroxy-ethylammonium) with a plasma concentration of 10-50 μmol in humans. Although it is not by strict definition a vitamin, it has been classified as an essential nutrient by the National Academy of Science (USA). Despite the fact that humans can autonomously synthesize it in small amounts, choline also needs to be part of the diet to maintain health [31]. Choline serves as or is involved in:

- a) cell signalling
- b) the structural integrity of cell membranes
- c) lipid (fat) transport and metabolism
- d) a methyl group donor
- e) nerve impulse transmission.

Apart from its role as a precursor molecule for the ubiquitous neurotransmitter acetylcholine, choline and its metabolites are involved in cell signalling, including the synthesis of lipid mediators like the platelet activating factor, dipalmitoylphosphatidylcholine (a component of pulmonary surfactant) and

lysophosphatidylcholine (a major structural feature of serum lipoproteins and precursor for the platelet activating factor).

In a healthy organism, choline and its related metabolites are part of the biochemical makeup of any cell. It is only through the changes triggered by carcinogenesis that the physiological choline equilibrium loses its balance.

The predominant use of choline in the human organism is the synthesis of lipid cell membrane components, such as phosphatidylcholine (PtdCho) (also known as lecithin), phosphatidylethanolamine and sphingomyelin. Choline serves as the hydrophilic group in the formation of those phosphoglycerides, amphiphilic molecules responsible for the separation of intra- from extracellular matrix (see fig. 1). All phosphoglycerides are thus crucial for metabolic processes as well as for cell proliferation. Biosynthesis and hydrolysis of PtdCho, for example, are essential processes for mitogenic signal transduction events in the cell [32]. Phosphocholine (PC) has also been shown to act as a second messenger in cell growth signalling [33].

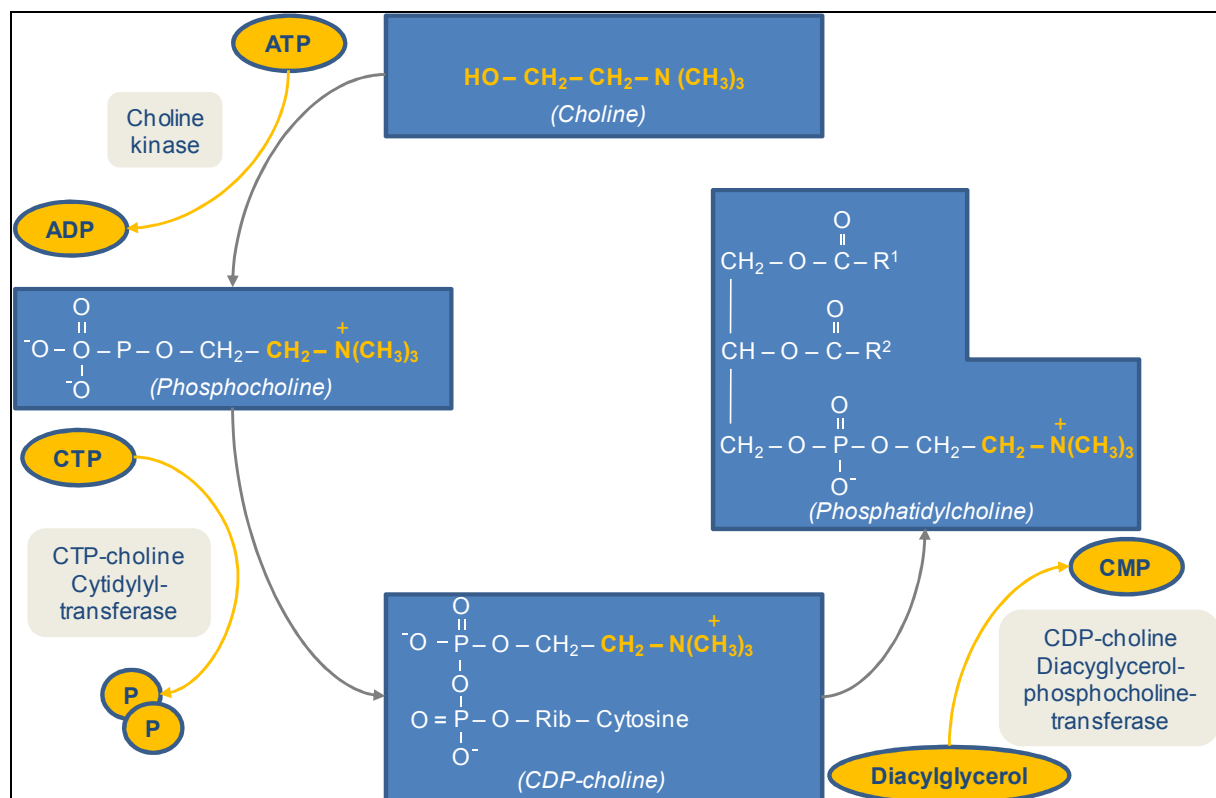


Figure 1 PtdCho biosynthesis pathway.

The main components of biological membranes are phosphoglyceride lipids composed of a glycerol unit esterified to two fatty acids and a polar alcohol group. One of the primary membrane phospholipids is PtdCho, in which the polar head group is composed of PC. The biosynthesis of PtdCho and phosphatidylethanolamine (PETN) follow similar routes. The first step in PtdCho is the phosphorylation of choline by ChoK to make PC, which is then activated by CTP. CDP-choline reacts with diacylglycerol to produce PtdCho [34].

Phosphoglycerids are in a state of constant dynamic transformation. Part of this transformation is the deconstruction through phospholipases. Each one of the phosphoglycerides' four ester-bonds is broken down by a specific lipase [35]. Phospholipase A, C and D all play a role in the synthesis of choline (or PC in the case of PLC), which constitutes the starting metabolite of the Kennedy pathway (see fig. 3), by breaking down either PtdCho or GPC.

7.4 Phosphoglycerid synthesis

Apart from the already mentioned de-novo-synthesis, phosphoglycerids can also be transformed from one into another (phosphatidylserin to phosphatidylethanolamin to phosphatidylcholin) by three successive methylations, as shown in fig. 2.

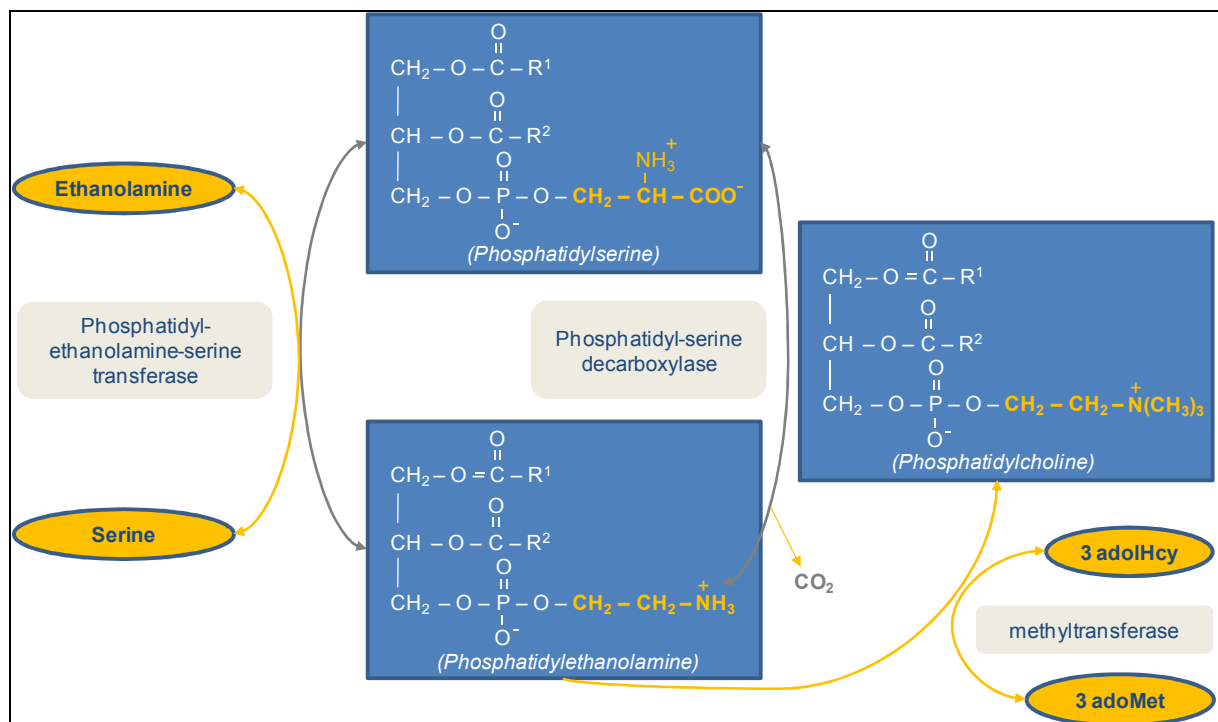


Figure 2 The salvage pathway from serine to PtdCho.

The biosynthesis of membrane phospholipids occurs through distinct pathways. For the synthesis of PETN, ethanolamine is first phosphorylated and activated to form CDP-ethanolamine. It then reacts with diacylglycerol to form PETN. PtdCho is synthesized by a similar route. Phosphatidylserine is synthesized through exchange of the polar head group with PETN. Phosphatidylserine is decarboxylated to form PETN, to which three methyl groups are added to form PtdCho [34].

This three-step methylation pathway - using S-adenosyl methionine (SAM) and catalyzed by phosphatidylethanolamine N-methyltransferase (PEMT) - appears to be quantitatively significant only in hepatocytes [36]. Thus, the major biochemical pathway for PtdCho in most cells appears to be the Kennedy pathway.

7.5 The Kennedy cycle

The intracellular pathway responsible for de-novo synthesis of cytidyldiphosphate-choline (CDP-choline) and ultimately PtdCho is known as the Kennedy pathway. The choline used for CDP-choline synthesis comes from three different sources: extracellular choline, intracellular choline and choline from GPC breakdown.

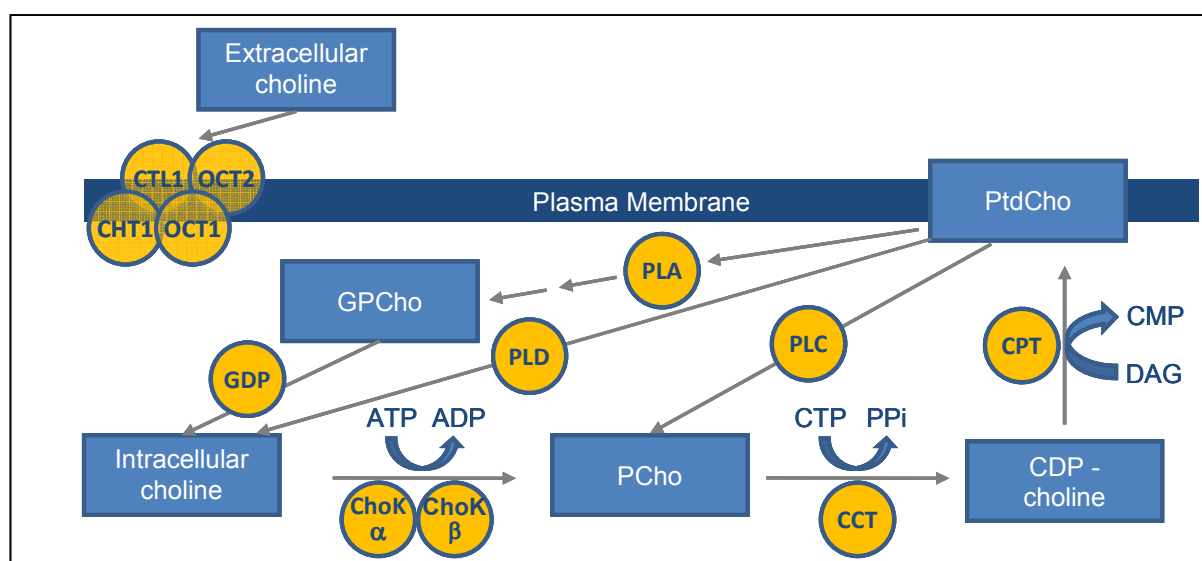


Figure 3 Schematic overview of the Kennedy cycle.

Shown are the choline transporters and the enzymes participating in the synthesis and degradation of choline phospholipids. Abbreviations used: CHT1: Choline high-affinity transport 1; CTL1: choline transport-like protein 1; OCT1 and OCT2: organic cation transporters 1 and 2; ChoK α and ChoK β : choline kinase α and β ; CCT: CTP:PC cytidylyltransferase; CPT: cholinephosphotransferase; PLA: phospholipase A; PLC: phospholipase C; PLD: phospholipase D; GPD: glycerophosphocholine phosphodiesterase; PtdCho: phosphatidylcholine; GPC: glycerophosphocholine.

In order to provide phosphoglycerides whenever they are needed (i.e. for cell growth and multiplication), the Kennedy cycle (basically an acylation cycle) provides a salvage pathway to produce new phosphoglycerides, using phospholipases [35], as shown in fig. 3.

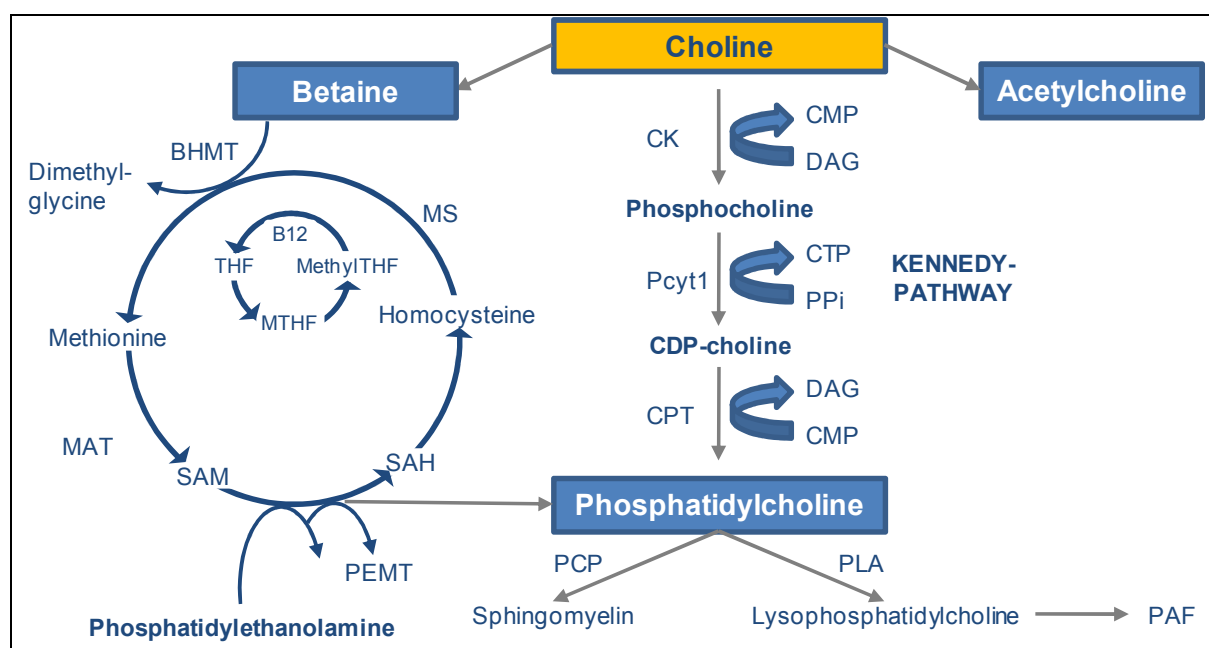


Figure 4 Use of choline in different metabolic pathways.

Choline serves as acetylcholine, betaine and membrane-building PtdCho, which itself serves as sphingomyelin (a sphingophospholipid present in almost all cellular membranes) and lysophosphatidylcholine, a precursor for the platelet activating factor (PAF). ADP: adenosine diphosphate; ATP: adenosine triphosphate; BHMT: betaine:homocysteine methyltransferase; B12: vitamin B12; CDP: cytidine diphosphate; CK: choline kinase; CPT: CDP-choline:DAG cholinephosphotransferase; CMP: cytidine monophosphate; CTP: cytidine triphosphate; DAG: diacylglycerol; MAT: methionine adenosyltransferase; methylTHF: 5-methyltetrahydrofolate; MS: methionine synthase; MTHF: 5,10-methylene-tetrahydrofolate; PAF: platelet-activating factor; PCP: phosphatidylcholine:ceramidecholine phosphotransferase; Pcyt1: CTP:phosphocholine cytidyltransferase; PEMT: phosphatidylethanolamine N-methyltransferase; PLA: phospholipase A2; PPI: pyrophosphate; SAH: S-adenosylhomocysteine; SAM: S-adenosylmethionine; THF: tetrahydrofolate.

Fig. 4 illustrates the use of choline and the consecutive products of PtdCho. Both are embedded in more than just one system. The intracellular choline is used in three ways by the cell:

- phosphoglycerids (i.e. choline) can be turned into one another by methylation
- choline can be turned into acetylcholine by acetyltransferase (using acetyl-coenzyme A)
- choline can be transformed to PtdCho using the Kennedy pathway which in turn can be used for the synthesis of sphingomyelin and platelet activating factor (PAF).

Since the discovery of cytidyltransferase (CCT) by Eugene Kennedy [37, 38] in 1956, the choline-PtdCho pathway has been extensively studied with respect to its significance in inflammation-related pathologies [39, 40] and neurological disorders such as multiple sclerosis [41], Gaucher's disease [42], M. Alzheimer [43] and M.

Parkinson. In Kennedy's honour, the pathway in which CCT is embedded was named after him.

The focus of this study is on enzymes involved in the Kennedy cycle, as it represents the main source of choline metabolites. The enzymes were selected for their direct involvement in the choline metabolism: they either have choline as one of their immediate substrates or catalyze a reaction that uses up one choline metabolite and thus could potentially indirectly trigger a reaction that in turn restores low choline levels (e.g. CCT). The genes selected for this study are listed in table 3.

Enzyme	Gene
Choline transporter OCT1	SLC22A1
Choline transporter OCT2	SLC22A2
Choline kinase α	CHKA
Choline kinase β	CHKB
Phosphocholine cytidylyltransferase α	PCYT1A
Phosphocholine cytidylyltransferase β	PCYT1B
Phospholipase D1	PLD1
Phospholipase D2	PLD2

Table 3 Enzymes and corresponding genes of the choline metabolism.

7.5.1 Selected enzymes of the Kennedy cycle

In the following, the enzymes that were studied will be explained more closely, with a focus on their function and biochemical properties.

7.5.1.1 Choline kinase

ChoK is the enzyme responsible for the generation of PC [44, 45]. Using both choline and ethanolamine as substrates, ChoK catalyzes the reaction of intracellular choline to PC by use of ATP [46].

There appear to be at least two genes coding for three isoforms of ChoK, the three isoforms being: ChoK α 1, ChoK α 2 and ChoK β , the two functional isoforms ChoK α 1 and ChoK α 2 resulting from alternative splicing of the ChoK α -transcript [46]. The functional difference between ChoK α 1 and ChoK α 2 (which differ by 18 amino acids) is currently unknown. The gene similarity between α 1 and β sequences is 59.7 % [47]. The enzyme exists as the hetero-dimer ChoK α / β and the homo-dimers α / α and β / β . Generally, the hetero-dimer is considered more active than the homo-dimers.

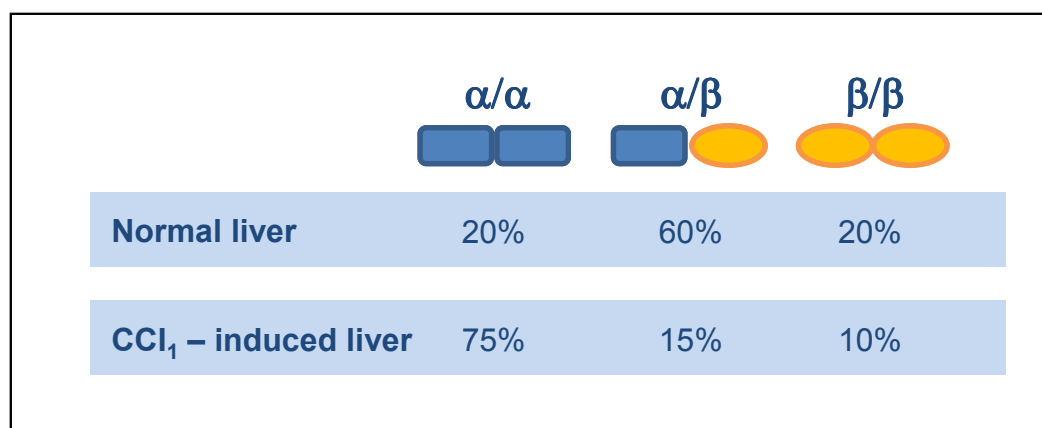


Figure 5 Configuration of the active ChoK enzyme.

Configuration of the active ChoK enzyme in normal and CCl_4 -induced mouse liver and the possible mechanism involved in the induction of ChoK- α gene expression in mouse liver by CCl_4 (a strong hepatotoxin) and polycyclic aromatic hydrocarbon (PAH). A relative contribution of active dimer configuration is indicated as percentage of the entire ChoK activity [47].

Aoyama [47] looked at ChoK activities in mice and found that, although some of the ChoK's active form actually consisted of an α/α or β/β homo-dimeric unit, a predominant part of ChoK activity in most mouse tissues was found to consist of an α/β hetero-dimer. In mouse liver, for instance, 20 % each of total ChoK activity was represented by the α/α and β/β homo-dimers with the remaining 60 % of the entire ChoK activity attributable to the α/β hetero-dimer. Injection of CCl_4 (a potent hepatotoxin and carcinogen) caused a shift in ChoK activity, with the homo-dimer α/α becoming the predominant isomer, contributing 75 % to the overall ChoK activity (fig. 5).

It has been reported in earlier purification studies that the specific activity of the α/α isoform can be much higher (with higher V_{max} and lower K_m for both choline and ATP) than that of β/β in in vitro ChoK assays. Thus, it is speculated that the specific activity of the α/β hetero-dimer may lay somewhere in between the two homo-dimer activities [47].

It has been suggested that ChoK is subject to a number of different regulatory influences. Among these are growth factors, hormones such as PKA (in mammalian cells) [47], and also oncogenes [48-51].

In 2002, Ramirez de Molina found a correlation between ChoK enzymatic activity and histological grade [52]. Three years later, her research team stated the “*definitive evidence of the oncogenic potential of choline kinase*” [53]. Overexpression of ChoK alone was sufficient to induce a 2,3 - fold increase in the number of colonies. These results suggest that ChoK is sufficient to induce oncogenic transformation displaying a transforming potential [53]. The article also points out the potent synergy of ChoK

when combined with RhoA, an upstream regulator¹. In mouse fibroblasts, oncogenes such as ras, src, raf and mos have been shown to increase ChoK activity [47].

A rapid induction of ChoK has also been associated with certain forms of cell stress, such as the one caused by polycyclic aromatic hydrocarbon (PAH) carcinogens [54] or carbon tetrachloride intoxication [47, 55]. This indicates that the ChoK gene must be a member of an acute responsive gene family, although the exact role of ChoK induction as well as of newly generated PC in various situations of cell stress needs yet to be clarified.

Whereas the fact of rising choline metabolite levels in tissues undergoing carcinogenic change appears to be extensively proven in previous studies, the sequence of events in this metabolic algorithm is not clear. Whether it is an aberration in the choline metabolite pathway and thus ChoK that triggers carcinogenesis or an alternative event leading to malignant transformation of the cell among other metabolic changes characterised by the induction of ChoK is still unclear.

Generally, it can be said that ChoK seems to be subject to a number of regulatory influences that cannot easily be categorized as stemming from one single biochemical process.

7.5.1.2 Phospholipase D 1/2

PLD is one of the four phosphodiesterases that catalyze the hydrolysis of phosphoglycerids at their terminal phosphodiester bond. It thereby produces a phosphatidic acid and releases the free polar head group, phosphocholine. Most mammalian PLD activity is found associated with membranes and appears to be specific for phosphatidylcholine [56-60]. PLD is known to be activated via multiple pathways involving G-proteins, Ca²⁺, unsaturated fatty acids, protein kinase C (PKC) and protein-tyrosine kinases [56, 61-69]. In addition PLD has been found to be induced by several members of the Rho family of GTPases and Ras families of GTPases, which thus serve as potent upstream activators of both PLD and ChoK [70].

¹ The Rho family of GTPases is a family of small (~21 kDa) signalling G-proteins (specifically a GTPase), and is a subfamily of the Ras superfamily. The members of the Rho/GTPase family have been shown to regulate many aspects of intracellular actin dynamics.

7.5.1.3 Cytidylyltransferase α/β

Cytidylyltransferase (CCT) is a dimer [71, 72], which catalyzes the formation of CDP-choline from phosphocholine by the use of one CTP. Four CCT isoforms are known in mammals: CCT α and CCT β 1, 2 and 3 [73-75]. They are biochemically similar in enzymatic activity and regulation. The gene PCYT1A encodes the CCT α isoform [76, 77], which is considered to be the major isoform [74], and PCYT1B encodes the CCT β 1/2/3 isoforms [77-79].

Cytidyltriphosphate (CTP):phosphocholine CCT is considered to be the rate-limiting enzyme in the Kennedy pathway [80] and is unique in that there is both a cytosolic and a membraneous form of the enzyme [74, 75]. It has been observed that the reversible translocation of CCT to membranes correlates with its activity within the cell [81].

Intriguingly, cellular content of CCT is clearly higher than what is required to sustain PtdCho production [82]. Jackowski suggests that this redundancy provides a mechanism for cell survival. Its activity is biochemically regulated over about a 100 - fold range based on its interaction with membrane lipid components and can rapidly respond to a range of metabolic changes and signaling stimuli [82].

CCT α is found in the cytoplasm associated with membranes, but the majority is in the nucleus [82]. In contrast, CCT β localizes exclusively outside the nucleus [78]. The nuclear CCT α is thought of as a reserve for a prompt response to an extranuclear PtdCho requirement, such as the membrane synthesis associated with mitogenic stimulation [83], or replacement of membrane due to pharmacological disruption of PtdCho synthesis [84]. Both hypotheses are possible and are not mutually exclusive [82].

Michel et. al. consider CCT to be the only rate-limiting step within the Kennedy pathway and deny a regulatory influence of any other mechanisms, such as for example choline transport rates [85]. Nevertheless, we decided to include transport enzymes in the study.

A current model states that interfacial packing defects, low lateral pressure, acyl chain disorder and bilayer curvature elastic strain is sensed by CCT and governs the degree of membrane association [74], thus providing a mechanism for both positive and negative regulation of activity. This indicates a certain degree of variability in the regulation of CCT through external factors and makes it all the more possible that

activity of the enzyme is influenced by cellular changes undergone by malignant tissue.

Already back in 1980, Sleight found that CCT translocates and activates in response to the depletion of PtdCho, either in PLC-treated cells [81, 86] or in cells starved for choline and supplemented with choline analogues [87]. It has been shown that CCT can be activated directly or indirectly by catabolic breakdown products from PtdCho [46, 74]. Thus, indirectly, CCT responds to a membrane surface deficit of PtdCho. This deficit could – at least in theory – result from increased synthesis of sphingomyelin and PAF from PtdCho.

7.5.1.4 Organic cation transporters

Choline has many physiological functions throughout the body. However, since choline is a charged hydrophilic cation, special transport mechanisms are required in order for it to cross biological membranes, as passive diffusion rates are low.

The primary choline transport mechanisms are described in tables 4 and 5.

Low affinity transporters	High affinity transporters
- choline $K_m \sim 30-100 \mu\text{M}$	- choline $K_m \sim <10 \mu\text{M}$
- location: ubiquitous	- location: presynaptic cholinergic nerve terminal
- function: provides choline for phospholipid synthesis	- function: provides choline for acetylcholine synthesis
- hemicholinium $K_i \sim 100 \mu\text{M}$ (μM range)	- hemicholinium $K_i \sim 0.001-0.1 \mu\text{M}$
- Na^+ -independent	- Na^+ -, Cl^- -dependent

Table 4 Two primary choline transport mechanisms. [88]

The transport mechanisms for choline include:

- sodium-dependent high-affinity uptake mechanism in synaptosomes
- sodium-independent low-affinity mechanism on cellular membranes and
- unique choline uptake mechanisms (e.g., blood-brain-barrier choline transport).

OCT 1/OCT2	CTL1-5	CHT1
Low affinity	Intermediate affinity	High affinity
- Choline $K_m \sim >30-100 \mu\text{M}$	- Choline $K_m \sim 20-200 \mu\text{M}$ [79]	- Choline $K_m \sim <10 \mu\text{M}$
- Location: ubiquitous	- Na^+ -independent	- Location: presynaptic cholinergic nerve terminal
- Function: provide choline for phospholipid synthesis	- immediate affinity for choline transport	- Function: provide choline for acetylcholine synthesis
- Hemicholinium $K_i \sim 100 \mu\text{M}$ (μM range)	- K_m most consistent with choline transport in cancer cell lines [81]	- Hemicholinium $K_i \sim 0,001-0.1 \mu\text{M}$
- Na^+ -independent		- Na^+ , Cl^- -dependent

Table 5 Comparison of different choline transport mechanisms. [88]

Low-affinity choline transport is typically characterized by sodium-independent carrier-mediated uptake. The average affinity for choline is $K_m > 20-30 \mu\text{M}$ and is a saturable process. Furthermore, low-affinity choline uptake is defined by stereospecificity and can be inhibited by similar nitrogen-methyl compounds (e.g. hemicholinium) [85, 88].

Choline transport characteristics are similar to those generally applying to transporters:

- translocation or uptake of choline across cellular membranes
- choline affinity and affinity for compounds that have a quaternary nitrogen coupled with a nitrogen–oxygen distance of approximately 3.26 \AA [89]
- translocation of the choline R(+)-enantiomer and not the S(-)-enantiomer (except for low-affinity transporters)
- competition with similar nitrogen-methyl compounds and
- demonstration of Michaelis-Menten saturability [88].

As shown in table 4, the low affinity transporters OCT1/2 are easily inhibited by hemicholinium, as opposed to high affinity transporters as CHT1, underlining their potential as a drug target.

Some experimental studies indicate that a large fraction of the intracellular choline represents non-metabolized choline [90] (i.e. non-phosphorylated choline), suggesting that choline transport and not phosphorylation is the key contributing factor for elevated choline levels within cells. This would suggest that the analysis of choline transporters could add crucial information to the explication of elevated intracellular choline levels.

This study looks at two of the low-affinity transporters, OCT1 and 2. Both are members of the SLC22 transporter family, which comprises organic cation transporters (OCTs), zwitterion/cation transporters (OCTNs), and organic anion transporters. OCTs function as uniporters that mediate facilitated diffusion in either direction. The OCT1-3 subgroup translocates organic cations, including weak bases. Transport of organic cations by any of the three OCT subtypes is:

- electrogenic
- independent of Na⁺ and
- reversible with respect to direction.

The driving force is supplied solely by the electrochemical gradient of the transported organic cation [91].

In 2007, the tissue distribution of polyspecific organic cation transporters was investigated by Koepsell [92]. It was found that mammary gland tissue expresses both OCT1 and 3, but not OCT2. Michel [85] describes OCT2 as mainly present in the kidney and specific brain regions. Specific and exclusive location of the transporters has still not been ultimately defined, and as Sweet puts it: “[...] *despite increased understanding of the individual transporters at the molecular and mechanistic levels, correlations of the functional differences between the OCT paralogs are still tenuous*” [93]. As both Glunde [11] and Eliyahu [15] include OCT1 and 2 in their detailed cell-line studies on the Kennedy cycle, both transporters were selected for this study, among other considerations as means of comparability between cell-line and tissue sample study setups.

7.5.1.4.1 OCT1

This transporter is most strongly expressed in hepatic tissue, but can also be found in mammary glands and epithelial cells [92, 94]. It has been found that expression and selectivity of OCT1 can be regulated by PKC, PKA, tyrosinkinase (stimulation) and cGMP (inhibition) [95, 96].

7.5.1.4.2 OCT2

In general, OCT2 has a more restricted expression pattern than OCT1, with its main concentration in the kidney and considerably lower concentrations in the brain,

neurons and epithelial cells [92]. Its expression has been found to be gender-dependent (expression of renal OCT2 is higher in males), steroid-hormone induced (testosterone application increased OCT2 expression in females) and regulated on a short-term basis [91].

Between OCT1 and 2, there is an overlap in substrates [92], among which are endogenous compounds (e.g. choline, acetylcholine, guanidine), drugs (cimetidine, procainamide), xenobiotics and model compounds.

7.6 Regulation of the choline metabolism

The regulation of choline phospholipid can occur through growth factor stimulation [97], oncogenes [98] and chemical carcinogens [99]. Also, transfection of human mammary epithelial cells with the erbB2 oncogene has been reported to cause a significant increase in PC levels [14, 100]. How these changes relate to one another is still unclear. In addition, regulation can occur on all levels and every step within the Kennedy pathway. Therefore, all regulatory influences identified for every enzyme within the Kennedy cycle also have an effect on the choline metabolism as a whole.

7.6.1 The Kennedy cycle and the rise in choline concentration

In order to explain the rise in choline-containing metabolites measured by ^1H MRS and NMR in malignant cells, we looked for possible causalities within the Kennedy cycle. Intracellular choline levels are determined by:

- the rate of choline synthesis and degradation
- the rate of PtdCho synthesis and degradation
- the rate of extracellular choline influx.

Consequently, choline kinase α and β (ChoK α/β), phospholipase D 1 and 2 (PLD1/2), cytidyltransferase α and β (CCT α/β) and organ cation transporters (OCT1/2) were chosen to analyse the variations in choline concentration.

PLC also figures among the enzymes of interest which could have a potential effect on choline metabolite concentration. Upon intensive discussions with Kristine Glunde and Zaver Bhujwala of Johns Hopkins University, Baltimore, MD, USA, two of the most active researchers in the field of choline metabolism and MRS in malignant cell populations and tissue, we decided not to include PLC, also because there is so far

no primer available to be used for PCR-analysis of choline-specific PLC. The only promising results in analysing this enzyme had been made in enzyme activity quantifications and were thus not feasible for our laboratory.

7.7 Nuclear magnetic resonance

As pointed out, changes in the metabolic makeup of a cell can give an indication of its histologic classification. The metabolome as a whole is dynamic, reflecting the continuous fluxes of metabolic and signalling pathways. There is no single preferential method of metabolic identification yet. A series of analytic techniques are available, each with distinct advantages and drawbacks. Two of the major NMR methods are ^1H MRS and mass spectroscopy (MS), which usually includes a separation stage based on gas chromatography or liquid chromatography, or optical spectroscopic techniques. ^1H MRS-based metabolomics has the advantage of being nondestructive, nonselective, cost effective and fast. MS on the other hand is considered to have more sensitivity than ^1H MRS (see table 6).

	MRS	MS
Equipment cost	High	High
Maintenance cost	High	High
Per sample cost	Low	High
Required technical skills	Yes	Yes
Sensitivity	<MS	>NMR
Reproducibility	High	Moderate
Quantitation	Yes	-
Resolvable metabolites	-	Advantage
Identification of unknown metabolites	-	Advantage
Potential for sample bias	Advantage	-
Data analysis automation	No	Yes

Table 6 Comparison of MRS and mass spectroscopy.
[101]

In order to effectively identify and quantify with sufficient sensitivity and precision the diverse range of metabolites, the so-called hyphenation approach (a coupling of a capillary separation method to mass spectrometry instruments or to high field NMR with capillary detection coils) would be needed. Suitably equipped facilities are scarce and their use extremely cost-intensive. With lower per-sample costs, quantitative evaluation potential and high reproducibility, ^1H MRS is an acceptable and feasible compromise for studies such as the one at hand.

The technique of Magnetic Resonance Spectroscopy (MRS) describes the reaction of nuclei in an external magnetic field that is perturbed by a second oscillating field [102]. Standard MRI scans are able to provide extremely detailed anatomical information. However, the findings in routine MRI do not necessarily correlate with tumour biochemical information. Only water protons are excited by the magnetic field and contribute to the tissue signal, whereas other metabolites do not [25]. In contrast, MRS provides extensive biochemical information on every sample, revealing information about the concentration of metabolites as well as changes of the biochemical environment [31, 46].

For a long time, classical MRS procedures could only be applied to aqueous solutions (solutions of tissue extracts and metabolites of lysed cells), where molecules are free from intermolecular interactions. They are destructive on solid structures as the molecules undergo anisotropic effects, resulting in spectral line broadening that makes a distinction of metabolites impossible. Thereby, classical MRS prevents further histopathological evaluation of the tissue, which is needed in order to correlate biochemical and pathological information of a sample [8, 12].

7.7.1 High resolution magic angle spinning

In 1972, Chapman et al. found a way to reduce the above-mentioned line broadening in solid samples [103]. This was done by spinning the sample rapidly around an axis which is oriented at an angle of $54,7^\circ$ with the direction of the magnetic field. By spinning at this so-called "Magic Angle" (the angle between the z-axis and the (1,1,1) - vector), at a rate larger than the anisotropic interactions, these interactions are averaged to their isotropic value, resulting in substantial line narrowing. The excess broadening under static conditions is due to a combination of residual dipolar interactions and variations in the bulk magnetic susceptibility [104]. For a variety of solid samples magic angle spinning is efficient at averaging these left-over components of the solid state line width and leads to NMR spectra that display resolution approaching that of liquid samples. Such methods have been termed High Resolution MAS (HRMAS) NMR.

HRMAS was used in this study to achieve spectral resolution sufficient for the identification and quantification of individual metabolites, while preserving tissue pathological structures for subsequent histopathological examination in order to

correlate spectroscopic data and quantitative pathology measured from the same specimen [105].

As one of the first to conduct a study on phosphorous-containing metabolites in different types of breast tissue (malignant, benign and non-involved human breast tissue) Merchant et al. found characteristic changes in malign tissue in 1988. Working with ^{31}P MRS, he suggested that an elevation in phosphocreatine plus a parallel elevation in an uncharacterized phosphate resonating at a chemical shift of 3,66 δ (expressed in ppm by its frequency) “*permits a differentiation between malignancy and benignancy in breast disease*” [23]. ^1H MRS delivers highly resolved spectra of hydrophilic - and to a lesser extent lipophilic - metabolites without any prior extraction step or other sample preparation necessary [106]. Among the metabolites undergoing specific changes in malign tissue, choline is a hydrophilic group and is therefore well suited for ^1H MRS detection.

Since Merchant’s discovery, the elevation of phosphocholine (PC), glycerophosphocholine (GPC), phosphatidylcholine (PtdCho) and free choline has become one of the most widely established characteristics in cancerous tissue of various origins: increased choline levels have been detected - among others - in breast, prostate and different types of brain tumours [13, 24, 45]. Likewise, several studies have shown that choline kinase (ChoK) is increased in human mammary tumours with high incidence, and this activation is associated with variable clinical indicators of higher malignancy [100]. As summarized in tables 7 (tissue) and 8 (cell populations), several studies have looked at choline levels in cancerous and corresponding normal samples.

Tissue/organ	Metabolite	Normal	Cancer
Human brain tissue extracts, ¹ H NMR (μmol/g ww) (Podo, 1999) [107]		White matter	Astrocytoma III/IV
	tCho	1.79±0.24	1.6±0.5 to 3.0±0.5
		Cortex	Anaplastic astrocytoma
Human breast tissue extracts, ¹ H NMR mean ± SD (μmol/g ww) (Gribbestad et al., 1999) [108]	PE	1.06±0.10	2.05±0.41
	tCho	0.64±0.10	1.326±0.079
	PC	0.029±0.025	0.79±0.55
	PE	0.16±0.011	2.1±1.1
	GPC	0.042±0.036	0.28±0.20
Human breast tissue extracts, ³¹ P NMR (μmol/g ww) (Podo, 1999) [107]	tCho	0.087±0.062	1.19±0.64
	PC	0.02 to 0.04	0.02 to 2.21
Human liver tissue extracts, ³¹ P NMR (μmol/g ww) (Bell and Bhakoo, 1998) [109]	PE	0.08 to 0.12	0.15 to 2.91
	PC	0.17±0.11	1.36±0.50
	PE	0.16±0.10	2.47±0.84
	GPC	2.46±0.37	0.59±0.15
	GPE	2.25±0.46	0.57±0.17
In-vivo clinical studies			
Brain, ¹ H MRS (Li et al., 2002) [110]	Volume of regions with metabolic abnormalities, based on indices obtained from tCho, tCr, NAA and lactate/lipid resonances, increased with tumour grade		
Brain, ³¹ P MRS (Negendank, 1992) [111]	PME/NTP	Normal<astrocytoma / high grade glial cancer	
	PDE/NTP	Normal>high/low grade glial cancer	
Brain, ¹ H MRSI (Kurhanewicz et al., 2000) [112]	tCho/NAA	Normal<cancer (no overlap)	
Breast, ³¹ P MRS (Negendank, 1992) [111]	PME	Normal<cancer	
Liver, ³¹ P MRS (Negendank, 1992) [111]	PME/NTP	Normal<cancer	
	PME/Pi	Normal<cancer	
Prostate, ¹ H MRSI (Kurhanewicz et al., 2000) [112]	Cho+tCr/citrate	Normal<cancer (minimal overlap)	
	tCho/tCr	BPH ≤ cancer	
Prostate, ¹ H MRS (Swindle et al., 2003) [113]	lipid/lysine	BPH ≤ cancer	
	PME/NTP	Normal ≤ cancer	
Prostate, ³¹ P MRS (Negendank, 1992) [111]	PME/PCr	Normal < cancer	
Abbreviations used: BPH, benign prostatic hyperplasia; Cho, free choline; GPC, glycerophosphocholine; GPE, glycerophosphoethanolamine; NAA, N-acetyl aspartate; NTP, nucleoside triphosphate; PC, phosphocholine; PCr, phosphocreatine; PDE, phosphodiester; PE, phosphoethanolamine; Pi, inorganic phosphate; PME, phosphomonoester; tCho, PC+GPC+Cho; tCr, creatine+phosphocreatine.			

Table 7 An overview of choline phospholipid metabolite levels.

Obtained from tissue in vivo and ex vivo. Data are from ¹H and ³¹P NMR spectroscopic studies of tumours and corresponding normal tissue [24]. In general, choline metabolite levels are elevated in malign tissue and cell population in comparison to benign cells.

A common feature found in both cancerous cell populations and tissue were increased choline, PC and GPC levels as opposed to lower choline metabolite levels in benign cells and tissues. The composite total choline resonance in ¹H MR spectra

(at 3,2 ppm) contains GPC, PC, choline, other trimethylamines and compounds such as inositol, phosphoethanolamine (PETN) and taurine.

Cells	Metabolite	Normal	Cancer
Brain cell extracts, ¹ HNMR, mean ± SD, (nmol/mg protein) (Bhakoo et al., 1996) [114]		Schwann cells (rat)	Meningioma cells
	PC	9.1±1.7	≥13.0±3.2
	GPC	18.9±2.7	≥4.2±2.2
	tCho	33.1±4.5	
			Glioblastoma cells
	PC		≥6.4
	GPC		≥2.3
			Neuroblastoma cells
HMEC extracts, ¹ HNMR, mean ± SE, (fmol/μm ³ or mM) (Aboagye, 1999) [14]	PC	0.027±0.010	≥0.390±0.021
	GPC	0.0307±0.0067	≥0.037±0.016
HMEC extracts, ³¹ PNMR, mean ± SD, (mol%) (Singer et al., 1995) [12]	tCho	0.077±0.022	≥0.491±0.017
	PC	0.4±0.2	≥5.8±0.6
	PE	6.7±1.9	≥7.5±1.0
	GPC	2.1±0.4	≥3.1±1.4
	GPE	2.2±0.9	≥2.5±1.9
Human prostate epithelial cell extracts, ¹ HNMR, mean ± SE (mM) (Ackerstaff et al., 2001) [115]	PC	0.0714±0.0031	≥0.56±0.12
	GPC	0.0244±0.0012	≥0.1437±0.025
	tCho	0.1173±0.0033	≥0.85±0.15
Intact HMECs, ³¹ PNMR and ¹³ CNMR, mean ± SE, (fmol/cell) (Bogin et al., 1998) [116]	PC		>17
	GPC		2.5±0.3
Intact HMECs, ³¹ PNMR, mean ± SE, (Met/NTP) (Ting et al., 1996) [13]	PC	<0.1	>1.3
	PE	<0.2	>0.8
	GPC	<0.3	>0.4
	GPE	<0.2	>0.4
Intact HMECs, ³¹ PNMR, mean ± SD, (mol%) (Singer et al., 1995) [12]	PC		10.3±3.4
	PE		22.2±2.7
	GPC		7.2±2.4
	GPE		6.8±1.0

Abbreviations used: BPH: benign prostatic hyperplasia; Cho: free choline; GPC: glycerophosphocholine; GPE: glycerophosphoethanolamine; NAA: N-acetyl aspartate; NTP: nucleoside triphosphate; PC: phosphocholine; PCr: phosphocreatine; PDE: phosphodiester; PE: phosphoethanolamine; Pi: inorganic phosphate; PME: phosphomonoester; tCho: total free choline: PC+GPC+Cho; tCr: creatine+phosphocreatine.

Table 8 An overview of choline phospholipid metabolite levels in cell lines.

Data are from ¹H, ¹³C and ³¹P NMR spectroscopic studies of normal and cancer cell lines [24].

7.8 Choline metabolites and MRS

As of 1992, following a review by Negendank [111], elevated choline and PC levels have been used to detect malign lesions, using ¹H MRS or NMR, for prostate [112], brain [117], breast [108], lung [118] and other cancers. Based on these observations,

ChoK, as a major catalyst in choline synthesis, has been studied extensively. Glunde [11] found that breast cancer cells exhibit increased PC ($p < 0,001$), increased total choline-containing metabolites ($p < 0,01$), and significantly decreased GPC ($p < 0,05$) compared to normal cell lines. It is this significant MRS pattern found across a multitude of different cancer forms that calls for an explanation on the biochemical level. This common feature of malign cells presents a promising lead into understanding metabolic changes that go along with carcinogenesis.

It has been found that PC can act as a second messenger in cell growth signalling [44, 119]. The activation of ChoK and the resulting increase in PC levels are assumed to be necessary events for fibroblasts to proliferate under the stimulation of certain growth factors (PDGF, bFGF etc.) [47]. The link from ChoK and its product PC to cellular transformation mediated by human oncogenes has so far been primarily researched by the teams of Hernandez-Alcoceba [51], Ramirez de Molina [53] and Bañez-Coronel [120]. Only recently it has been found that specific inhibition of ChoK leads to apoptosis in tumour-derived cell-lines from breast tissue [120]. Furthermore, a family of ChoK inhibitors has been shown to have anti-tumoural activity both in vitro and in vivo against human xenografts [120, 121]. This has opened up a possible therapeutic implication of the ChoK pathway as a target for pharmaceutical intervention.

8 Materials and methodologies

8.1 Design of the study

When designing the study, we looked in particular at two other articles by Glunde and Eliyahu that were closely related to our topic. Those two studies looked extensively at the changes in the choline metabolism in breast cancer and the relation to enzymes of the Kennedy pathway. Compared to one another, Glunde and Eliyahu came to very different results, as shown in table 9:

Author	Activity / concentration increase ↑	Activity / concentration decrease ↓
Eliyahu [15]	OCT2	PLD
	CHT1	
	ChoK α	
	Choline transport rates	
Glunde [11]	ChoK	Glycerophosphocholine
	PLC	PLD
	Total choline	PLA ₂
	Phosphocholine	Lysophospholipase 1

Table 9 Comparison of related studies by Eliyahu and Glunde.

The studies have been conducted on changes of enzymes of the Kennedy cycle between normal and cancerous cell lines. Listed findings refer to the cancerous cell lines. Abbreviations used: CHT1: choline high affinity transporter 1; OCT2: organic cation transporter 2; PLA₂/C/D: phospholipase A₂/C/D.

Glunde attributes the increase in intracellular choline metabolite concentration to a higher activity of both ChoK and catabolic PLC.

Eliyahu - in contrast - stresses the importance of an increase in transmembraneous transporters such as OTC and CHT. They found both choline transport rates and ChoK activity to be increased. Choline transporters were found to be expressed in the following order (both in normal and cancerous mammary epithelial cells): CTL1>OCT2>OCT1>CHT1. In malignant cells, OCT2 and CHT1 were upregulated. This went in order with an upregulation of transport rates within these cells and also increased PC levels.

The results of these studies clearly illustrate the differing findings and explanations surrounding the choline metabolism in cancerous cells so far. The setup of the study at hand differs in two major points from the work done by Glunde and Eliyahu:

- instead of normal to malignant cells, the study at hand looks at differences between tissue of histological grade 2 and 3

- while the other studies worked with cell lines, the study at hand is performed on intact tissue.

8.2 Tissue samples

The study has been approved by the institutional review board (IRB) of Massachusetts General Hospital (MGH IRB Approval: Metabolomic Profiles of Breast Tissue in Patients with Breast Cancer).

For the study, biopsy-proven breast cancer samples were used which were obtained during lumpectomy performed at Massachusetts General Hospital, Boston (USA). Selection of tissue samples was performed retrospectively according to their histological classification. All samples were histologically staged as invasive ductal carcinomas (IDC), grades 2 and 3. They were previously banked for molecular studies without identifier. The samples were kept at -80 °C at all times.

Patients were selected ex post upon histological determination of the tumour form: this study was performed on invasive ductal carcinoma tissue. Table 10 gives an overview of all samples initially selected for the study with their respective TNM-grading and patient age.

Sample number	TNM	Age of the patient at time of surgery
1	G3 N+ M0	51
2	G2 N+ M1	64
3	G2-3 N+ M0	58
4	G2 N+ M0	56
5	G3 N+ M0	49
6	G3 N- M0	54
7	G2 N+ M1	69
9	G3 N+ M0	72
10	G2 N+ M0	48
11	G2 N+ M0	70
12	G3 N- M0	57
13	G3 N- M0	68
18	G2 N- M0	73
19	G2 N+ M0	54
20	G2-3 N- M0	53
21	G3 N+ M0	48
22	G2 N+ M1	70
23	G2 N- M0	47
24	G2 N- M0	69
25	G3 N+ M0	73
26	G3 N+ M0	69

Table 10 Complete sample list including TNM staging and patient age.

The average patient age is 61. Based on the histopathological report, patients were retrospectively included in the study, following selection criteria IDC and grades 2 or 3. Age and overall TNM staging were not taken into consideration.

From the original sample group of n=21, two samples were excluded since they could not be assigned correctly to either one of the two grades (see table 11). The final number of samples was n=19.

Grade	Number of samples	Pathology
II	10	IDC
III	9	IDC
II-III	2	IDC

Table 11 Overview of samples.

From every sample, consecutive serial slides were used for HRMAS ¹H MRS analysis and LCM and subsequent rt-q-PCR. Both sets of data were then merged and jointly analysed.

8.3 HRMAS ¹H MR Spectroscopy

8.3.1 Spectroscopic procedures

Specimens were weighed before HRMAS ¹H MRS and transferred to a HRMAS sample rotor containing a permanently-attached external standard (silicone rubber) that functioned as a reference both for resonance chemical shift identification and quantification. HRMAS ¹H MRS measurement was carried out at 4 °C to minimize tissue degradation during the measurement. Spectra were acquired on a 600 MHz (14.1 T) Bruker AVANCE™ spectrometer (Bruker Instruments, Inc., Billerica, MA, USA) with magic angle spinning rates of 600~700 Hz using rotor synchronized DANTE Carr-Purcell-Meiboom-Gill (CPMG) pulse sequences. The 90 ° pulse length was adjusted for each individual sample. The 16 to 64 transients was acquired with a spectral width of 12 kHz and 16 k data points at a repetition rate of 5 sec. Measurement time for each sample was less than 6 minutes, and total testing time was less than 20 minutes.

8.3.2 Spectral analysis

Spectra were analysed by both Bruker software equipped with the spectrometer and the Nuts program (Acorn NMR for Windows systems). Before Fourier transformation, and phasing, all free induction decays were subjected to 1 Hz apodization, integrating appropriate resonances of choline kinase relative to the external (Si) and internal (H₂O) standards.

8.3.3 Transfer of MRS data to JMP

For the evaluation and correlation of MRS and PCR data, JMP 7.0.2 was used. MRS data were transferred to the JMP program for statistical analysis.

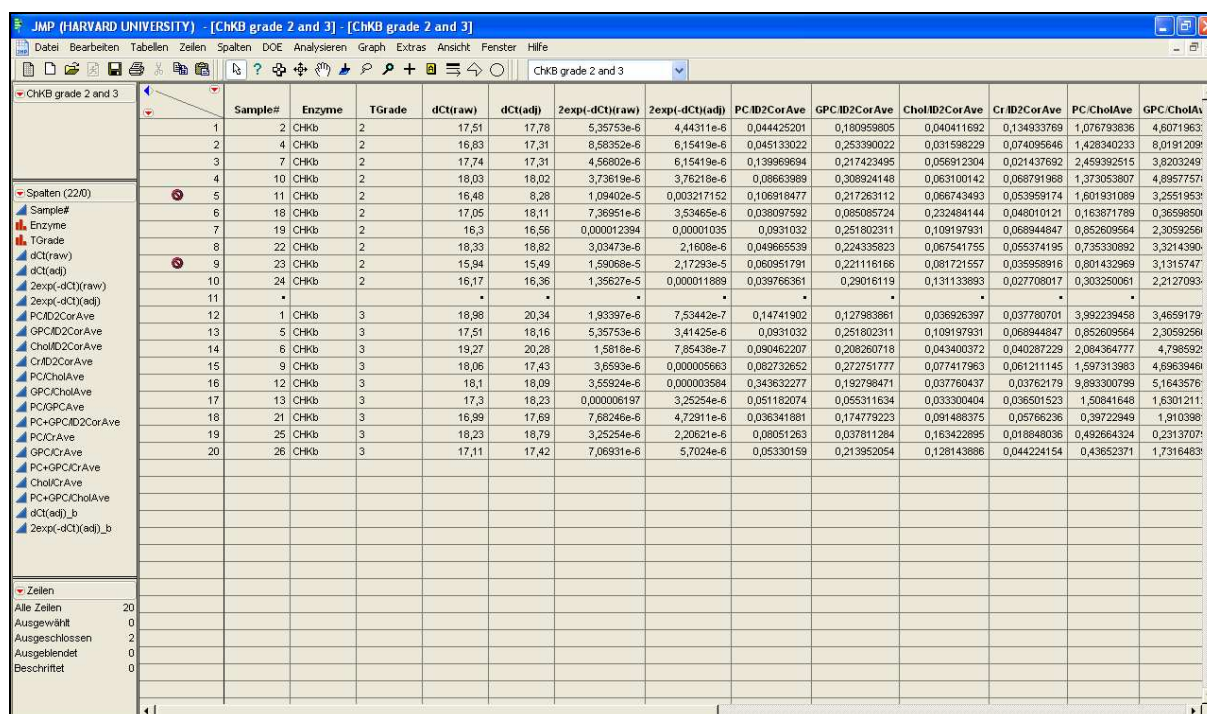


Figure 6 Screenshot of JMP program. Used for statistical analysis and correlation of MRS and PCR data.

Figure 6 shows the starting screen for ChoKβ and HRMAS ¹H MRS data. JMP allows for individual comparison of enzyme concentrations and tumour grade or metabolite concentrations.

Continuous modelling types:	Nominal modelling types:
dCt (raw)	enzyme
dCt (adj)	tumour grade (TGrade)
2exp (-dCt) (raw)	
2exp (-dCt) (adj)	
PC / ID2CorAve	
GPC / ID2CorAve	
Chol / ID2CorAve	
Cr / ID2CorAve	
PC / CholAve	
GPC / CholAve	
PC / GPCave	
PC+GPC / ID2CorAve	
PC / CrAve	
GPC / CrAve	
PC+GPC / CrAve	
Chol / CrAve	
PC+GPC / CholAve	
dCt (adj)_b (= dCt for ChoKβ)	
2exp(-dCt)(adj)_b (=2exp(-dCt)(adj)_b for ChoKβ)	

Table 12 Variables used for MRS data presentation in JMP.

Table 12 lists all variables on exported from MRS to JMP. In addition, data gained through PCR and known data like the tumour grade for every sample were then added.

One MRSI item listed in JMP is ID2CorAve. It is a measure of total spectrum intensity. Spectrum intensity varies across samples. It covers the total region of metabolites except for fat. In order to provide comparability between samples, choline concentration was standardized by use of a ratio of choline to total spectrum intensity rather than the absolute choline concentration. This choline intensity/total spectrum intensity ratio is expressed by the term ID2CorAve.

8.4 Histopathological analysis

Every sample used in the study was evaluated by an MGH pathologist. Frozen (-80 °C) tissue sample sections were serially sectioned, using a Leica CM 3050 cryostat. Table 13 lists the material used for the preparation of the serial slides.

Product	Manufacturer
Cryostat CM 3050	Leica
Gold seal slides, uncharged	Thermo Fisher Scientific, USA
Optimal temperature tissue compound	Sakura Seiki, Tokyo, Japan

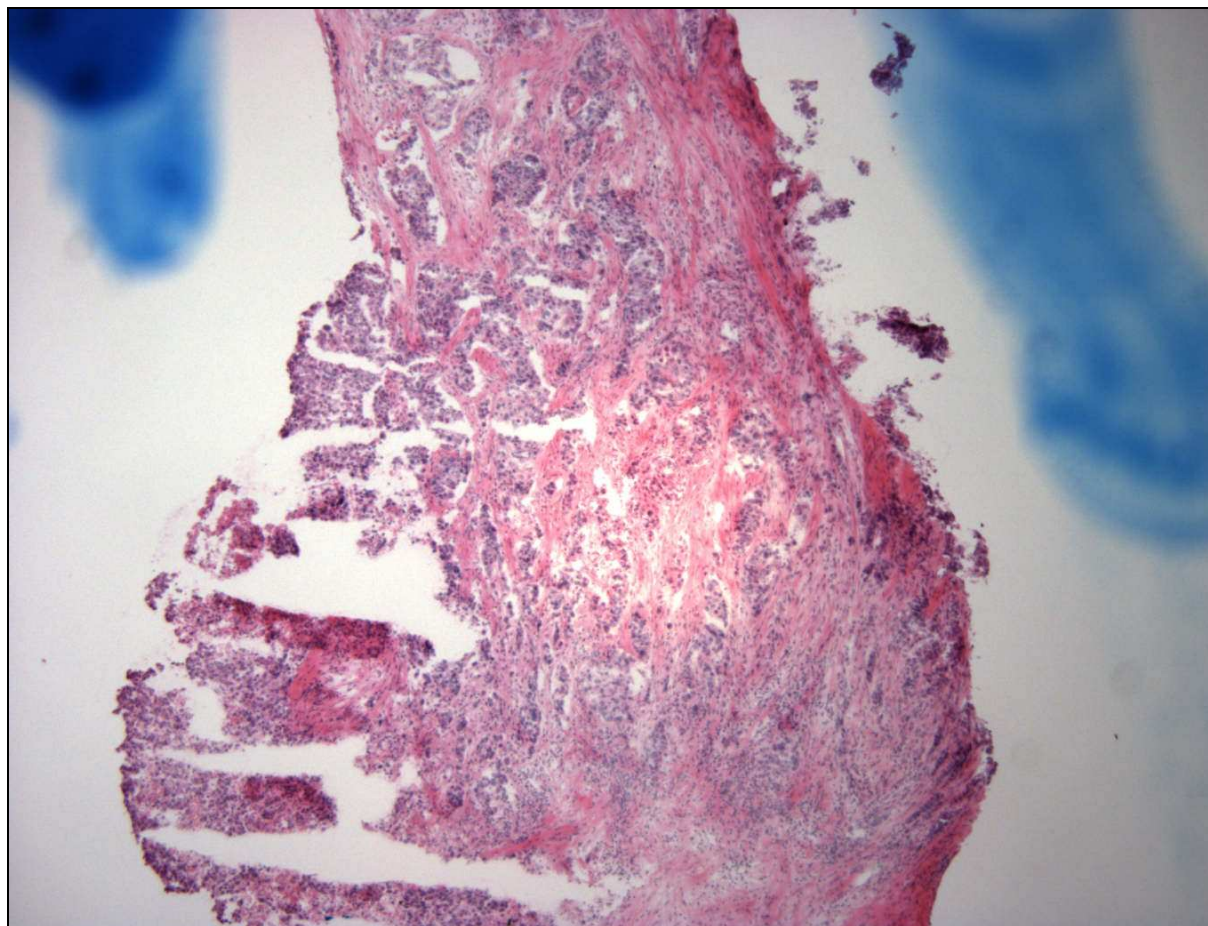
Table 13 Material used for cryostat work and preparation of serial slides.

Per sample, six slides each with three 10 µm cuttings were produced. Thus, serial sections of a 180 µm overall range were produced and subsequently stained using the hematoxylin/eosin staining protocol described in table 14.

Step	Substrate	Time
1	Xylene	12 min
2	100% EtOH	4 min
3	95% EtOH	2 min
4	Rinse in dd-water	1 dip
5	Hematoxylin	5 min
6	Rinse in dd-water	1 dip
7	Bluing reagent	15 dips
8	Rinse in dd-water	1 dip
9	95% EtOH	10 dips
10	Eosin	3 min
11	95% EtOH	10-15 dips
12	95% EtOH	10-15 dips
13	100% EtOH	10-15 dips
14	100% EtOH	10-15 dips
15	Xylene	≥ 2 min

Table 14 H/E staining protocol.

To make sure where and if the part of the specimen that was being used for LCM contained malignant cells, the first and last slides were screened by an MGH pathologist who would mark the malignant cell accumulations in the tissue and thus give an indication which areas of the section were to be acquired during LCM. Picture 1 shows an H/E serial slide of a tissue section. The blue marks in the upper left and right hand corners indicate the area of unequivocal malignity, as identified by the pathologist.



Picture 1 Invasive ductal carcinoma in breast tissue x20.

H/E staining. The blurred blue lines to the right and left are the pathologist's demarcations to indicate the part of the tissue that is infiltrated by tumour cells. In the adjoining cuts, these areas were then chosen for LCM. Picture taken with Olympus BX41 Microscope and Imaging System, magnification x20.

8.4.1 Handling of samples

Samples were stored at $-80\text{ }^{\circ}\text{C}$. For the preparation of LCM, samples were removed from the freezer and stored on dry ice. During cryostat cutting, samples were exposed to temperatures of $-22\text{ }^{\circ}\text{C}$ within the cryotome. The slides were then again stored on dry ice and moved to laser capturing or back to the $-80\text{ }^{\circ}\text{C}$ freezer.

8.5 Laser Capturing Microdissection

Slides containing frozen sections were fixed in 75% ethanol for 1 minute, in purified and distilled water for 2 minutes, stained with hematoxylin/eosin, followed by dehydration steps of 30 seconds in 75% ethanol, 2 minutes in 95% and 1 minute in 100% ethanol, with a final 5 minute dehydration step in xylene (see table 15).

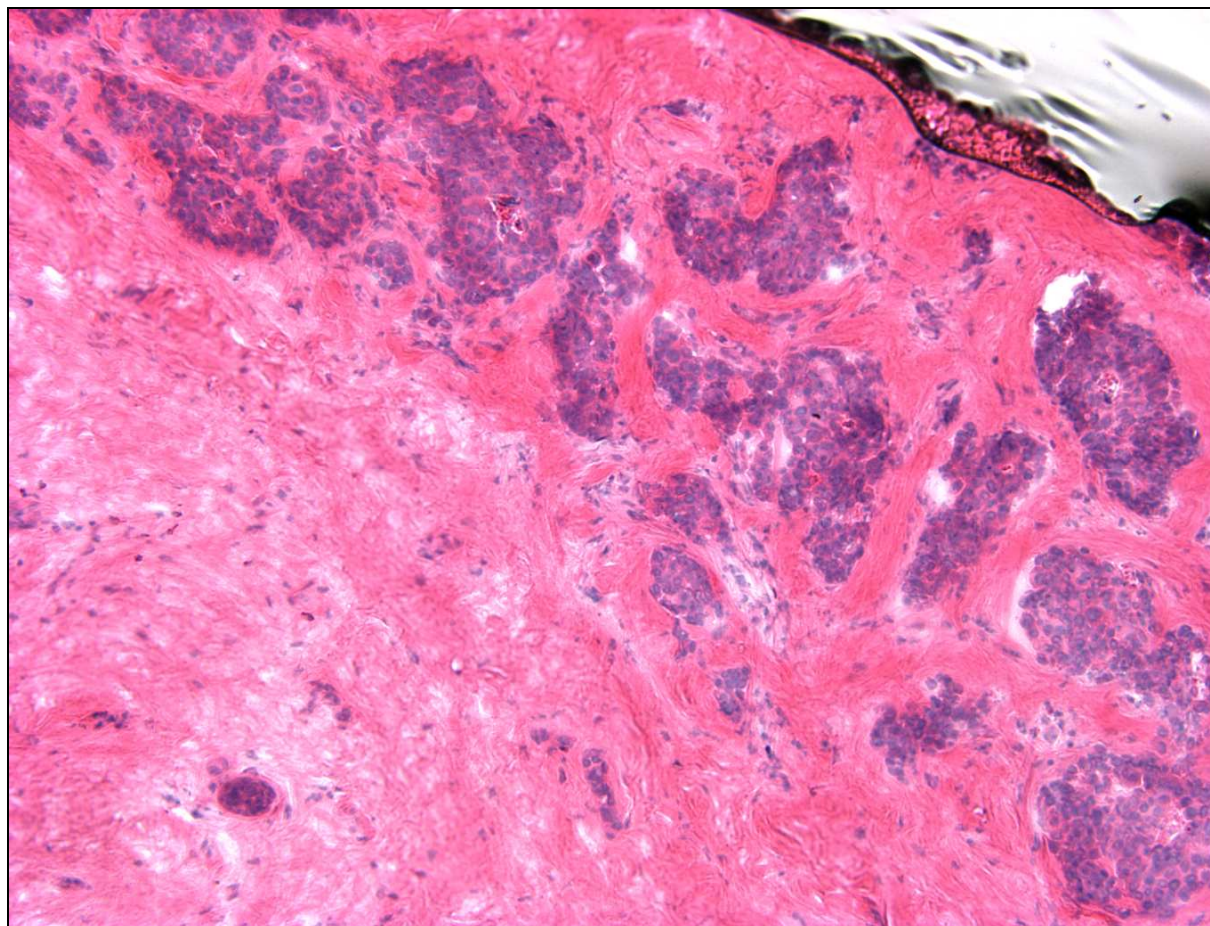
Step	Substrate	Time
1	75% EtOH	1 min
2	Purified, distilled water	2 min
3	H/E	2 min
4	75% EtOH	30 sec
5	95% EtOH	2 min
6	100% EtOH	1 min
7	Xylene	5 min

Table 15 Staining protocol for LCM.

The sections were air-dried and LCM performed on them using PixCell II Laser Capture Microdissection System (Arcturus Engineering, Mountain View, CA). LCM works by melting thermoplastic films mounted on transparent LCM caps (CapSure Macro LCM caps, Arcturus Engineering Inc., CA., USA) on the selected populations of cells. For the smallest spot size, the system was set to the following parameters:

- 35 Mw for the laser power
- 4,5 msec pulse duration and
- 7,5 μm spot size.

Every microdissection session was performed in less than 30 minutes, during which no more than three sections were processed in order to assure mRNA integrity and protection from degradation. For each section typically 5.000 pulses were used. Picture 2 shows the view through the LCM before capturing.



Picture 2 Invasive ductal carcinoma in breast tissue x60.
H/E staining. Picture taken with Olympus BX41 Microscope and Imaging System, magnification x60.

The caps with the selected cells were then put into vials filled with 25 μ l extraction buffer (Absolutely RNA Miniprep Kit, Stratagene, La Jolla, CA, USA), a mercaptoethanol-based lysis buffer and incubated for 10 minutes at 40 °C, at which time all captured cells from the cap dissolve within the lysis buffer. Vials were then spun at 30.000 rpm for 1 minute and consecutively stored at -80 °C until PCR was performed.

The use of LCM allows for a highly specific selection of malignant cells only and minimizes the unwanted selection of adipose and fibrous tissue surrounding the malignancy.

8.6 RNA techniques

Working with RNA requires protective measurements against RNase-contamination. The use of single-use latex gloves, frequent disinfection of the working area with RNase-Zap and autoclaving of pipettes and vials were obligatory.

8.6.1 Real-time quantitative PCR

For a correct performance of PCR, the following steps were taken:

- selection of an appropriate reference gene ("housekeeping gene")
- preparation of serial dilutions of cDNA for both the gene of interest and housekeeping gene to ensure similar efficiencies and for testing of primers (eight dilution series for a total of eight enzyme primers and the housekeeping gene)
- performing of PCR
- calculation of amplification efficiency
- use of amplification efficiency adjustment tool
- accuracy check as a means of internal quality control for triplicates.

8.6.2 Relative quantification

As opposed to absolute quantification, gene expression levels can be calculated by determining the ratio between the amount of a target gene and an endogenous reference gene that can be found in all samples. This ratio is then compared between different samples. Usually, housekeeping or maintenance genes are chosen as an endogenous reference. The target and reference gene are amplified from the same sample in the same reaction. The normalized value is determined for each sample and can be used to compare differential expression of a gene in different tissues. When gene expression levels are compared between samples, the expression level of the target is referred to as being, for example, 100 - fold higher in stimulated cells than in unstimulated cells.

8.6.3 Housekeeping gene

Housekeeping genes are commonly used in quantitative real time reverse transcriptase PCR. They serve as an internal control gene - based on the assumption that these housekeeping genes are constantly expressed, do not vary in their concentration and are unaffected by experimental conditions - , since the amount of assayed mRNA may fluctuate in between samples. This is due, among other things, to differences in tissue mass, the number of cells, experimental treatment or varying efficiency of RNA preparation. To make up for these confounding factors, genes of

interest are measured in relation to their control gene rather than in absolute terms. Also, normalizing to an endogenous reference provides a method for correcting results for differing amounts of input RNA [122].

Several housekeeping genes have been commonly used for PCR validation, such as glucose 6-phosphat dehydrogenase (G6PDH), hypoxanthine phosphoribosyltransferase (HPRT) and β 2-microglobulin [123]. For this particular study, 18s was used as housekeeping gene, because it displays practically no variation between benign and malign cells [124, 125].

8.6.4 Process of PCR

As it was only until later in the study that we decided to include additional enzymes of the Kennedy pathway to look for additional information as to why choline metabolite concentration in malignant tissue was elevated, some enzymes could not be run on all samples for lack of sample material. Therefore, additional enzymes could only be measured in 16 out of the original 19 samples. Table 16 lists the products used to perform PCR.

Product	Manufacturer
Dithiothreitol (DTT)	Promega, Wi.; USA (P1171)
Reverse transcriptase (RT)	Promega, Wi., USA (M1701)
Random hexamers	Roche, Germany (11034731001)
Desoxynucleosid triphosphate (DNTP)	Roche, Germany (3622614001)
RNAse inhibitor for cDNA	Promega, Wi., USA (N2111)
Mastermix	Superarray, now SABiosciences
RNA extraction kit	Stratagene, Tx., USA
Primers	SABiosciences, Md., USA
Reverse transcriptase	Gibco©, Invitrogen, Ca., USA

Table 16 Material used for PCR.

For maximum consistency, all primers were ordered from one company, in this case SABiosciences (see table 17).

Protein	Gene	SABiosciences primer number
Choline transporter OCT1	SLC22A1	PPH11376A-200
Choline transporter OCT2	SLC22A2	PPH20579E-200
Choline kinase α	CHKA	PPH10046A
Choline kinase β	CHKB	PPH66782A
Phosphocholine cytidyltransferase α	PCYT1A	PPH20489A-200
Phosphocholine cytidyltransferase β	PCYT1B	PPH12192A-200
Phospholipase D1	PLD1	PPH02835A-200
Phospholipase D2	PLD2	PPH02787A-200

Table 17 Overview of primer provenance.

For PCR, the cells in lysis buffer were reheated to 37 °C and RNA was prepared from captured cells using the Absolutely RNA Miniprep Kit (Stratagene) and reversely transcribed to cDNA by murine leukemia virus reverse transcriptase.

To the RNA in lysis buffer, 80 ml of 70 % ethanol were added, put in a spincap and spun for 1 minute at maximum speed. 600 ml of lowsalt buffer were added and spun again for 1 minute at maximum speed. The filtrate was discarded and the cap spun again for 2 minutes in order to dry the matrix. Then, a mixture of 5 ml of DNase and 25 ml of DNase buffer were put on the filter and incubated for 15 minutes at 37 °C. After that, 500 ml of highsalt buffer were pipetted on the filter and spun for 1 minute at maximum speed, after which the filtrate was discarded. Then, 600 ml of lowsalt buffer were pipetted on the filter and again spun for one minute at maximum speed and the filtrate discarded. The vial was then spun for the fifth time at maximum speed and the filtrate discarded. Next, 300 ml of lowsalt buffer were put on the filter, spun for two minutes at maximum speed, after which the filter was placed in a 1,5 ml tube and pipetted with 30 ml of elution buffer to clean the RNA out of the filter. At last, the vial was put in a heating block at 37 °C for two minutes, spun for one minute at maximum speed, the filtrate pipetted on the filter once more and spun for one minute at maximum speed. RNA was then stored at -80 °C until further use.

Mathematically, PCR has three phases: the exponential, linear and plateau phase as shown in fig. 7.

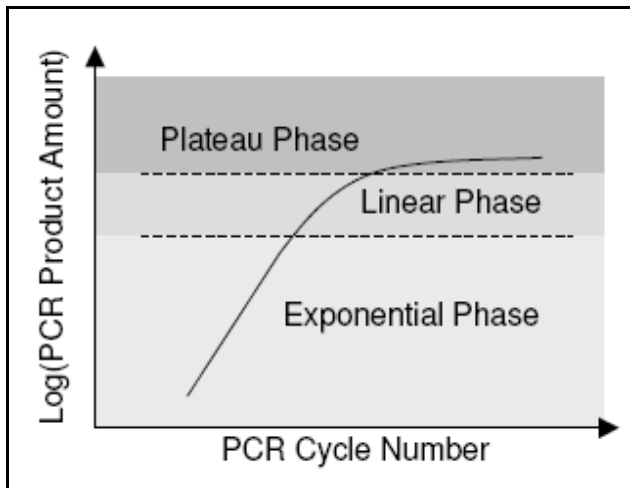


Figure 7 Theoretical plot of PCR.

The PCR cycle number and corresponding logarithm PCR product amount. The graph gives an indication of the different phases undergone during the PCR process.

The exponential phase is the earliest segment in the PCR, in which the product increases exponentially since the reagents are not limited. Graphically, this phase is represented by a linear slope (log-linear). The linear phase is characterized by an increase in product as PCR reagents become limited. The PCR-replication process will eventually reach the plateau phase during later cycles, when the amount of product will not change because some reagents become depleted. Real-time PCR exploits the fact that the quantity of PCR products in the exponential phase is in proportion to the quantity of initial template under ideal conditions [126].



Picture 3 Sample amplification plot 7000 System SDS Software.

The curves to the left represent the housekeeping gene 18s in a duplicate. The three curves to the right are the triplicate of one single gene of interest.

As shown in picture 3, the plot of logarithm 2-based transformed fluorescence signal versus the cycle number will yield a linear range at which the logarithm of fluorescence signal correlates with the original template amount. For further analysis, a threshold was set at a point where both the amplification curves of the housekeeping gene and the gene of interest were in the linear growth phase. The cycle number at the threshold level of log-based fluorescence is defined as C_t number, which is the observed value in most real-time PCR experiments, and therefore the primary statistical metric of interest [127].

PCR reactions were performed by using an ABI PRISM 7000 Fast Lightcycler (Applied Biosystems, Foster City, CA., USA). Relative quantification was assessed by using the formula $2^{-\Delta C_t}$ and normalizing the amount of the target gene to the housekeeping gene 18s. All PCRs were run as triplicates (genes of interest) and duplicates (housekeeping gene). The excel program used for adjustment of efficiency automatically calculated the mean of the triplicate measurements. A cycle difference of $>0,5$ between triplicates led to a re-run of that particular sample.

For PCR evaluation, 7000 System Sequence Detection Software BioAnalysis (Version 1.2.3 Applied Biosciences) was used. Spectroscopy, cryostat cutting, laser capturing and PCR analysis were performed in the facilities of Massachusetts General Hospital, Charlestown Navy Yard, Boston, USA.

8.6.5 Correlation of MRS data and PCR results

The data gained through spectral analysis was later combined with the data gained through PCR. Thus, a determination of the value (or lack thereof) of choline metabolite concentrations measured from HRMAS ^1H MRS as a function of the different histological tumour grades and of the sensitivity and specificity of expression levels of enzyme mRNAs in the choline synthesis/degradation pathways measured with LCM-rt-q-PCR could be tested.

For correlation between MRS data and the PCR values for every enzyme, ANOVA was used. A p-value $<0,05$ was considered significant.

9 Preliminary measures

To assure comparability and reliability of the PCR data, serial dilutions and pre-runs were performed.

9.1 Serial dilutions

Serial dilutions were run on every set of primers that was used in the study by use of the cDNA material. The purpose was to give a proof of concept and to test the correct functioning of the primers.

As can be seen in the plotting of concentration versus the cycle threshold (C_t), the values for the genes of interest (GOI) (in this case, ChoK α and β) and the housekeeping gene (18s) are practically the same (fig.8). This correlation is at the basis of the q-rt-PCR-method, therefore serving as a proof of concept for this method: C_t and concentration are almost perfectly correlated, with R^2 ranging between 0,9965 and 0,9967. Therefore, it is justified to infer the concentration difference from the C_t -difference.

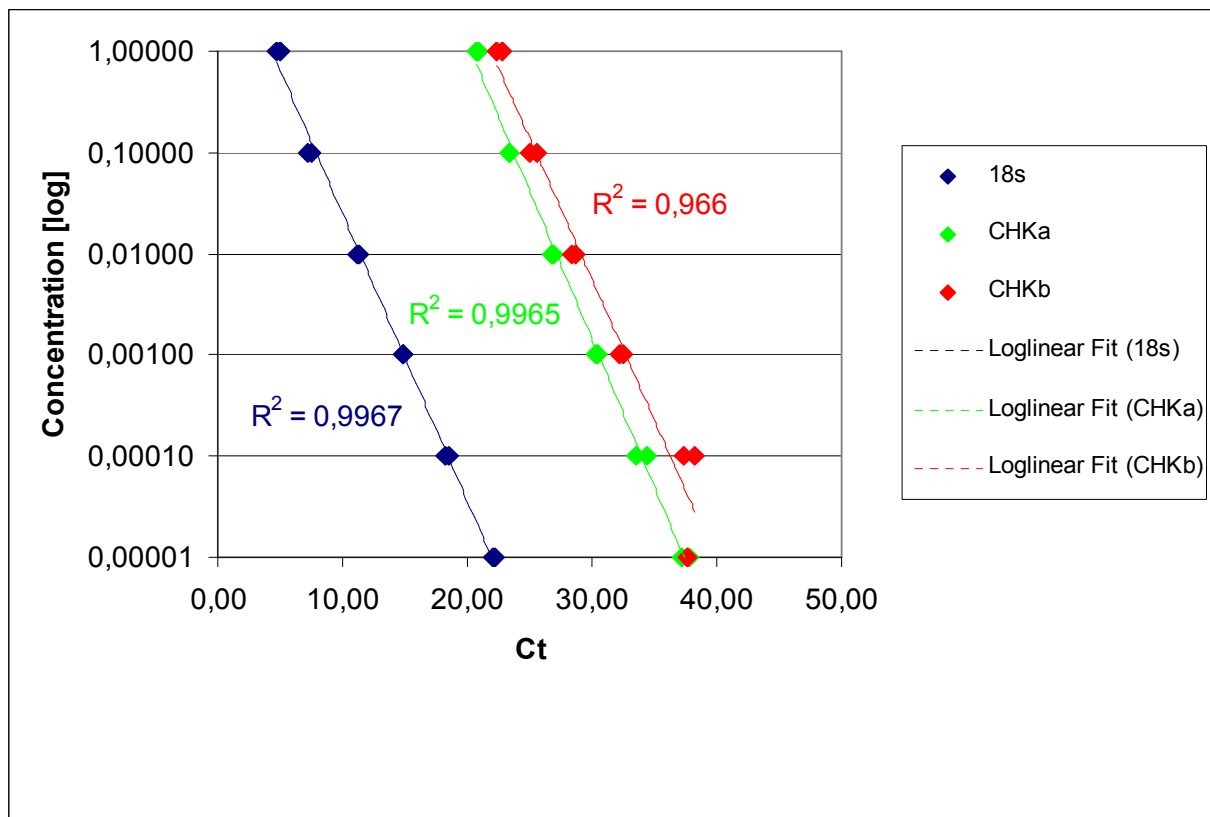


Figure 8 Concentration and C_t relation.

Proof of concept for q-rt-PCR, which suggests that a high C_t infers a low concentration and vice versa.

Serial dilutions were also used to test the primer: would there be extreme differences between the housekeeping gene and the GOI, a malfunctioning primer could not be excluded as one possible reason for the discrepancy.

As suggested by Livak and Schmittgen [122]:

- an internal control (housekeeping) gene was selected and
- serial dilutions of cDNA were performed for both the GOI and the housekeeping gene to ensure that the efficiencies are similar.

9.2 Amplification efficiency

In the serial dilution plots it was found that the slope in the amplification plot changed with differences in RNA-concentration. As depicted in fig. 9, the average amplification efficiency (AE) ranges between 1,7 and 2,0, with the housekeeping gene 18s generally displaying lower, GOI usually higher AEs. The smaller the initial cDNA concentration (i.e. the higher the Ct) the higher is the AE in the linear stretch for a particular well. This is true both across enzymes, but more importantly, also for each enzyme taken by itself (fig. 10).

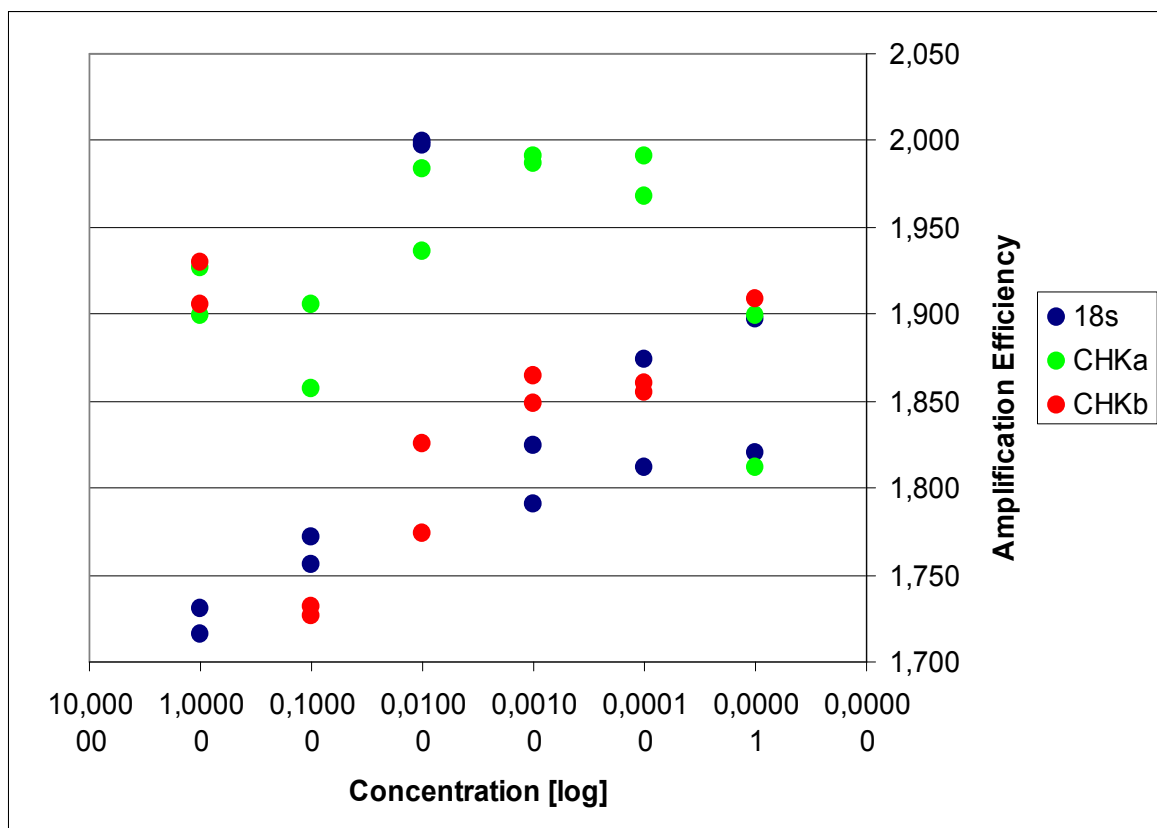


Figure 9 Amplification efficiency for different concentrations.

Higher AEs in higher C_t -values consequently imply higher AEs for lower cDNA concentrations, which are really underlying the higher C_t -values. This is depicted in fig. 10.

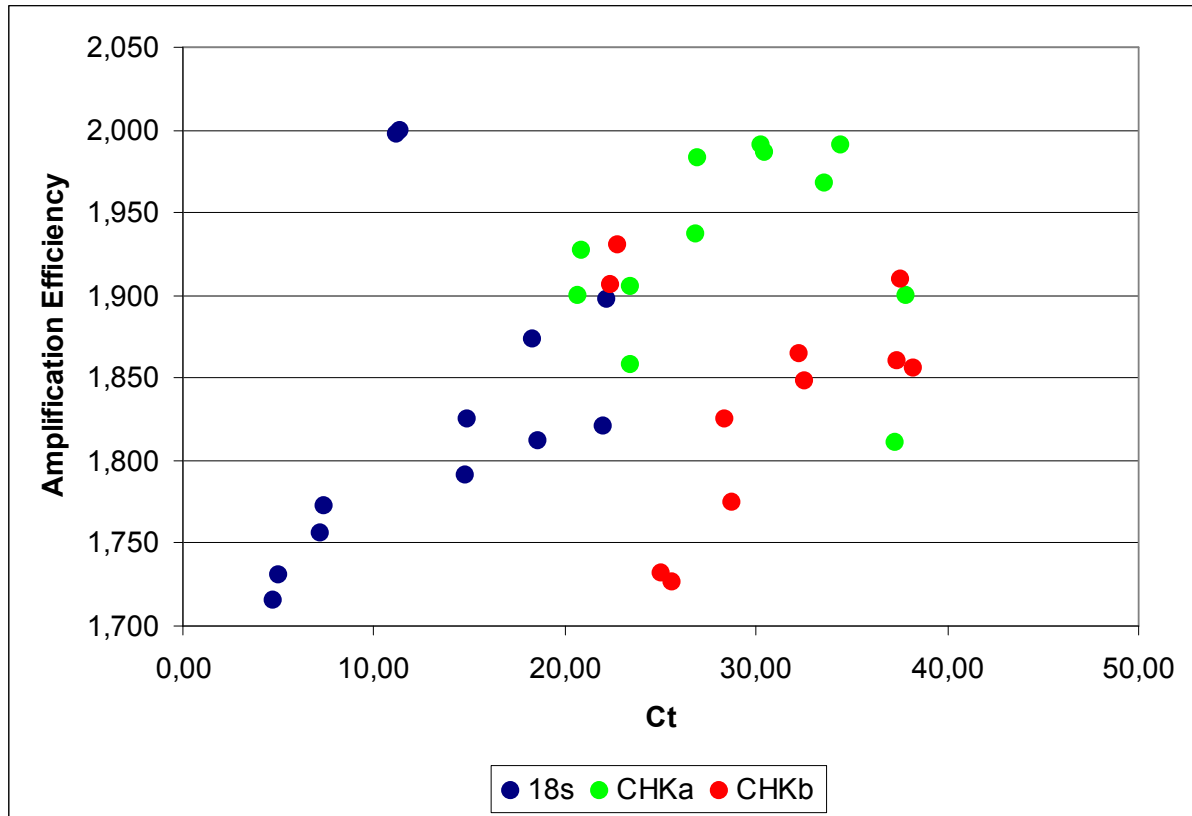


Figure 10 Amplification efficiency for different C_t -values.

Amplification efficiency tends to be higher for lower C_t -values (the basis of which are lower cDNA concentrations).

As becomes clear by looking at the chart, this relationship is only convincing for 18s and possibly ChoK β , and only when outliers are not being considered.

Two factors causing a divergence of amplification efficiencies could be identified:

- AE correlates with the initial input amount of RNA. To account for this factor, a pre-run was done before every actual PCR-run to detect any differences in initial RNA concentration. Adjustment for this difference was done by diluting the higher concentrated samples.
- AE varies between the different enzymes.

Amplification efficiencies differed, not only between different primers, but also between triplicates.

The amplification plot of the PCR delivers an illustration for every gene that is being amplified. In theory, every amplification cycle doubles the amount of the gene.

However, it has been shown that AES vary from 70-100 % [128]. These variations can be explained by the quality of the primer, template purity, amplicon length, assay design, PCR reagents, PCR equipment and human error.

At the start of a PCR reaction, there is an excess of reagents, but both template and product are at low enough concentrations that a renaturation of the PCR product does not compete with primer binding. Amplification proceeds at a constant, exponential rate. However, at one point, the reaction rate ceases to be exponential and enters a linear phase of amplification. The specific time for this shift in amplification efficiency is extremely variable and appears to be primarily due to product renaturation competing with primer binding (since adding more reagents or enzyme has little effect). At some later cycle the amplification rate drops to near zero, graphically illustrated by the plateau in the amplification plot.

In order to compare the PCR-curves of the genes of interest, they need to be adjusted so that their AE is equal (i.e. equal slopes in the amplification plots). When data of lower or unequal AE are analyzed with the current available models, the inferred result is much different from the actual gene expression. Upon analysis of the first results, a significant difference between the samples' AE was noticed. If the actual AE turned out to be suboptimal, meaning that the product of the PCR less than doubled every cycle, C_t -values could not be compared across different PCR runs. To compensate for these differences, we introduced a routine calculation of AE and a consecutive adjustment for the differences in AE between the samples. We compensated for the differences in AE by adjusting the C_t -values. These values will be referred to as C_t (adj).

9.3 C_t -value

The C_t is determined from a log-linear plot of the PCR signal versus the cycle number. Thus, C_t is an exponential and not a linear term. As Livak and Schmittgen propose, this is the reason why every statistical analysis of C_t should use the adjusted $2^{-\Delta\Delta C_t}$ and not the raw C_t -value [122].

The ΔC_t -value for each sample is determined by calculating the difference between the C_t value of the target gene and the C_t -value of the endogenous reference gene.

- ΔC_t (sample) = C_t target gene – C_t reference gene

Next, the $\Delta\Delta C_t$ -value for each sample is determined by subtracting the ΔC_t -value of sample A from the ΔC_t -value of sample B.

- $\Delta\Delta C_t = \Delta C_t (\text{sample A}) - \Delta C_t (\text{sample B})$

If the PCR efficiencies of the target gene and endogenous reference gene are comparable, the normalized level of target gene expression is calculated by using the formula:

- Normalized target gene expression level in sample A = $2^{-\Delta\Delta C_t}$

However, if the PCR efficiency is not the same between the target gene and endogenous reference gene, this method of quantification may lead to inaccurate estimation of gene expression levels. The error is a function of the PCR efficiency and the cycle number and can be calculated according to the formula:

- $\text{Error (\%)} = [(2^n / (1+E)^n) \times 100] - 100$

where:

E = efficiency of PCR

n = the cycle number

The $\Delta\Delta C_t$ method should only be chosen if the PCR efficiency of target gene and endogenous reference gene are the same, or if the difference in expression levels is sufficiently high to tolerate the resulting error [24, 129]. This is the reason for the introduction of the amplification efficiency adjustment tool.

9.4 Calculation of amplification efficiency

This method calculates the amplification efficiency of a single reaction, without the use of standard curves.

9.4.1 Assumption

The amplification plot has an exponential (log-linear) phase during which it can be described by

$$(1) \quad R_n = R_0 \times E^n$$

where

n = number of cycles

R_0 = fluorescence at start of exponential phase

R_n = fluorescence at cycle n

E = amplification efficiency

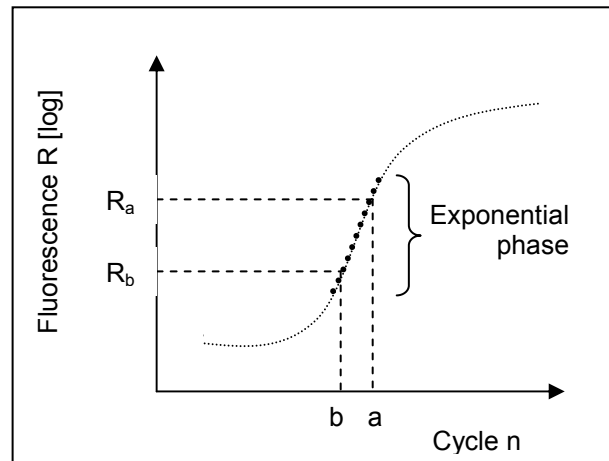


Figure 11 PCR replication cycle.

9.4.2 Method

Two points (R_a, a) and (R_b, b) on the exponential stretch of amplification plot are chosen randomly. This gives a system of two equations:

$$(2) \quad R_a = R_0 \times E^a$$

$$(3) \quad R_b = R_0 \times E^b$$

The system can be solved for the unknown E , i.e. the amplification efficiency:

$$(4) \quad R_a/R_b = R_0/R_0 \times E^a/E^b \quad (\text{dividing 2 by 3})$$

$$(5) \quad R_a/R_b = E^a/E^b$$

$$(6) \quad R_a/R_b = E^{a-b}$$

$$(7) \quad \log_k (R_a/R_b) = \log_k E^{a-b} \quad (\text{for any } k)$$

$$(8) \quad \log_k (R_a/R_b) = (a-b) \log_k E$$

$$(9) \quad [\log_k (R_a/R_b)] / (a-b) = \log_k E$$

$$(10) \quad E = k^m \quad \text{where } m = [\log_k (R_a/R_b)] / (a-b)$$

Ultimately, a total of five points on the exponential stretch of the amplification plot were chosen to deliver as exact a result as possible.

9.4.3 Adjusting C_t -values for differences in amplification efficiency

As the PCR-results still needed to be compared to the data raised through HRMAS $^1\text{HMRs}$, strict measures had to be taken to assure the comparability between all 38 PCR runs needed to test the enzymes for all tissue samples. Therefore, we opted for a general adjustment of C_t -values to make up for possible differences in AE. If amplification efficiency is sub-optimal and differs across reactions, C_t -values need to be adjusted to be truly comparable.

9.4.3.1 Assumptions

During the exponential phase of the amplification plot, the following relation holds true:

$$(1) \quad R_n = R_0 * E^n$$

where

n = number of cycles

R_0 = fluorescence at start of exponential phase

R_n = fluorescence at cycle n

E = amplification efficiency

9.4.3.2 Method

If C_t is measured during this exponential phase, it relates to the threshold fluorescence R_t as follows:

$$(2) \quad R_t = R_0 * E^{C_t}$$

If the actual $E < 2$ (i.e. if the efficiency is suboptimal and the product of the PCR less than doubles each cycle), the C_t actually measured at R_t will differ from the C_t that would have been measured were the amplification efficiency E optimal.

Optimally:

$$(3) \quad R_t = R_0 * E^{*C_t^*}$$

where

E^* = optimal amplification efficiency = 2

C_t^* = C_t adjusted to optimal amplification efficiency

The system of equations (2) and (3) can be solved for the unknown c_t^* , i.e. the adjusted c_t :

$$\begin{aligned}
 (4) \quad R_t/R_0 &= R_0/R_0 \times E^{c_t}/E^{*c_t^*} && \text{(dividing 2 by 3)} \\
 (5) \quad 1 &= E^{c_t}/E^{*c_t^*} \\
 (6) \quad E^{*c_t^*} &= E^{c_t} \\
 (7) \quad \log_2 E^{*c_t^*} &= \log_2 E^{c_t} \\
 (8) \quad c_t^* \times \log_2 E^* &= c_t \times \log_2 E \\
 (9) \quad \boxed{c_t^*} &= c_t \times \log_2 E && \text{(since } E^* = 2\text{)}
 \end{aligned}$$

To normalize to optimal amplification efficiency conditions, c_t has to be adjusted by the factor $\log_2 E$, where E is the actual amplification efficiency of the reaction. In consequence, by adjusting the slopes we imitated a perfect amplification of 2 per cycle and thus make up for amplification inefficiencies.

9.4.3.3 Note

If percentile amplification efficiency (PAE) is used instead of E , the formula for adjusting c_t to c_t^* is different, namely:

$$(10) \quad \boxed{c_t^*} = c_t \times \log_2 (\text{PAE} + 1)$$

where

$$(11) \quad E = \text{PAE} + 1$$

PAE is sometimes also defined as

$$(12) \quad E = 2^{\text{PAE}}$$

In that case, the formula for adjusting c_t is:

$$(13) \quad \boxed{c_t^*} = c_t \times \text{PAE}$$

⇒ Each of the three adjustment formulae (9), (10) and (13) uses its own definition of amplification efficiency, but all deliver the same adjusted c_t^* .

9.4.4 Amplification efficiency adjustment tool

This excel tool was designed by Florian Sturm² in order to adjust for differences in amplification efficiency. The tool refers back to the actual amplification plot of the

² A Charité co-student, member of Prof. Cheng's research team.

PCR (7000 System Sequence Detection Software BioAnalysis). For each enzyme, a common threshold within the log-linear phase of the plot for the set of triplicates is chosen. Then, two points above and two points below the threshold are randomly picked and its coordinates plugged into the amplification efficiency adjustment tool (an excel macro application). Using these four points, the tool optimizes the slope by performing a regression analysis. Picture 4 gives an impression of what the excel program looks like. The tool was used to test and adjust AE for all 38 PCR runs.

Step 1 Paste your raw data

- In the 7000 System Software, look for the loglinear stretch on each curve
- Choose the threshold at which you want the C_t to be measured
- Export the results from the 7000 System Software into a csv-file
- Choose four further points on the loglinear stretch - two above and two below the first threshold
- So, for each curve, there are five points in total - and accordingly five sheets named "Raw data"
- Copy-paste the data for all the points into this Excel file (middle point to "Raw Data (central)")

Step 2 Check your pipetting accuracy

- Give Excel the names of the samples you want to check
- Excel will automatically find the duplicates/triplicates for you
- You can adjust the criteria for excluding duplicates/triplicates
- Excel will then suggest which samples to run again

Step 3 Check the efficiency estimates

- Amplification efficiency can never be greater than 2. If it is, there must be a mistake.
- You can check the efficiencies here and review the raw data input if necessary.

Step 4 Group and normalise your samples

- You can now group your samples by up to three criteria
- Which groups you choose will depend on your experiment design
- A criterion might, for example, be "gender" with either "male" or "female" as groups
- Next, choose the genes of interest ("targets") you want to examine
- For each "target", choose the housekeeping gene ("reference") you want to use for normalisation

Step 5 Get your results

- Choose your hypothesis design and Excel will calculate the $\Delta\Delta C_t$ values for you
- For each hypothesis, it also does a significance check

Note: Instead of Steps 2 to 5, you can also just export the efficiency adjusted C_t values (eg from the sheet "Grouping&Matching") to a statistics program of your choice - and do all further analysis there.

Options

- User Mode
- Programming Mode

Picture 4 Adjustment tool instructions page.

The tool then calculates the minimum-to-maximum-stretch of the C_t -values and the standard deviation of the triplicates for every sample. According to the previously set cut-off values for both standard deviation and minimum-to-maximum span, the tool proposes re-runs for the samples that do not concur with the preset values.

As a next step, the tool calculates efficiency estimates: amplification efficiency (values from 1-2), percentile amplification efficiency 1 (PAE1) (values from 0-1; defined as $PAE1 = AE - 1$) and PAE2 (defined as $PAE2 = 2^{PAE1}$). The tool automatically displays a warning should one of the values lie outside of their defined range.

In a next step, the user can choose between a comparison of ΔC_t s between two GOIs ($\Delta\Delta C_t$) or one GOI and the housekeeping gene (ΔC_t) (calculated by subtracting

the C_t number of target sample from that of the housekeeping gene). The tool will then give raw and adjusted ΔC_t -values.

As an additional feature, the tool also lets the user test several hypotheses (see picture 5). For example, enzyme concentration in grade 2 may be compared to concentration in grade 3. The tool will then deliver the $\Delta\Delta C_t$, $2^{-\Delta\Delta C_t}$ and the p-value for this particular hypothesis.

Use of the adjustment tool explains the existence of two values in the JMP-file: raw and adjusted data. Throughout the analysis of the data, only adjusted values were used.

Hypothesis design				Results						
	Enzyme	Tumor Grad	Use sample	n	$\Delta\Delta C_t$		$2^{-\Delta\Delta C_t}$		p-value	
					raw	adjusted	raw	adjusted	raw	adjusted
1	Compare... CHKa	3	yes	9	0,02	0,44	0,986	0,736	0,974	0,546
	with...	CHKa	2	yes	9					
2	Compare... CHKb	3	yes	9	0,85	1,18	0,554	0,440	0,045	0,033
	with...	CHKb	2	yes	9					
3	Compare... CHKb	2	no	1	-0,70	-0,95	1,619	1,932		
	with...	CHKa	2	no	1					
4	Compare... CHKb	2-3	yes	2	-0,88	-0,08	1,845	1,056	0,456	0,965
	with...	CHKa	2-3	yes	2					

Picture 5 Adjustment tool hypothesis page.

The page allows a juxtaposition of two enzymes in different tumour grade tissue and returns $\Delta\Delta C_t$ and $2^{-\Delta\Delta C_t}$ and their corresponding p-values.

9.4.4.1 Accuracy check

The accuracy check was introduced as a measure of internal quality control within the group of triplicates. To minimize potential inaccuracies in pipetting, samples as well as positive and negative controls were run as triplicates. Two sets of accuracy controls were introduced: standard deviation and absolute spread of C_t , whereas the threshold for a re-run was 0,3 for the standard deviation and 0,5 for the absolute C_t spread.

9.5 Use of $\Delta\Delta C_t$ versus use of $2^{-\Delta\Delta C_t}$

ΔC_t is defined as the cycle difference between a specific gene of interest with the household gene within one PCR run. It is an absolute quantification. Absolute quantification determines the input copy number of the transcript of interest, usually by relating the PCR signal to a standard curve. In some situations, it may be unnecessary to determine the absolute transcript copy number and reporting the relative change in gene expression will suffice.

$\Delta\Delta C_t$ is the number of cycle differences between two genes of interest.

$2^{-\Delta\Delta C_t}$ is an expression of the fold difference, a relative quantification method, defining the change in expression of the gene of interest relative to some reference group, such as an untreated control or another sample. For example, a $2^{-\Delta\Delta C_t}$ of 2 for gene x between tissue a and tissue b would indicate a difference of gene concentration of 2. According to literature, the $2^{-\Delta\Delta C_t}$ -method may be used to calculate relative changes in gene expression determined from real-time quantitative PCR experiments [122, 130, 131].

According to their definition, $\Delta\Delta C_t$ - and $2^{-\Delta\Delta C_t}$ -values should be comparable, being a different expression of the same fact. However, they are not equal in terms of their significance [128]. This can be observed by comparing analyses using $\Delta\Delta C_t$ with the same ones using $2^{-\Delta\Delta C_t}$ -values: the latter constantly display higher p-values. Although this difference in significance has not been explained so far by the scientific community, literature suggests the use of the $2^{-\Delta\Delta C_t}$ -values: the endpoint of real-time PCR analysis is the threshold cycle or C_t . The C_t is determined from a log-linear plot of the PCR signal versus the cycle number. Thus, any statistical presentation using the raw C_t -values should be avoided. For a demonstration of this effect and the different p-values, see Results: ChoK β in grade 2 and 3.

When looking at the results, one has to keep in mind the contrarian assertion of the two values: whereas a high cycle difference $\Delta\Delta C_t$ suggests a relatively low concentration of the measured gene (as opposed to the housekeeping gene), a high $2^{-\Delta\Delta C_t}$ -value a high fold-difference, meaning that the gene with the higher $2^{-\Delta\Delta C_t}$ -value also is higher concentrated than one with a lower one.

10 Results

For the samples ultimately analyzed, population sizes were $n=10$ for grade 2 and $n=9$ for grade 3 samples for ChoK.

Enzyme	N	
	Grade II	Grade III
ChoK	10	9
PLD	7	7
PCYT1		
SLC22A		

Table 18 Sample overview.

For the enzymes included in the study at a later stage, some samples could not be analysed for lack of sample material, and therefore have a lower n (see table 18).

10.1 Exclusion of samples

At the stage of data evaluation and statistic analysis, some PCR-runs on specific enzymes in individual samples had to be excluded from further analysis for several reasons:

- 1) insufficient enzyme concentration: concentration of the enzyme was so small that no correlation with the housekeeping gene was possible
- 2) insufficient pipetting accuracy: either the absolute minimum-to-maximum span of $C_t > 0,5$ or the standard deviation was $> 0,3$
- 3) $> 0,5$ cycle difference between triplicates
- 4) amplification aberrations: no linear amplification stretch on plot could be identified.

Table 19 provides an overview of the samples which were excluded and the reasons leading up to the decision.

Sample number	Enzyme	Reason for exclusion
1	SLC22A2	1
3	SLC22A1	1;3
3	SLC22A2	1
4	SLC22A1	1;3
4	SLC22A2	2;3
5	PCYT1B – 1 st	4
5	SLC22A1	1
5	SLC22A2	1
7	SLC22A2 – 2 nd , 3 rd	1
20	SLC22A1 – 3 rd	1

Table 19 Excluded enzymes.

(1st-3rd indicates the triplicate number), by sample number and reason for exclusion.

There are several possible explanations for the problems leading to data exclusion:

- possibly the concentration of enzymes in the tissue was generally too low for accurate measurement
- q-rt-PCR is not sensitive enough for measurement of apparently very low concentrations of transporter enzymes.

Even when running the primers on commercial RNA, concentration of SLC22A and PCYT1 were very low. The lower the concentration of the enzyme measured with PCR, the higher the standard deviation of the triplicates. Therefore, very low concentrated enzymes were more likely to fail the required standard deviation threshold.

For the second set of enzymes (PCYT1A/B, SLC22A1/2, PLD1/2), five samples (samples 19, 23, 24, 25 and 26) had to be excluded altogether for lack of sufficient cDNA substrate. Thus, sample size for PCYT1A/B, SLC22A1/2 and PLD1/2 is n=14 (grade 2: n=7; grade 3: n=7)

10.2 Statistic procedures

10.2.1 Handling of outliers

Based on quantitative analysis and the JMP box plot function, several outliers were identified in the PCR analysis of the enzymes. Outliers were defined as either $3 \times \text{IQR}$ or more above the third quartile or $3 \times \text{IQR}$ or more below the first quartile. Table 20 gives an overview of all outliers.

Enzyme	Grade	Outlier
ChoK α	II	11
	III	-
ChoK β	II	11
	III	-
PLD1	II	22
	III	12
PLD2	II	4
	III	5
PCYT1A	II	10
	III	12
PCYT1B	II	4
	III	12
SLC22A1	II	4
	III	12
SLC22A2	II	-
	III	12

Table 20 Summary of outliers.

Analysis of the PCR-results was done with and without the identified outliers. The comparison of both results – inclusion and exclusion of outliers – was done because no plausible reason within the process of the study was found that could have explained the extreme values. Good statistical practice demands the inclusion of extreme values if no scientific explanation for their appearance and thus a reason for their exclusion can be found. However, the various and multiple chances for errors in scientific laboratory work are acknowledged and also the fact that outliers are often simply bad data points. Therefore, both analyses with and without outliers are provided and subsequently discussed.

10.2.2 Use of ANOVA

Statistical analysis of the data gathered includes ANOVA, correlation coefficients, p-values and confidence intervals. Most of the comparable studies completed on the topic of metabolomics in MRS use ANOVA for their statistical analysis. Sample size of the study at hand is $n < 20$, increasing the inherent danger of overlooking certain effects in the statistical analysis. Except for ChoK α in grade 3 and ChoK β in grade 3, data are not normally distributed. Good statistical practice demands a Mann-Whitney-U test for this kind of data. It allows for nonparametric data analysis. This test was run on the statistically significant findings. The Mann-Whitney-U test is the most powerful rank test for errors with logistic distributions. Subsequently, the Mann-

Whitney-U test was conducted on onevariate statistically significant findings to validate the findings. None of the statistically insignificant findings using ANOVA turned significant when applying the Mann-Whitney-U test.

10.2.3 Statistical power

(1- α) was set at 0,95. A p-value of < 0,05 was considered significant.

10.3 Choline kinase

10.3.1 PCR results without MRS-correlation

The following table (table 21) summarizes our findings from PCR without correlation to MRS data. The table reads as follows: For ChoK α , there is a 0,736-fold difference between tumour grades 2 and 3. The corresponding p-value is 0,546.

Enzyme	Grade	Grade	$2^{-\Delta\Delta Ct}$ (adj.)	p-value (adj.)
ChoK α	2	3	0,736	0,546
ChoK β	2	3	0,440	0,033
ChoK α vs. β	2	2	0,894	0,753
ChoK α vs. β	3	3	1,495	0,431

Table 21 Concentration differences between enzymes and grades.

PCR results without correlation with MRS data (taken from the Excel tool for testing of hypotheses). Outliers included.

As can be seen in the table 21, the only significant finding of the ChoK-PCR-results without MRS-correlation is a 0,44-fold decrease in ChoK β in grade 3 compared to grade 2 with a p-value of 0,033.

None of the p-values for any of the ChoK α correlations are significant ($p < 0,05$).

ChoK α concentration ($2^{-\Delta Ct}$ (adj)) decreases by 1,66E-04 (app. 96,2 %) in grade 3 as opposed to grade 2, whereas ChoK β decreases by 3,25E-04 (app. 99 %) (see table 22). In grade 2, ChoK β is lower concentrated than ChoK α , but higher in grade 3.

	Difference $2^{-\Delta Ct}$ (adj) grade 3 to grade 2	
	ChoK α	ChoK β
Absolute	0,000166	0,00032539
Relative	96,2 %	99 %

Table 22 Concentration differences of ChoK α and ChoK β between grades 2 and 3. Outliers included.

In general, we found the level of ChoK to decrease with increased grading (see fig. 11). The measurements regarding ChoK α are not statistically significant with a p-value of 0,85, in contrast to ChoK β .

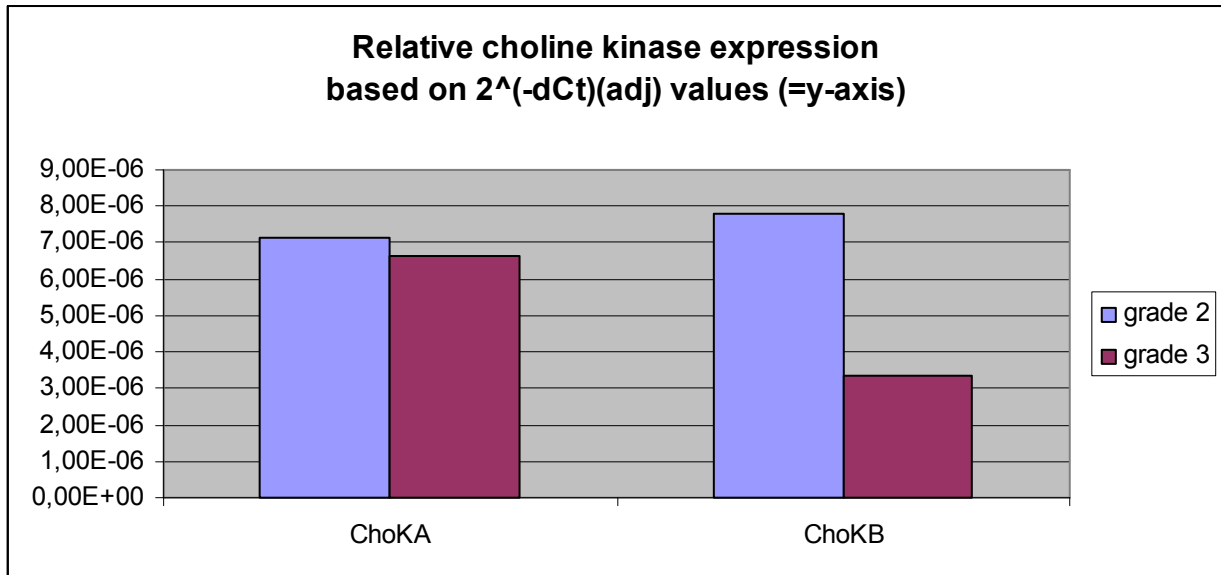
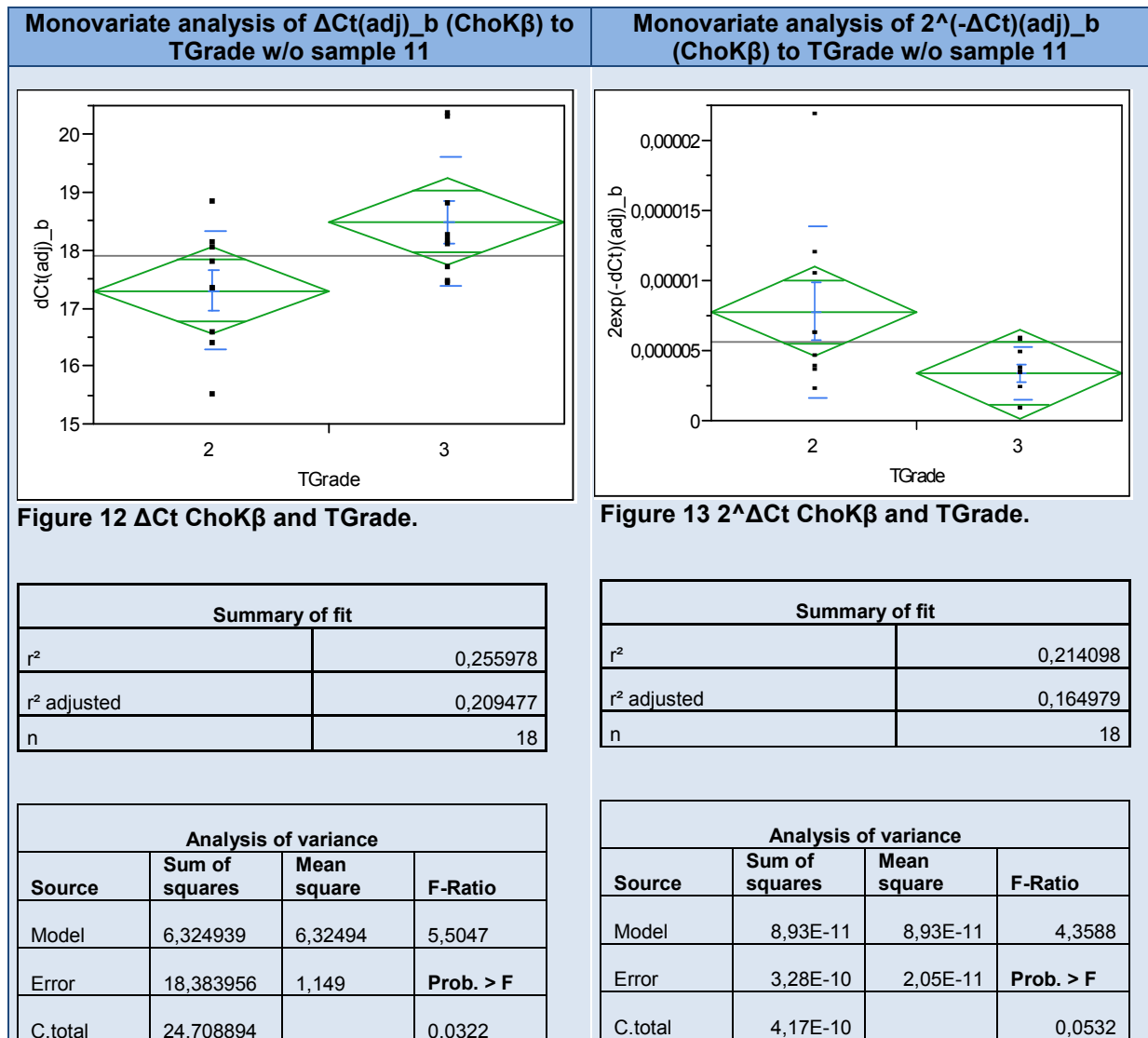


Figure 11 Comparison of $2^{-\Delta C_t(\text{adj})}$ of ChoK α and ChoK β in grades 2 and 3. Grade 2 n=9; grade 3 n=9.

10.3.1.1 Choline kinase β in grade 2 and 3

Figures 12 and 13 illustrate the concentration of ChoK β in both grades. The differences in the graphic illustration are a result of the differing underlying equations of ΔC_t and $2^{-\Delta C_t}$.



The comparison of figure 12 and 13 illustrates the difference in significance between the use of ΔC_t and $2^{-\Delta C_t}$. Here, the p-value mounts to 0,0532 from 0,0322 when $2^{-\Delta C_t}$ is used instead of ΔC_t . For both graphs, sample 11 was excluded, since it was identified as an outlier. Both figures illustrate the decrease of ChoK β in grade 3 as opposed to grade 2 with a significant p-value of 0,0532.

When looking at ChoK β expression levels and tumour grades, concentration of ChoK β is higher in grade 2 than in grade 3. The average ΔC_t (adj) ($2^{-\Delta C_t}$ (adj)) of ChoK β in grade 2 is 16,404 (3,28E-04) as opposed to 18,49 (3,34E-06) in grade 3 (n=18, without outlier sample 11).

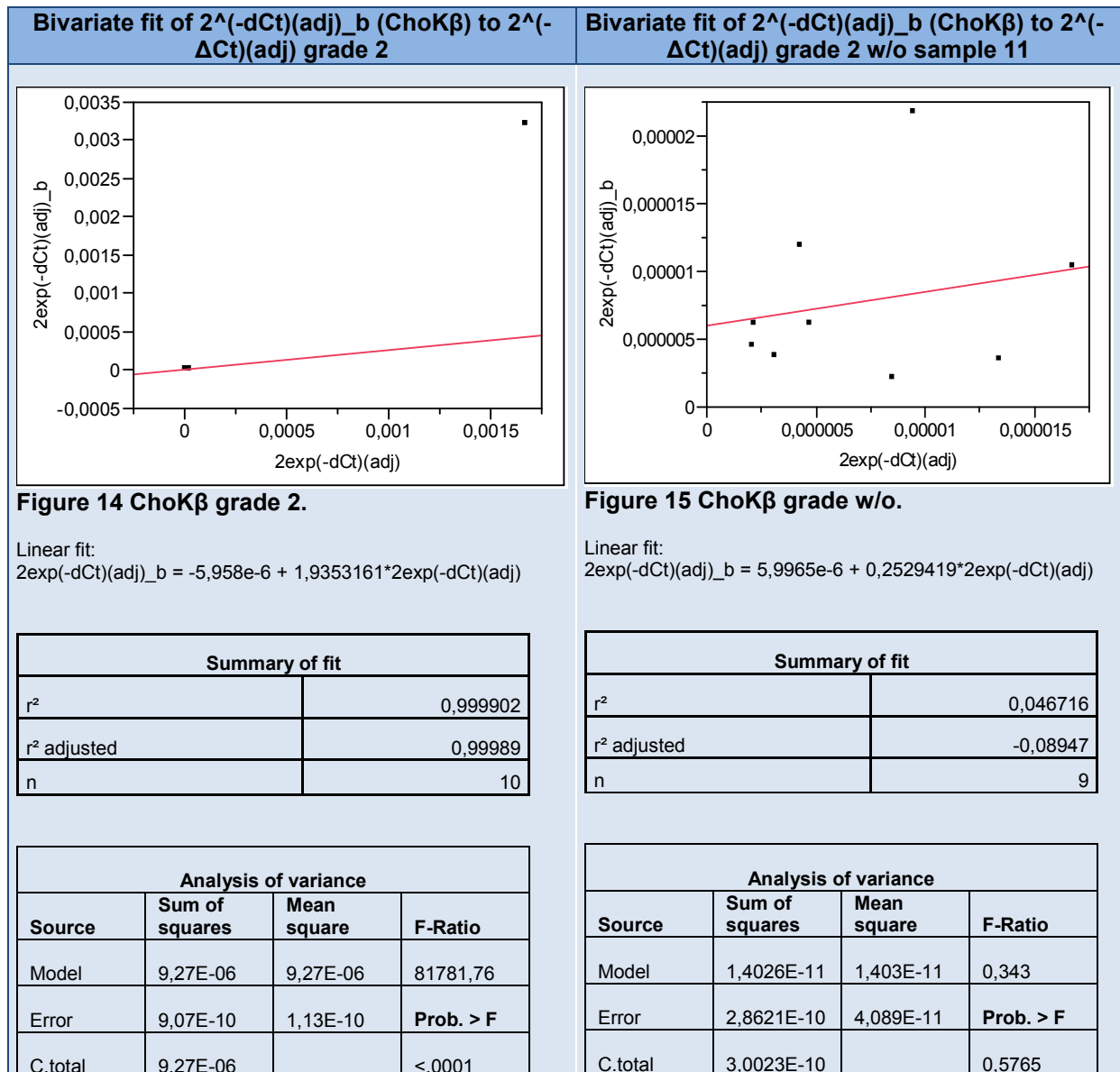
Mann-Whitney-U test: TGrade and 2 [^] (-ΔCt)(adj)_b (ChoKβ)				
Mann-Whitney-U (rank sums)				
Level	Count	Score sum	Score-mean	(Mean/mean0)/Std.0
2	9	109,000	12,1111	2,032
3	9	62,000	6,8889	-2,032
2 sample-test, normal-approximation				
S	Z	Prob > Z 		
62	-2,03200	0,0422*		
1-way test, chi-square-approximation				
Chi²	DF	Prob.>Chi²		
4,3105	1	0,0379*		

Table 23 Mann-Whitney-U test: TGrade and ChoKβ.

At p-value = 0,038, this correlation is also statistically significant when analyzed using the Mann-Whitney-U test.

10.3.1.2 Comparison of ChoKα and ChoKβ in grade 2

Figures 14 and 15 compare ChoKα and ChoKβ in grade 2. The apparent correlation shown in fig. 4 (left box) is solely dependent on sample 11, which is an outlier with more than seven standard deviations to the mean ΔC_t -values of both ChoKα and ChoKβ. (ΔC_t (adj) mean of both ChoKα and β: 16,52; ChoKα 16,65/ChoKβ 16,4). Including sample 11, p is < 0,001. With the outlier removed, the p-value rises to p=0,5765.



With the outlier removed, no significant correlation can be found between the concentration of ChoK α and ChoK β in grade 2 tissue.

10.3.1.3 Comparison of ChoK α and ChoK β in grade 3

Figure 16 shows ChoK α and ChoK β in grade 3. It depicts an apparent correlation between the two isoforms. The apparent correlation of $r^2=0,39$ and a p-value of $p=0,07$ is not significant. As there are no outliers in grade 3 for either isoform, no second plot is needed.

Bivariate fit of $2^{(-\Delta Ct)(adj)_b}$ (ChoK β) to $2^{(-\Delta Ct)(adj)}$ (ChoK α) grade 3

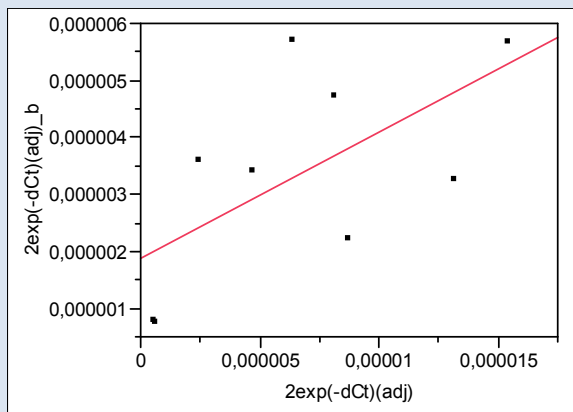


Figure 16 ChoK β and ChoK α .

Linear fit:

$$2\exp(-dCt)(adj)_b = 1,8706e-6 + 0,2216841 * 2\exp(-dCt)(adj)$$

Summary of fit	
r^2	0,394782
r^2 adjusted	0,308322
n	9

Analysis of variance			
Source	Sum of squares	Mean square	F-Ratio
Model	1,08E-11	1,09E-11	4,5661
Error	1,66E-11	2,38E-12	Prob. > F
C.total	2,75E-11		0,07

10.3.1.4 Additional potential enzyme correlations

All other possible comparisons of interest between different enzymes analysed in the PCR were insignificant according to their p-values.

10.3.2 PCR results in correlation to MRS data

In all PCR/MRS correlations for ChoK α and β in grade 2, sample 11 was excluded because of its high standard deviation and therefore biasing outlier position.

10.3.2.1 (PC+GPC)/Choline and choline kinase

Due to limitations of the analysis of the spectra, an individual measurement of PC concentration is not possible. However, PC can be analysed as a compound figure paired with GPC in relation to total choline concentration.

10.3.2.2 (PC+GPC)/Choline in relation to ChoK α

There is a negative correlation between ChoK α and the (PC+GPC)/choline ratio ($p=0,032$) in both grades (fig. 17). Thus, an increase of ChoK α goes along with a decrease in (PC+GPC)/choline concentration.

Inclusion of both ChoK β into the calculation leads to a decrease in the correlation coefficient r^2 and also a decrease of the p-value (fig. 18).

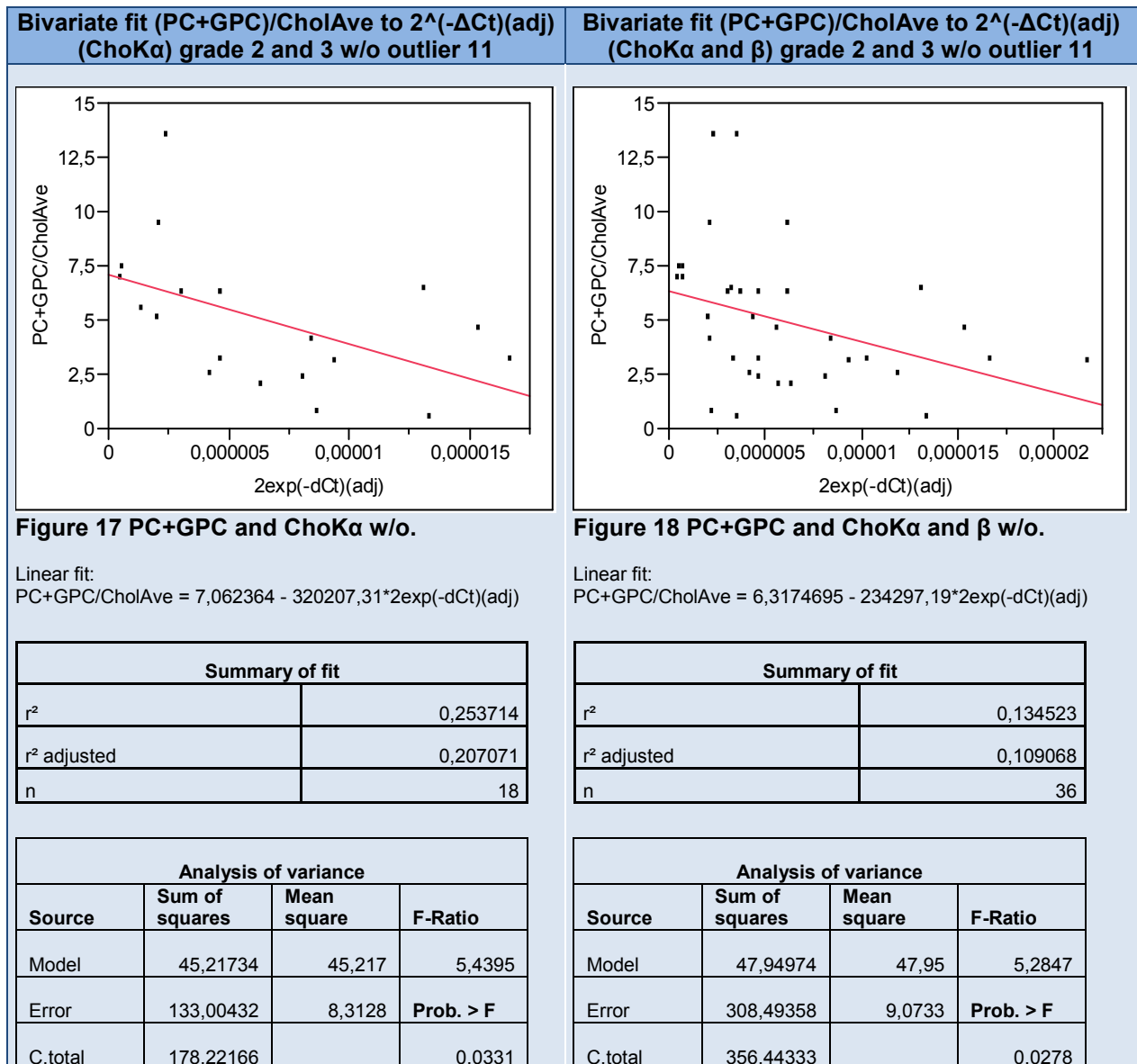


Fig.17 shows the correlation of ChoK α to the ratio of (PC+GPC)/CholAve in grade 2 and 3. The negative correlation is statistically significant with a p-value=0,0331. 25 % of the fall in (PC+GPC)/CholAve can be explained by the decrease in ChoK α concentration. Once ChoK β is included, statistical power increases with a rise of the p-value to 0,0278, and the correlation coefficient r^2 falls to appr. 13 % (fig. 18). There is a statistically relevant negative correlation between PC+GPC levels and ChoK α - and β -concentration over both grades.

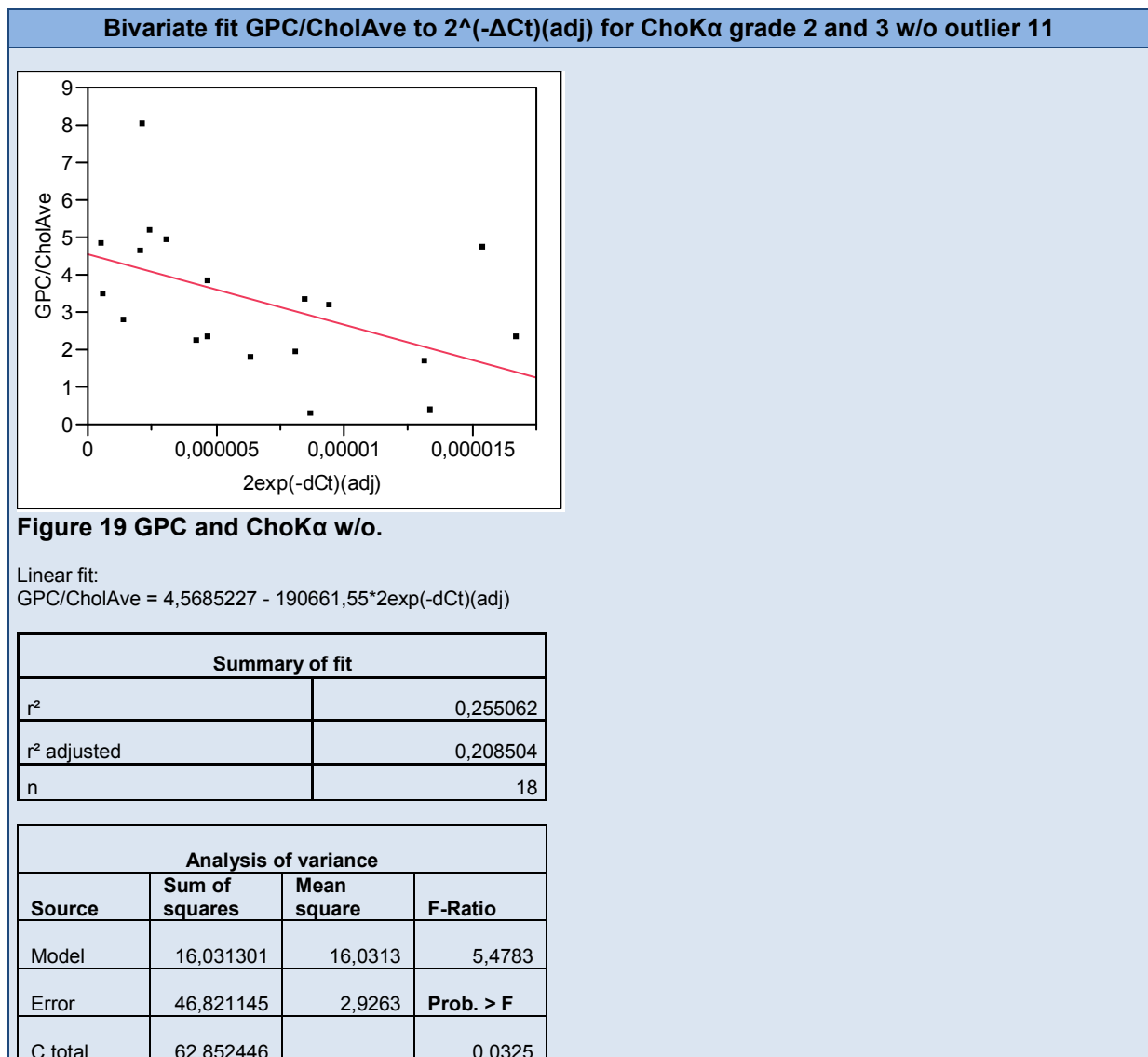
10.3.2.3 (PC+GPC)/Choline in relation to ChoK β

Individual correlations of (PC+GPC)/Choline levels with ChoK β led to non-significant results.

10.3.2.4 GPC and choline kinase

In contrast to PC, GPC can be accurately distinguished within the MR spectrum, at approximately 3,22 ppm close to the choline peak at appr. 3,2 ppm (a sample spectrum can be found in the appendix). Fig. 19 looks at GPC in relation to ChoK α levels in grade 2 and 3.

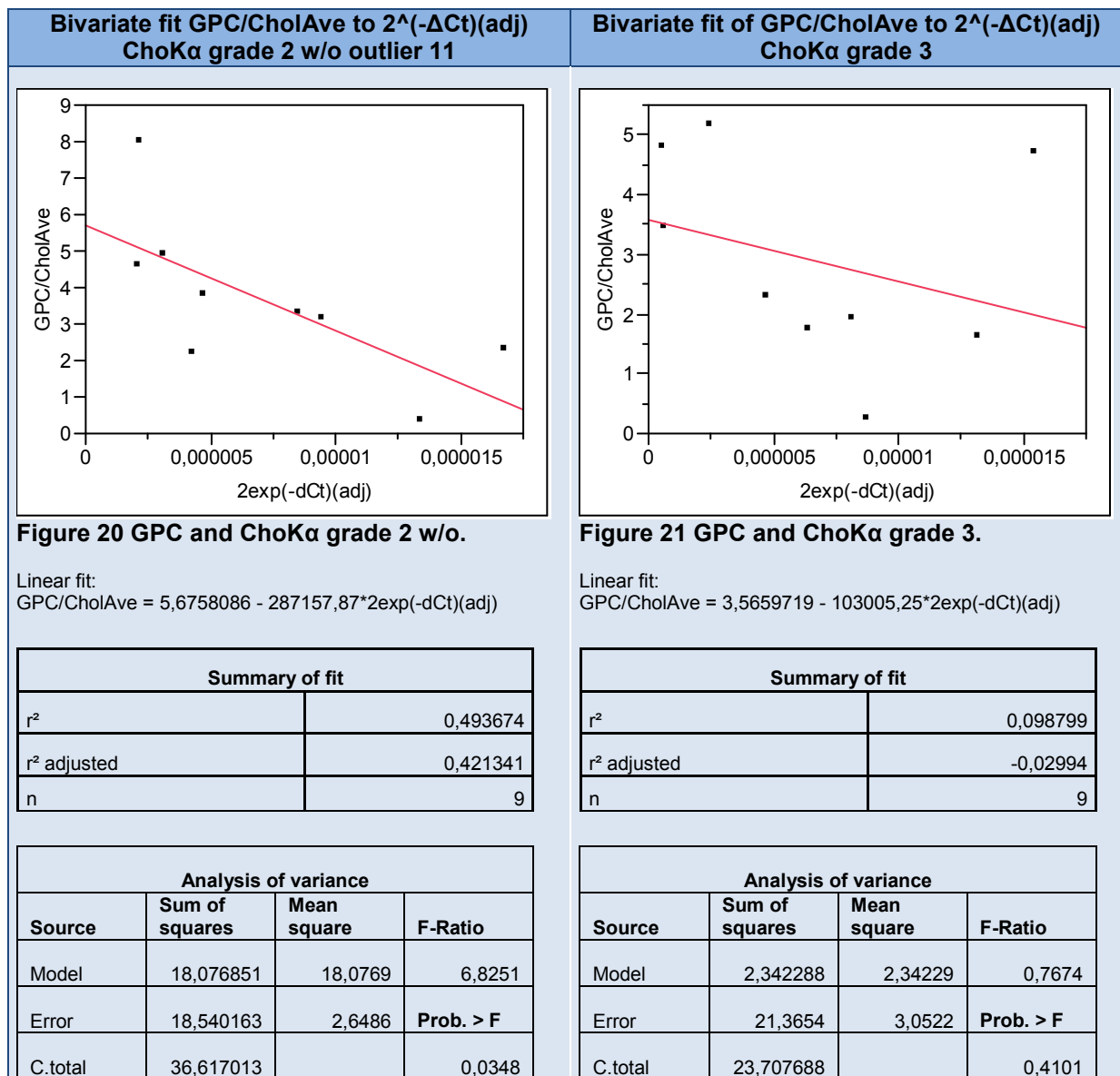
Fig. 19 describes a negative correlation between ChoK α and GPC. The coefficient of determination is $r^2 = 0,26$ with a p-value of 0,033. Thus, only 26 % of the variation of GPC can be explained by linear regression with ChoK α levels.



The correlation that can be observed for the combined grades 2 and 3 in general (fig. 19) also holds true for individual analysis of the grades (fig. 20 and 21). A negative

correlation between GPC levels and ChoK α can be observed in grade 2 (fig. 20). With a coefficient of determination of nearly 50 % ($r^2 = 0,49$) and a p-value of 0,034, this appears to be a strong correlation.

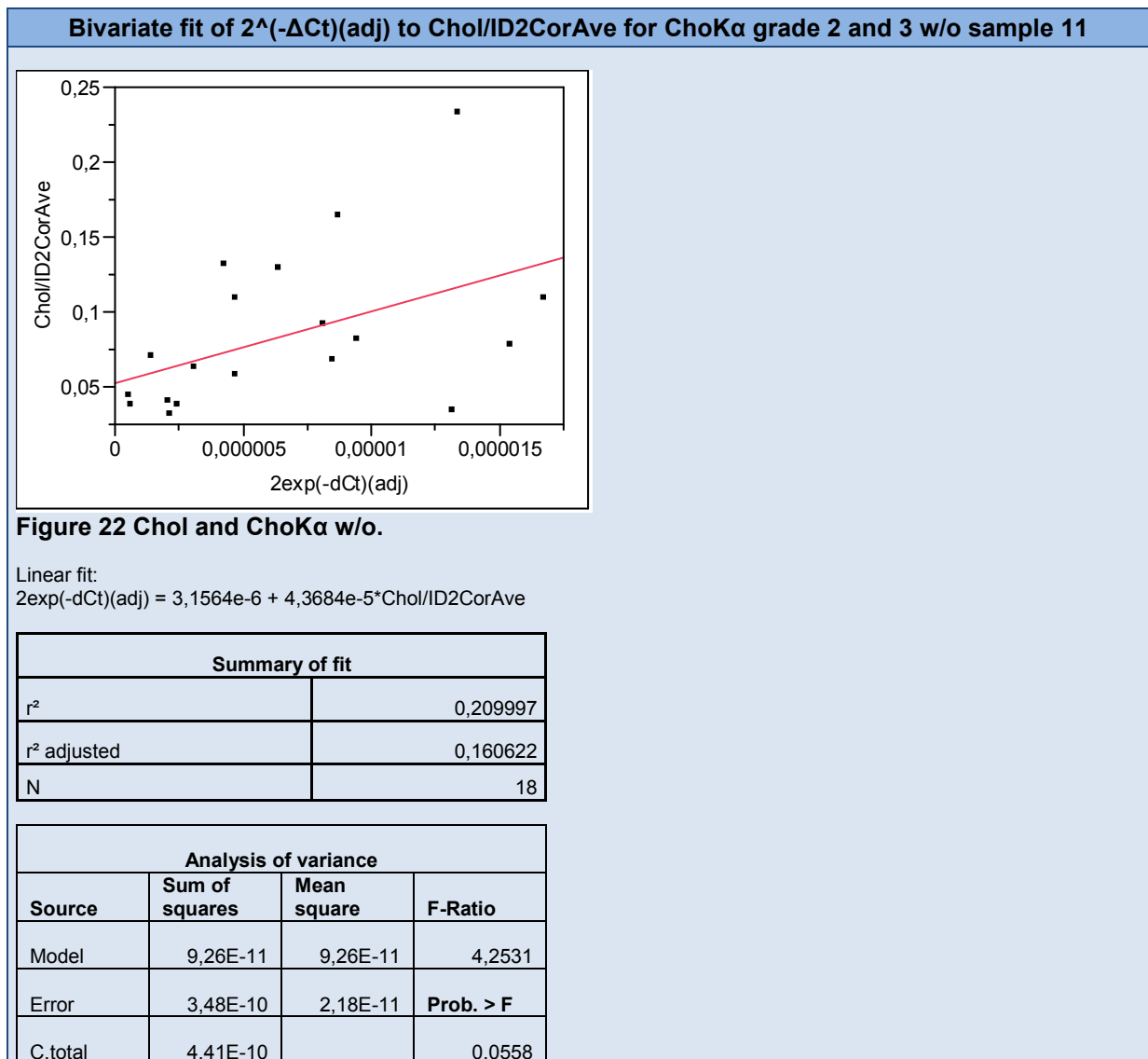
When looked at individually in grade 3, negative correlation between GPC and ChoK α appears to be only weak and with a non-significant p-value of 0,4 (fig. 21).



GPC/choline concentration in correlation to ChoK β is statistically insignificant for both grades.

10.3.2.5 Total choline and choline kinase

As depicted in fig. 22, there is a significant positive correlation between total choline levels and ChoK α concentration in grade 2 and 3. The correlation coefficient is $r^2=0,21$ and $p=0,056$ (which – strictly speaking – does not meet requirements for statistical significance).



Taken by itself, the p-value for choline concentration in grade 2 and ChoK α is statistically insignificant with $p=0,07$ and for grade 3 of only $p=0,54$. Correlations between choline concentration and ChoK β for combined grades 2 and 3 display a p-value =0,6712 and are therefore insignificant.

Based on the studies we had done so far, we were not able to fully explain the nature of and reason for the positive correlation of choline levels and ChoK α -concentration, negative correlation of ChoK β and TGrade, nor the negative correlations of PC+GPC

and GPC and ChoK α -concentration. Consequently, we decided to measure additional enzymes of the Kennedy cycle in search of additional changes in enzymes also participating in the metabolism of choline compounds. Due to lack of cDNA for certain samples, additional enzymes could only be measured in 14 out of the original 19 samples.

10.4 Phospholipase D

10.4.1 PCR results without MRS-correlation

PCR results for phospholipase D showed a correlation between increased tumour grade and concentration of both PLD 1 and 2.

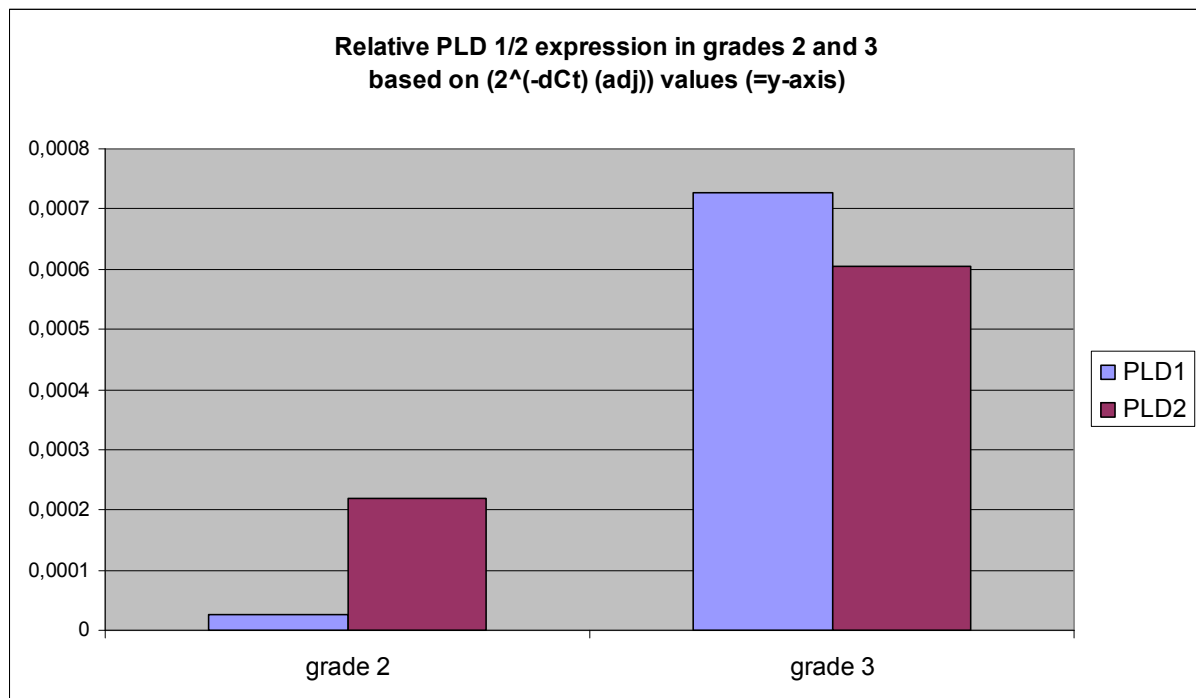
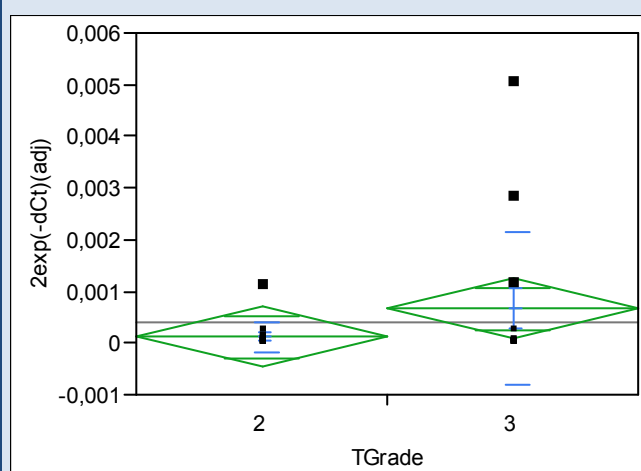


Figure 23 PLD 1 and 2; $2^{-\Delta Ct}$ (adj) in grades 2 and 3. Grade 2 n=7, grade 3 n=7.

As illustrated in fig. 23, both phospholipases D 1 and 2 increase with progressive tumour grade. PLD1 rises 27-fold, PLD2 rises to the 2,7-fold concentration. In absolute terms, PLD2 is higher concentrated in grade 2, but PLD1, undergoing a 27-fold increase in between grades, is higher concentrated in grade 3. The absolute concentration of both PLD1 and 2 is higher in grade 3.

Monovariate analysis of $2^{(-\Delta Ct)}(\text{adj})$ to TGrade; PLD1 and 2 in grades 2 and 3 w/o four outliers

Figure 24 PLD and TGrade w/o.

Summary of fit	
r^2	0,065849
r^2 adjusted	0,02992
n	28

Analysis of variance			
Source	Sum of squares	Mean square	F-Ratio
Model	0,00000206	2,06E-06	1,8328
Error	0,00002924	1,12E-06	Prob. > F
C.total	0,0000313		0,1875

The statistical analysis shows that there is no significant correlation between the rise in PLD1 and 2 and the histological grade, as indicated by the p-value=0,19 (see fig. 24).

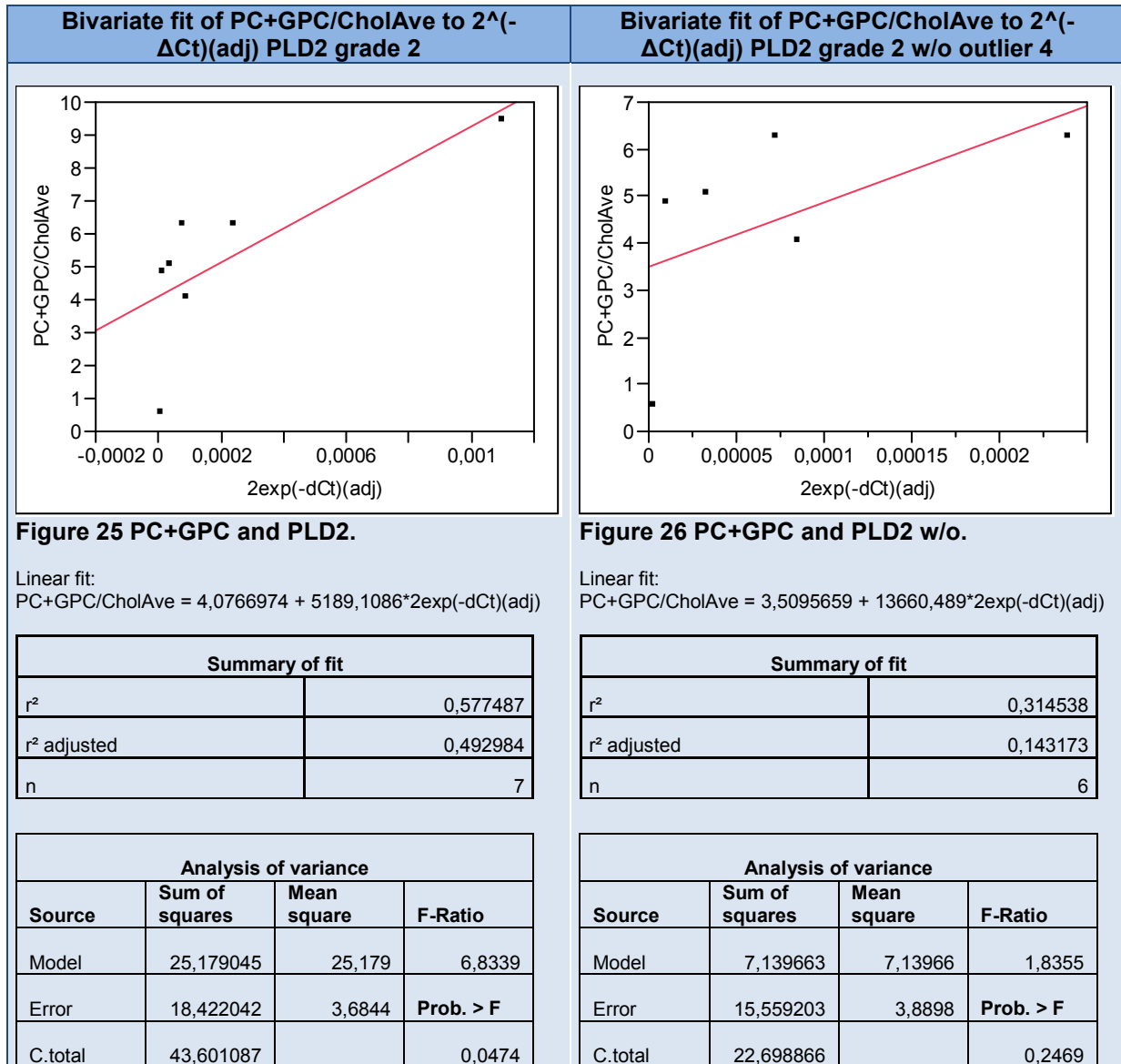
10.4.2 PCR results for PLD with correlation to MRS data

10.4.2.1 PLD1 and choline levels

For PLD1, we found no significant correlation between choline levels and the enzyme concentration. Graphic illustration suggests a negative correlation between the two variables, which lacks significance (p-value=0,61 in grade 2; p=0,46 in grade 3).

No correlation whatsoever can be described for PLD1 and the (PC+GPC)/choline or GPC/choline concentration in neither one of the grades.

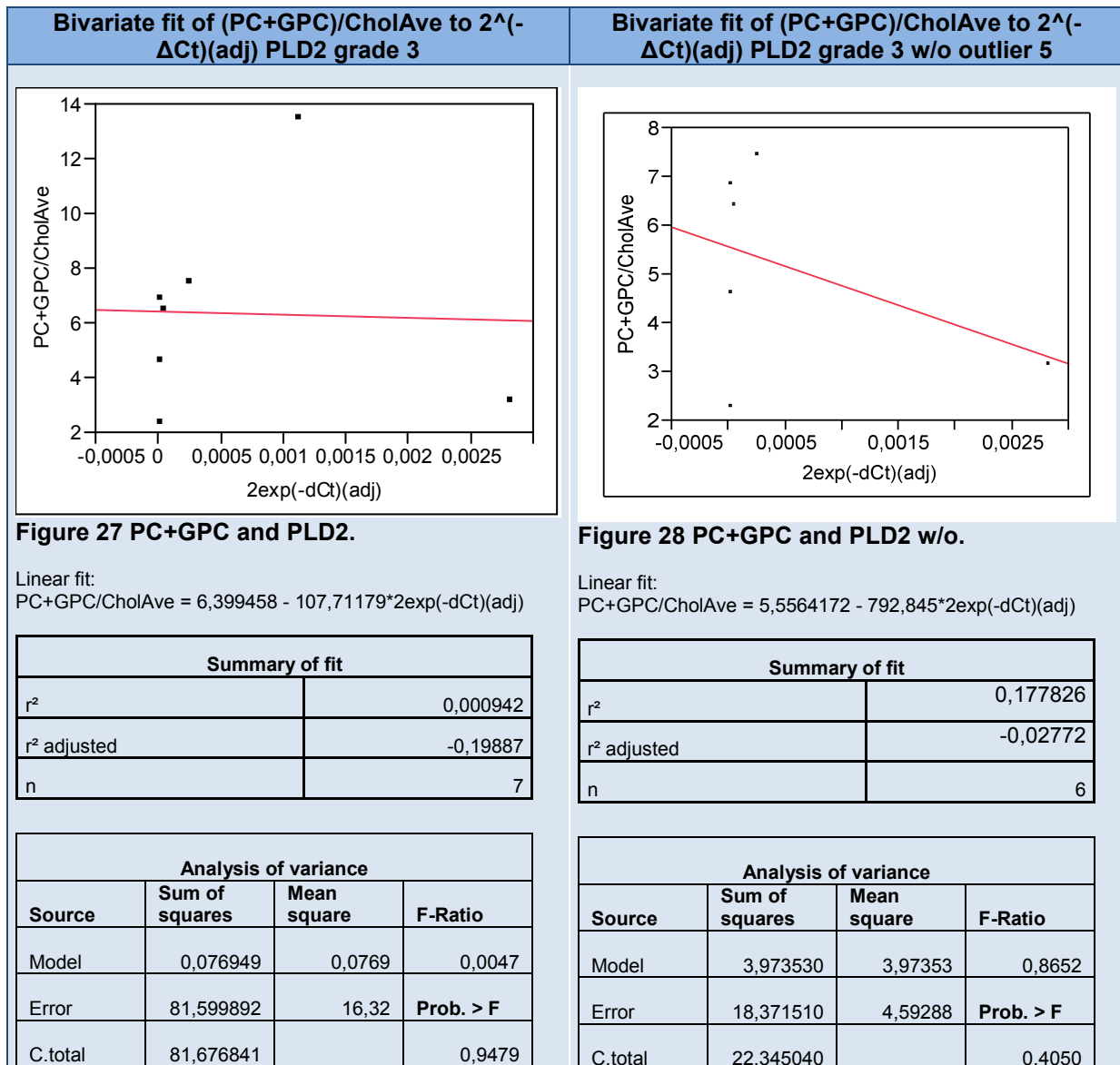
10.4.2.2 PLD2 and (PC+GPC)/choline



In grade 2, (PC+GPC)/Choline and PLD2 are positively correlated with a p-value of 0,0474 (fig. 25). The higher the PLD2 concentration, the higher the (PC+GPC)/Choline ratio. Here, appr. 58 % of the increase in PC+GPC concentration can be explained by the increase in PLD2.

Without outlier (sample 4), the p-value rises to 0,25 (fig. 26).

This correlation does not hold true for grade 3 (see fig. 27), both with and without outlier 5 (figg. 27 and 28).



In general, PLD2 increases with tumour grade: its concentration is 2,7-fold higher in grade 3 than in grade 2.

10.4.2.3 PLD1/2 over both grades

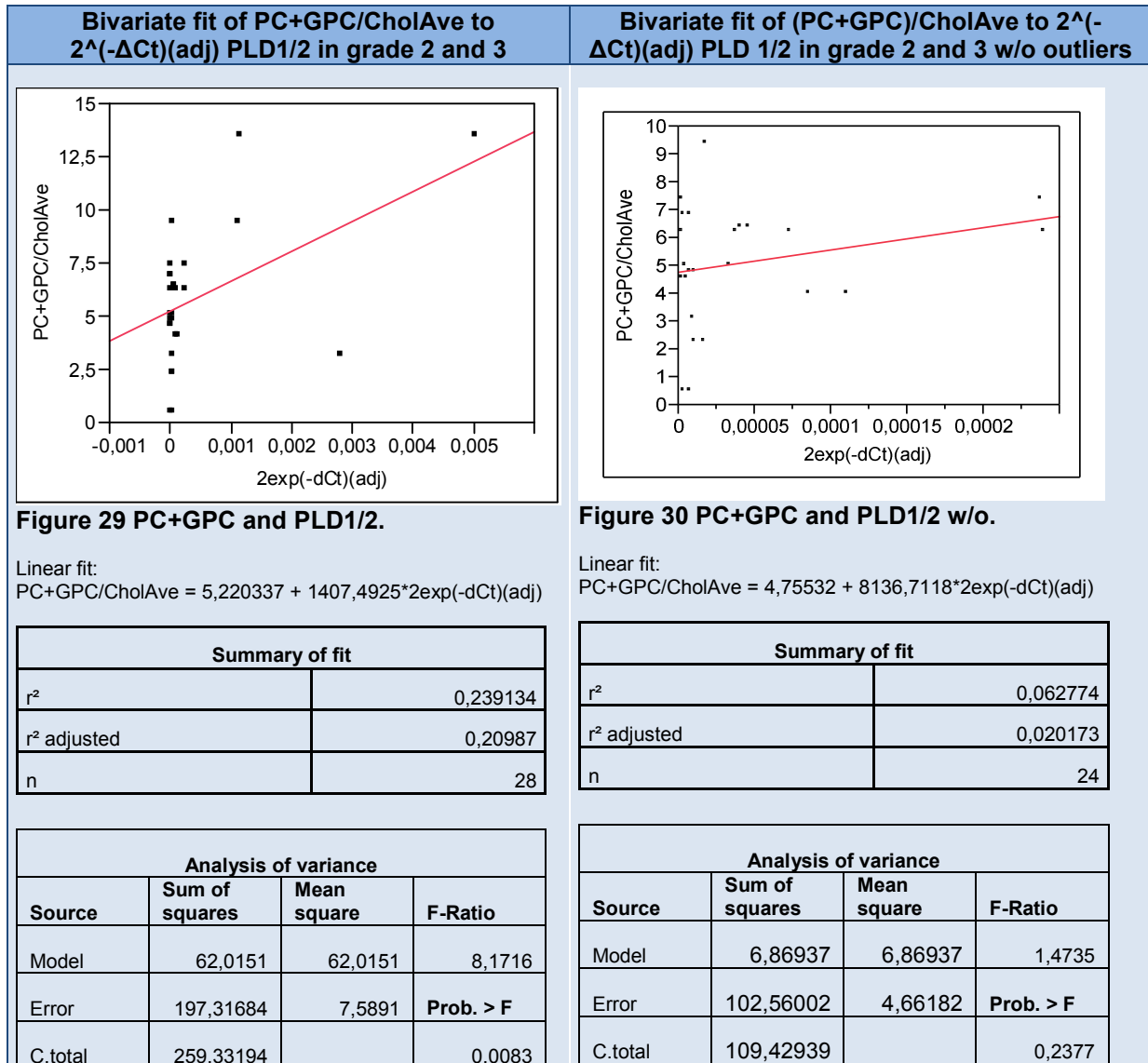


Fig. 29 shows PLD 1 and 2 in grades 2 and 3 in correlation with (PC+GPC)/choline. There is an apparent correlation between the concentration of both PLD isoforms and the PC+GPC level. This correlation relies to a great extent on the sample in the upper right hand corner (sample 12) and three other, in comparison to the rest relatively higher concentrated samples (samples 4, 5 and 22). With the outliers removed, the p-value rises from 0,0083 to 0,2377 (see fig. 30).

10.5 PCYT1

10.5.1 PCR results without MRS-correlation

Phosphocholine cytidyltransferase (PCYT1) has been repeatedly assumed to be the rate limiting step of the Kennedy cycle. In our study, both isoforms A and B displayed an increase in concentration with higher tumour grade.

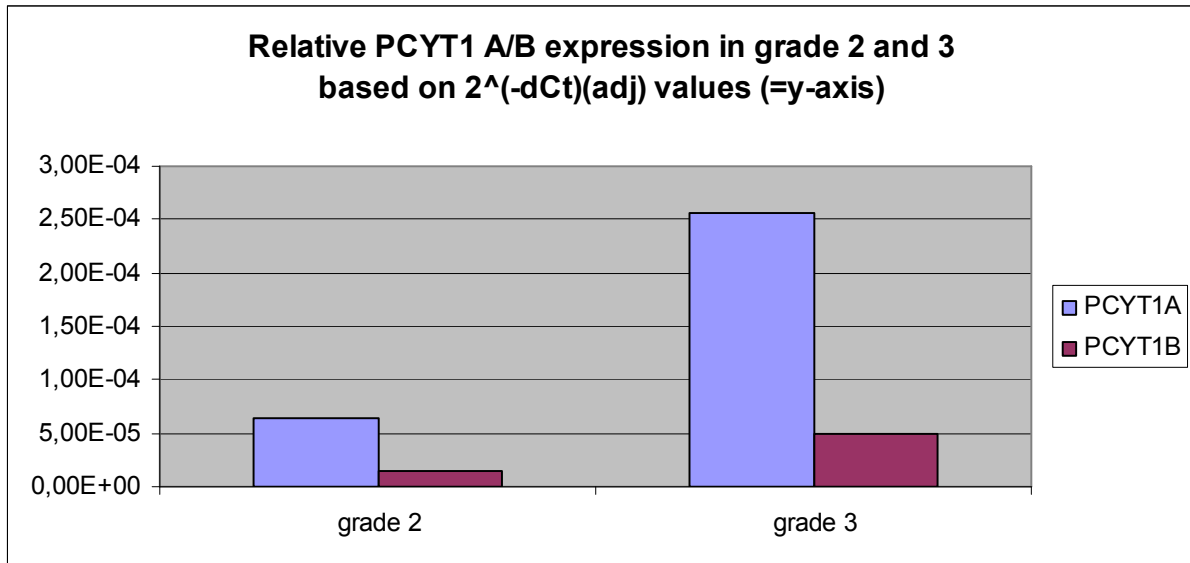
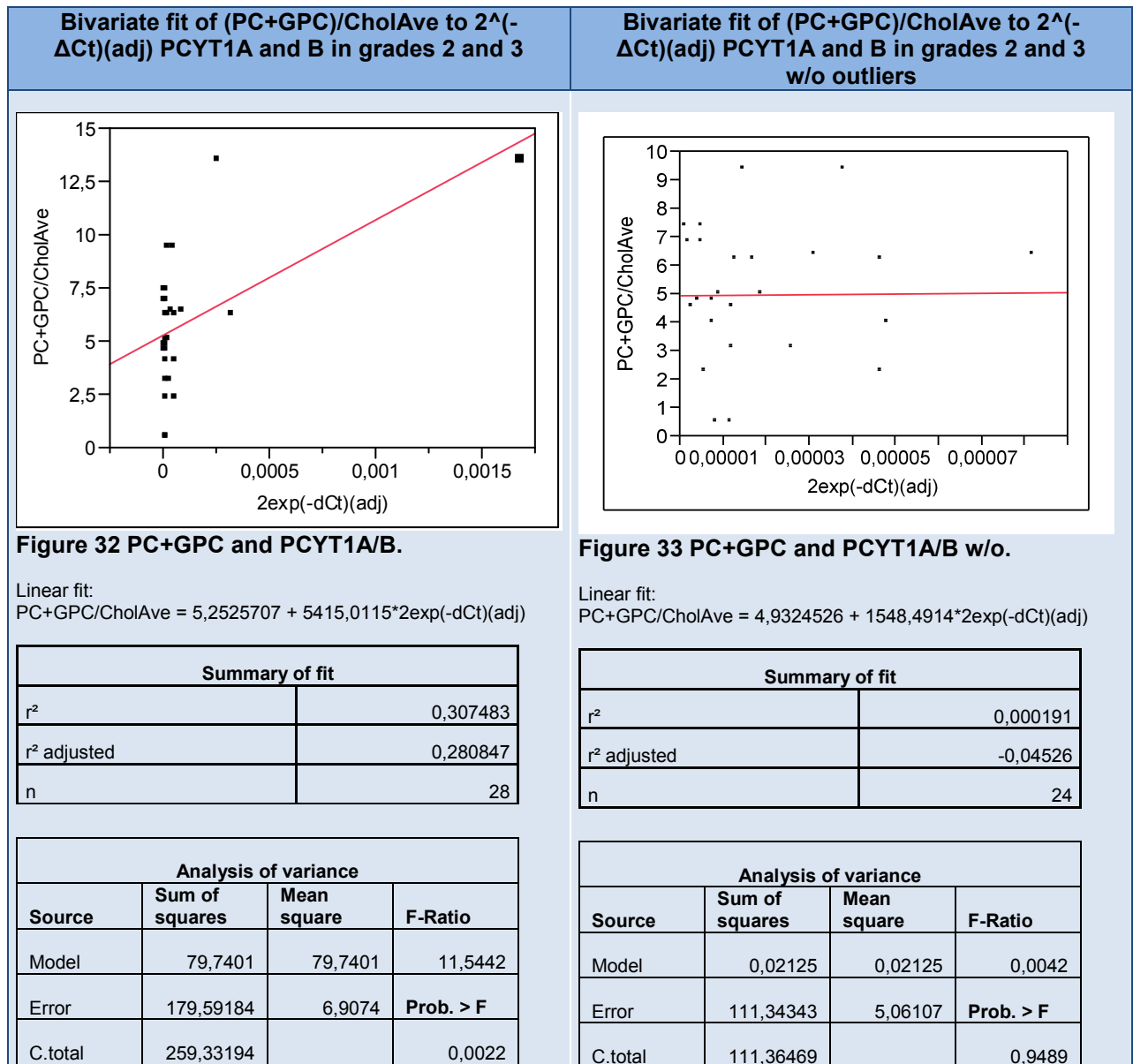


Figure 31 PCYT1A/B ($2^{-dCt}(adj)$) in grade 2 and 3. (n=14; grade 2: n=7; grade 3: n=7)

Fig. 31 compares PCYT1A and B in grades 2 and 3. In both grades, PCYT1A is higher concentrated than B. Both PCYT1A and B concentrations increase in grade 3 as opposed to grade 2. PCYT1A, starting from a higher concentration already in grade 2 than PCYT1B, rises about 4,02-times in grade 3, whereas PCYT1B rises 3,27-fold from grade 2 to 3.

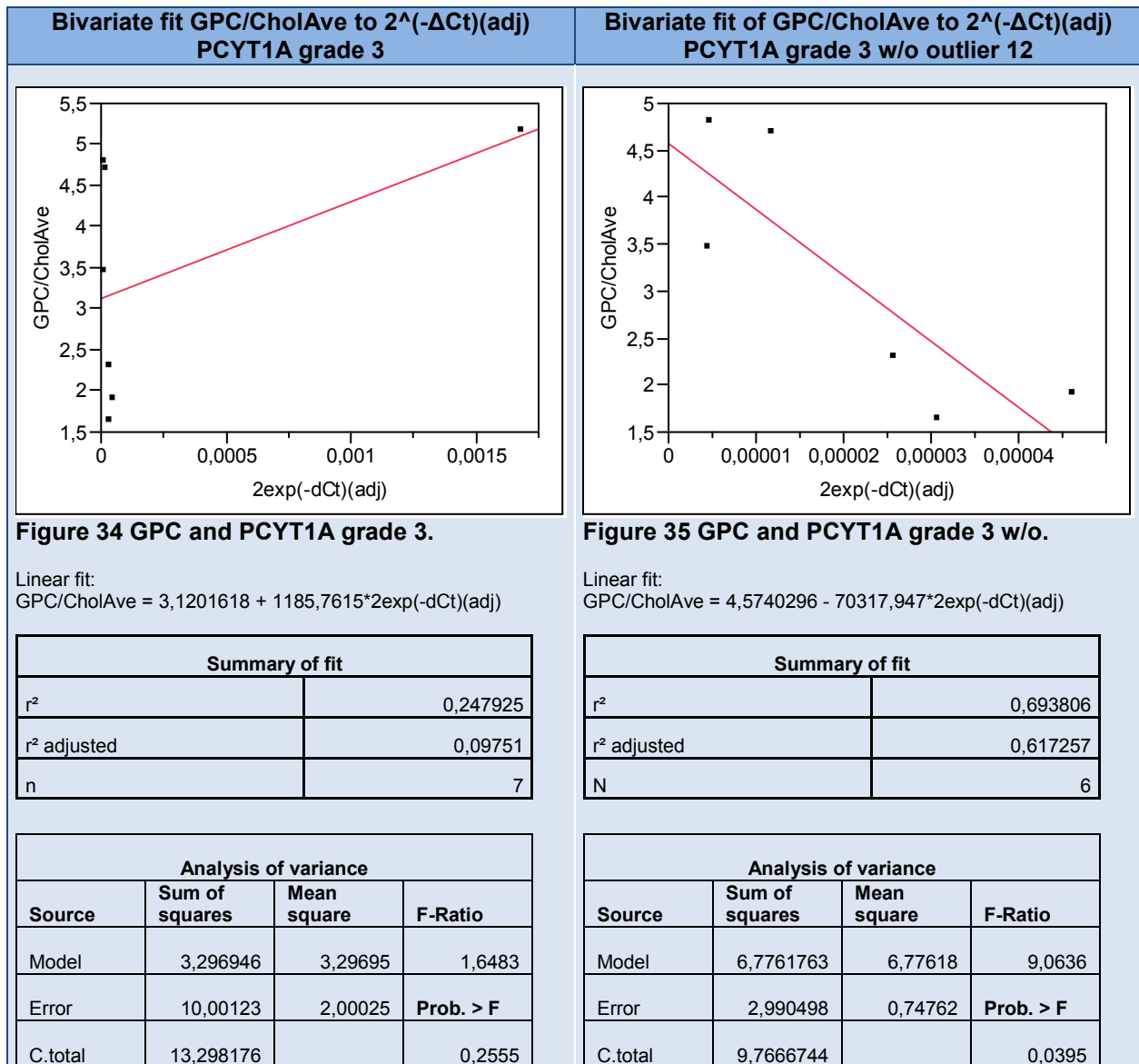
10.5.2 PCR results with MRS-correlation



Considering all samples, there is a positive correlation between (PC+GPC)/choline and the two isoforms PCYT1A/B across both grades (p -value=0,0022) (fig. 32). As shown in fig. 21, after the exclusion of all four outliers of PCYT1, the p -value rises to 0,95.

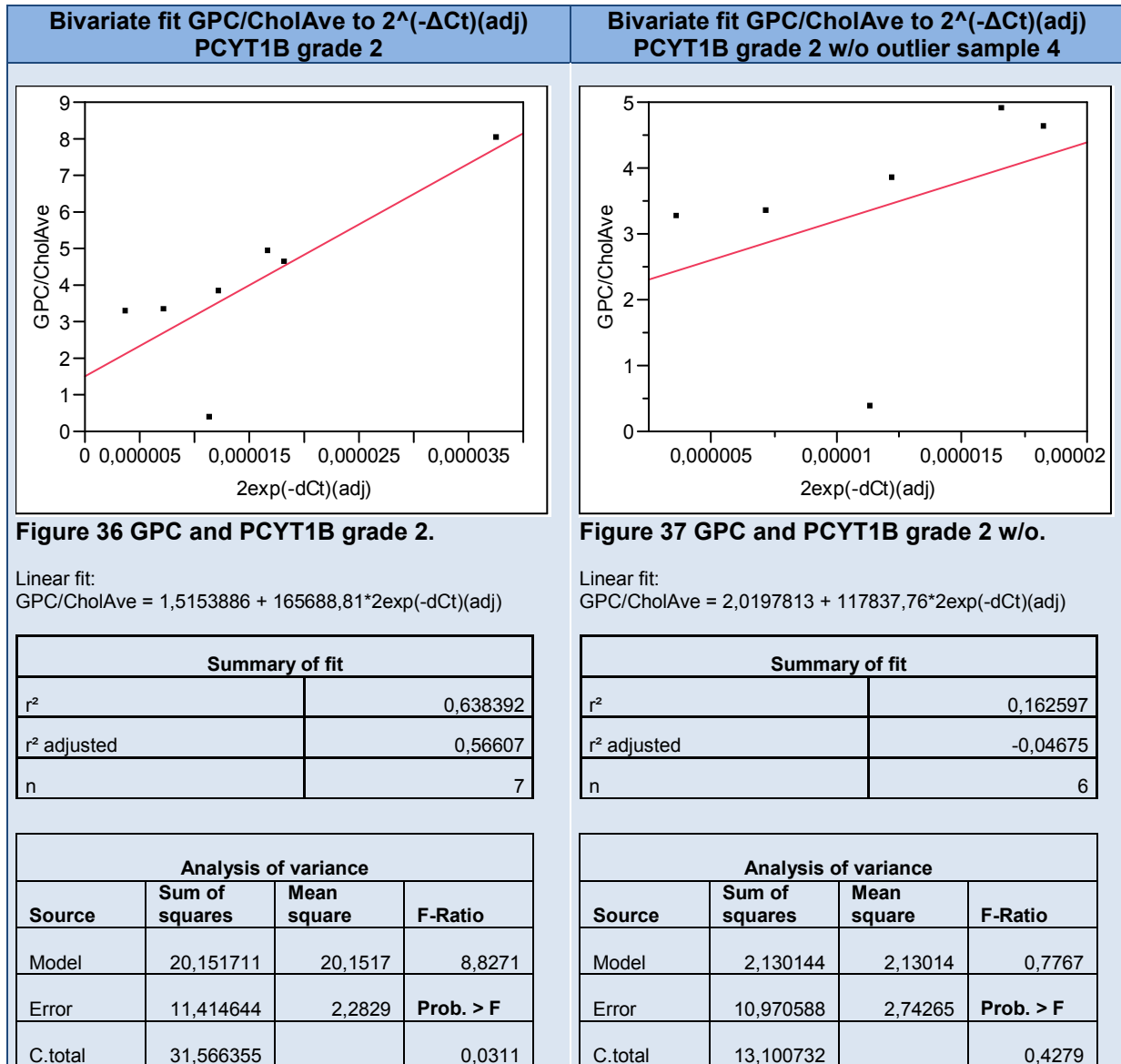
10.5.2.1 PCYT1A

For grade 2, no correlation between PCYT1A concentration and overall choline levels can be found. PC+GPC levels are not significantly correlated with PCYT1A either. In grade 3, PCYT1A and GPC/choline are apparently positively correlated (fig. 34). This correlation is greatly dependent on outlier sample 12. Without it, the correlation even turns into a negative one (fig. 35).



As can be seen in figg. 34-35, there is a significant negative correlation between PCYT1A and GPC/choline concentration in grade 3. Intriguingly, the exclusion of sample 12 leads to a drop of the p-value to 0,039, leading to a statistically significant negative correlation between the GPC/choline ratio and PCYT1A in grade 3.

10.5.2.2 PCYT1B



In fig. 36, we find a positive correlation between PCYT1B and GPC/choline in grade 2 with a p-value of 0,03 and an $r^2=0,64$. This apparent correlation is only dependent on the strong impact of outlier sample 4 in the upper right hand corner. When removed, the p-value rises to 0,43 and the correlation coefficient r^2 falls to 16 % (fig. 37).

No significant correlation can be reported for PCYT1B and choline or GPC in grade 2.

In grade 3, our data suggest no correlation of PCYT1B with either choline or GPC. PC+GPC concentration display an apparent positive correlation with PCYT1B levels.

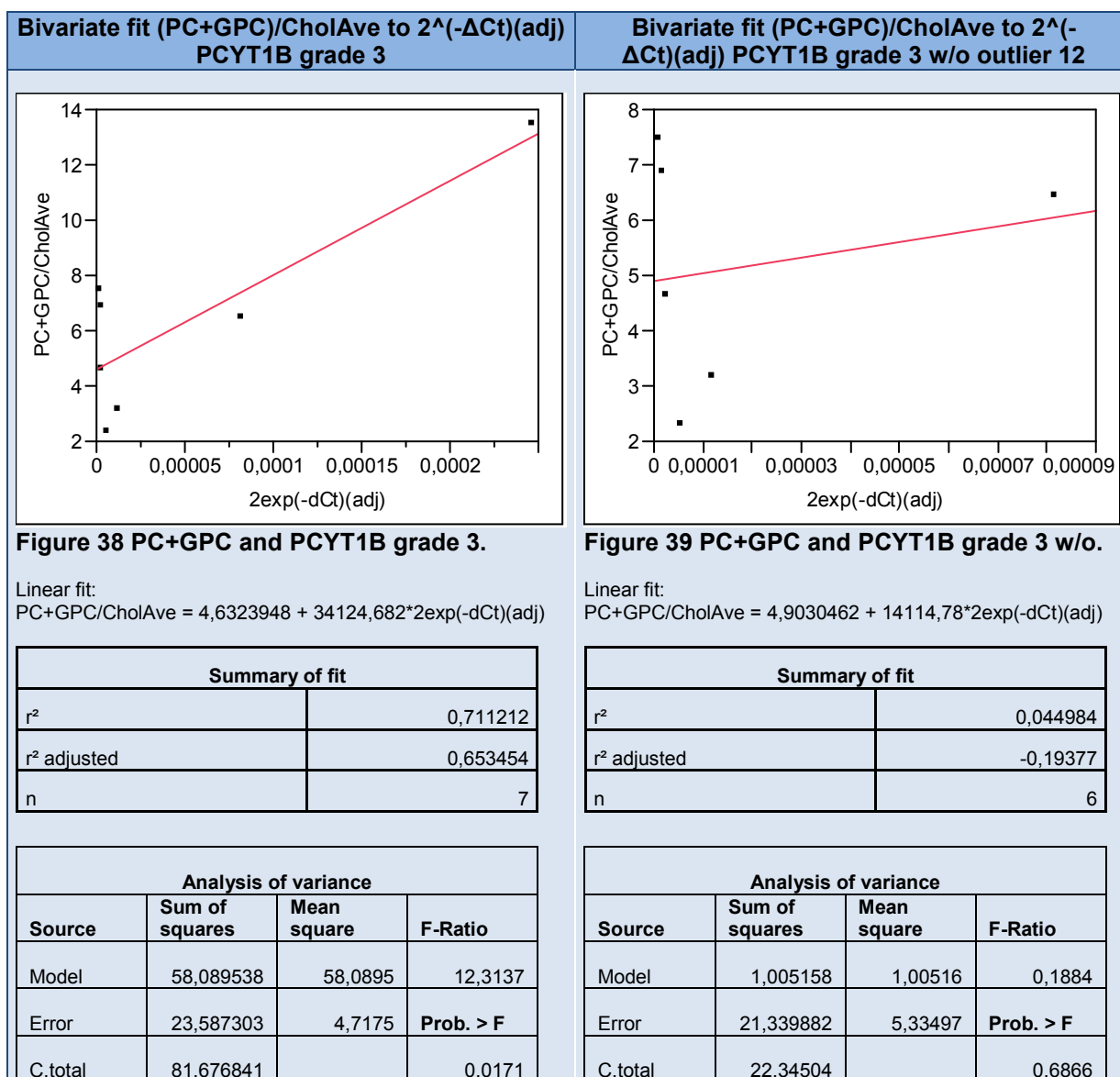


Fig. 38 illustrates this highly positive correlation of PCYT1B and (PC+GPC)/choline concentration in grade 3, which displays a correlation coefficient of $r^2=0,71$. After the exclusion of outlier sample 12, the p-value rises from 0,017 to 0,69 and the adjusted correlation coefficient even turns negative (fig. 39), indicating a simultaneous decrease in PC+GPC concentration with rising PCYT1B levels.

There was no significant correlation of PCYT1B concentration and tumour grade for neither of the histological grades.

10.6 SLC22A

10.6.1 PCR results without MRS-correlation

The transporter family OCT1/2 as a whole sees an increase in concentration in grade 3 as opposed to grade 2.

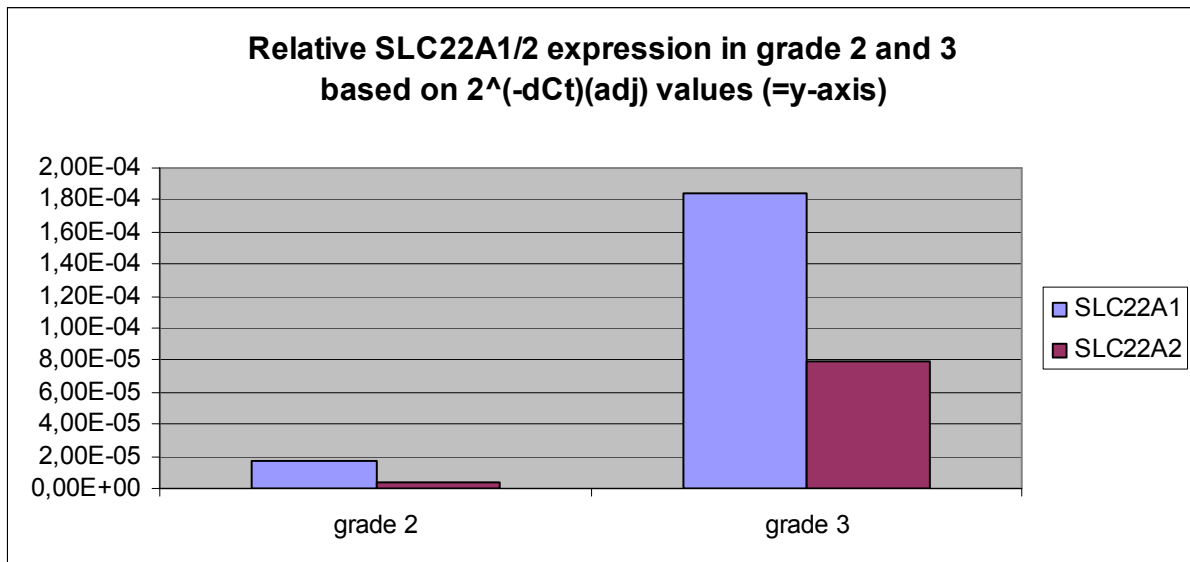


Figure 40 Comparison of SLC22A1/2 expression ($2^{-\Delta Ct}(\text{adj})$) in grade 2 and 3. (n=13; grade 2: n=7; grade 3: n=6)

SLC22A1, starting from a higher level of concentration already in grade 2 stays above the level of SLC22A2 in grade 3, although both transporter enzymes rise noticeably.

The only statistically significant correlation that could be found for SLC22A was a positive one for SLC22A1 and GPC/choline in grade 2, and for SLC22A2 and (PC+GPC)/choline in grade 3.

10.6.2 PCR results with MRS-correlation

10.6.2.1 SLC22A1

For SLC22A1 in grade 2, there is a positive correlation between GPC/choline and the enzyme (fig. 29). With the outlier (sample 4) removed, the p-value rises from 0,0242 to 0,34, as shown in fig. 30.

Bivariate fit of GPC/CholAve to $2^{(-\Delta Ct)(adj)}$ SLC22A1 grade 2 **Bivariate fit of GPC/CholAve to $2^{(-\Delta Ct)(adj)}$ SLC22A1 grade 2 w/o outlier 4**

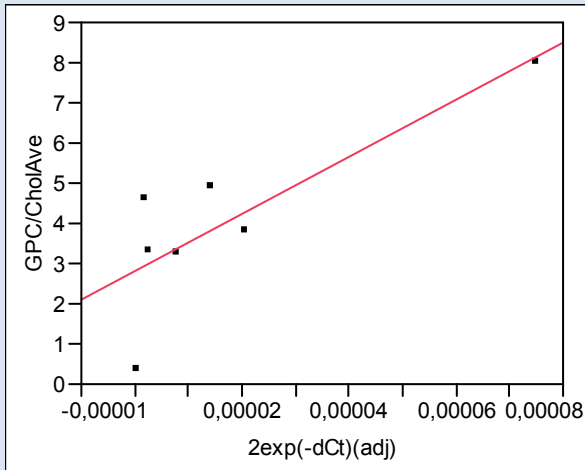


Figure 41 GPC and SLC22A1 grade 2.

Linear fit:
 $GPC/CholAve = 2,8126277 + 71230,576 * 2exp(-dCt)(adj)$

Summary of fit	
r ²	0,67094
r ² adjusted	0,605128
n	7

Analysis of variance			
Source	Sum of squares	Mean square	F-Ratio
Model	21,179135	21,1791	10,1948
Error	10,38722	2,0774	Prob. > F
C.total	31,566355		0,0242

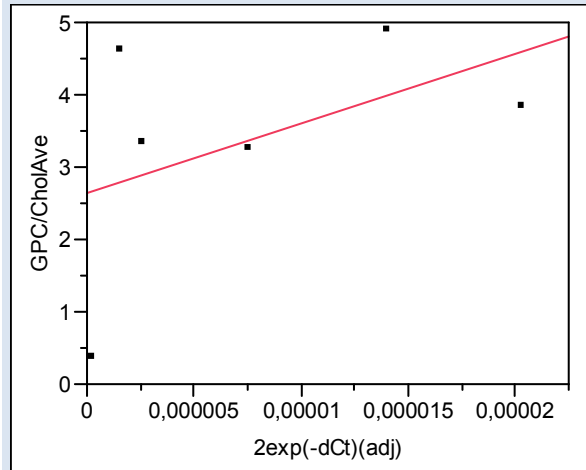


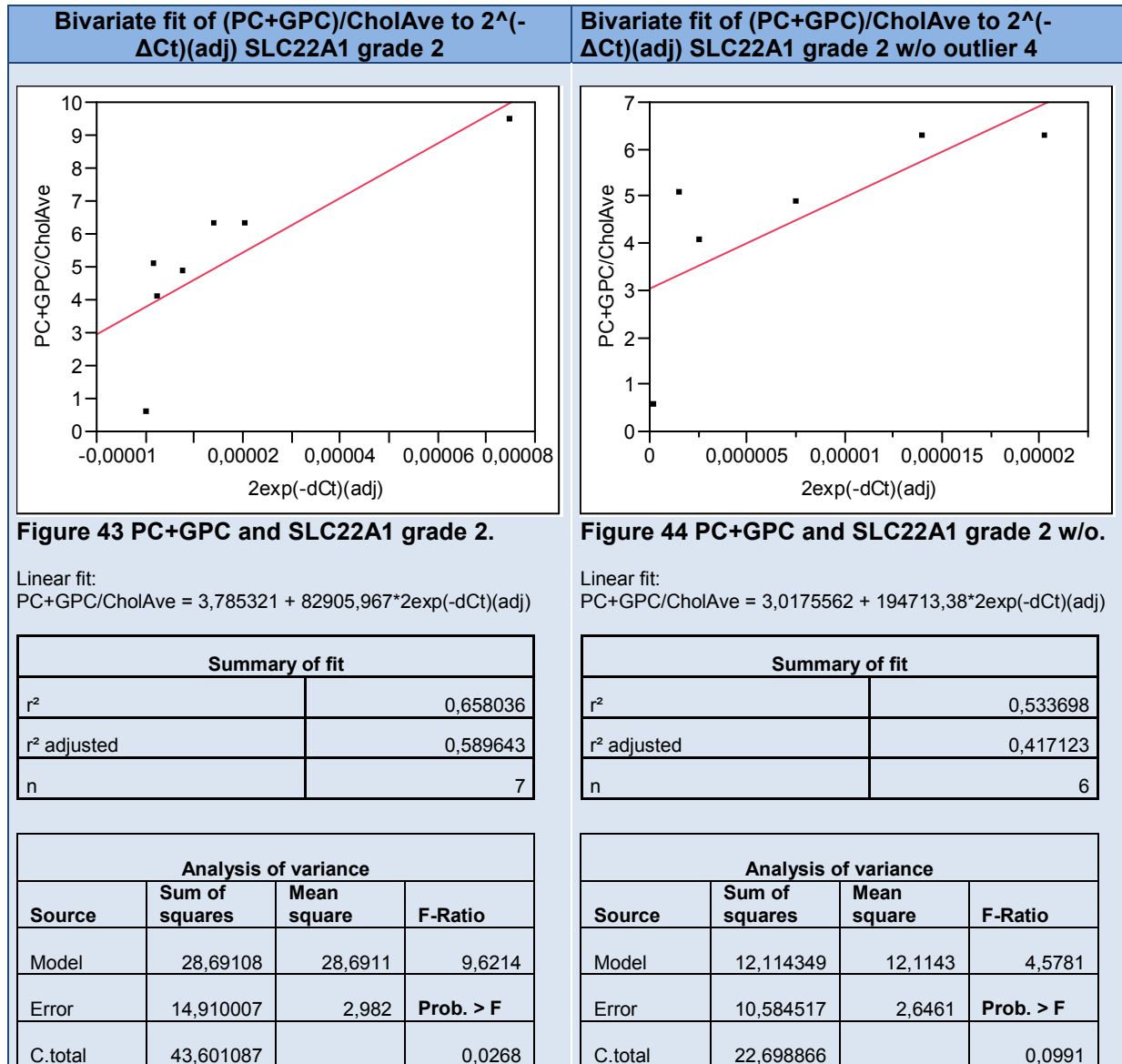
Figure 42 GPC and SLC22A1 grade w/o.

Linear fit:
 $GPC/CholAve = 2,6454852 + 95571,072 * 2exp(-dCt)(adj)$

Summary of fit	
r ²	0,222775
r ² adjusted	0,028468
n	6

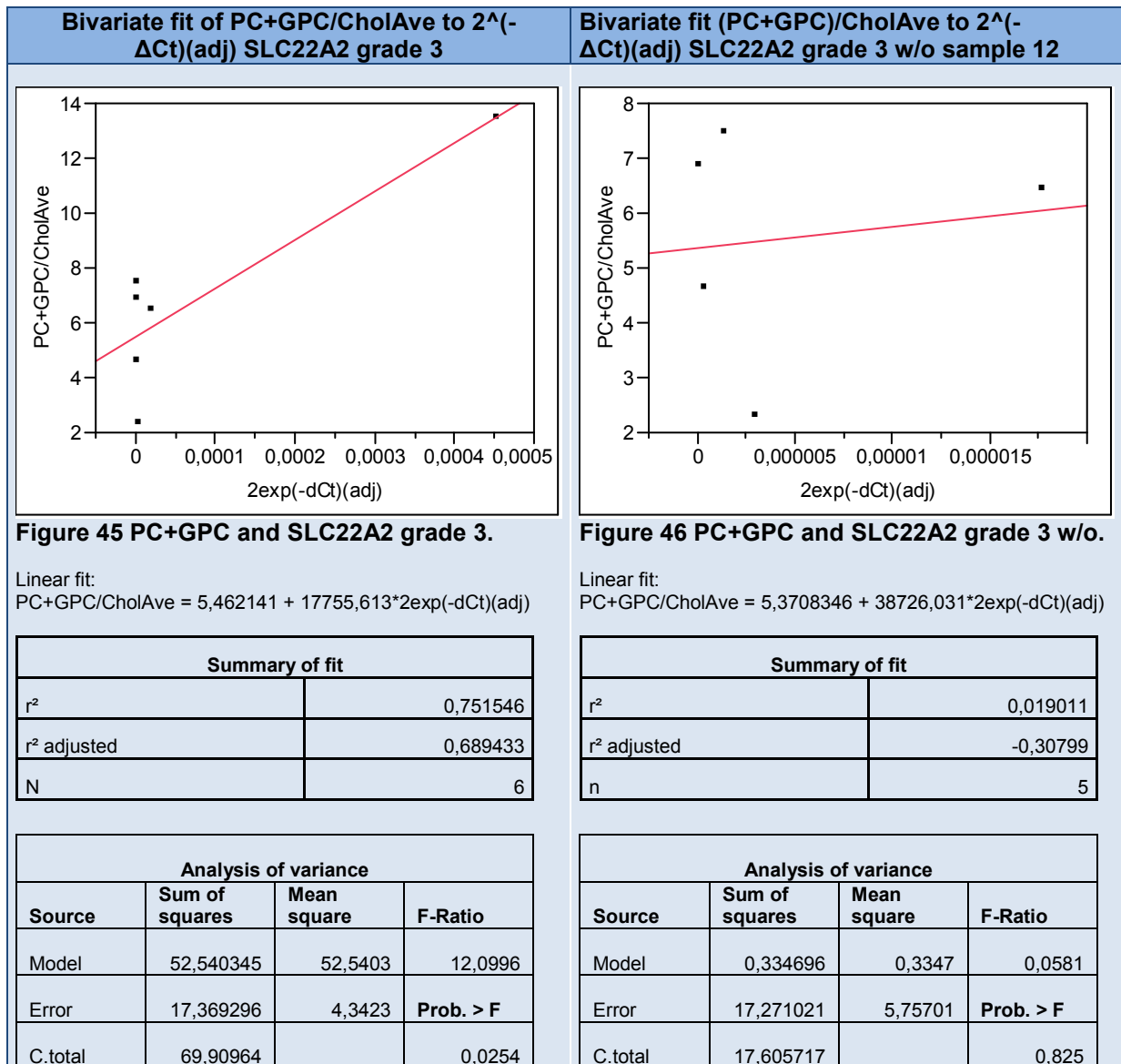
Analysis of variance			
Source	Sum of squares	Mean square	F-Ratio
Model	2,918511	2,91851	1,1465
Error	10,18222	2,54556	Prob. > F
C.total	13,100732		0,3446

A similar correlation as seen for GPC/choline can be observed for (PC+GPC)/choline and SLC22A1 in grade 2 (fig. 31). Again, this apparent correlation relies on an outlier (sample 4). Without it, the p-value rises to 0,099 (from 0,027 when included) (fig.32).



10.6.2.2 SLC22A2

No significant correlations could be found for SLC22A2 in grade 2 and GPC, PC+GPC or choline/ID2CorAve.



For SLC22A2 in grade 3, a correlation can be shown for (PC+GPC)/choline with a p-value of 0,025 and a correlation coefficient attributing 75 % of the variance of the (PC+GPC)/choline concentration to a rise in SLC22A2 (fig. 45). After exclusion of sample 12, the p-value rises to 0,82, leaving the correlation insignificant (fig.46).

10.7 GPC to PC switch

In a paper from 2003, Ackerstaff reports the detection of a GPC to PC switch as an early phenotypic change during carcinogenesis [24]. We observed the same changes in GPC and PC+GPC concentrations in our study, as shown in fig. 47.

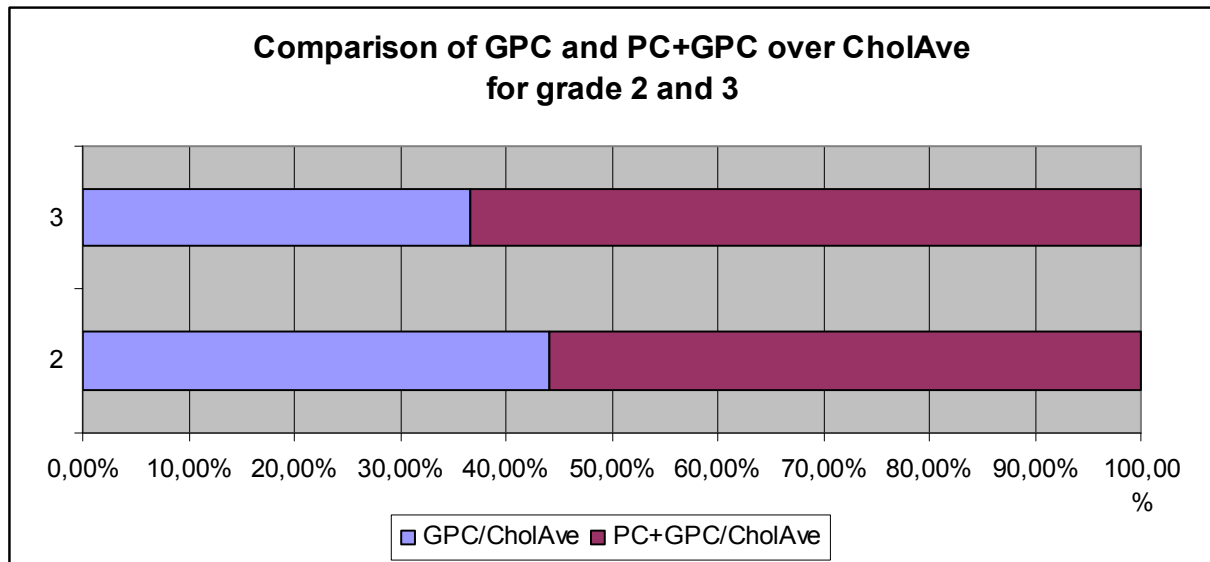


Figure 47 GPC to PC switch.

Comparison of ratios GPC/CholAve and (PC+GPC)/CholAve between grades. Calculation based on the average values from grade 2 (n=10) and grade 3 (n=9).

There is an increase of 7,53 % in (PC+GPC)/CholAve in grade 3 as opposed to grade 2. This increase can be either attributed to an increase in PC or a decrease in average choline concentration the higher grade.

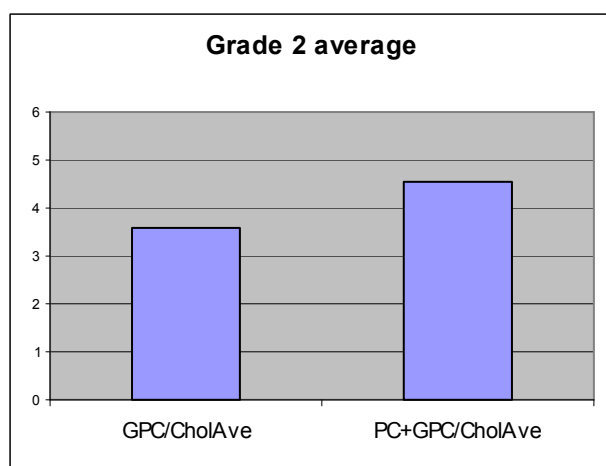


Figure 48 Average concentration ratios measured by MRS (y-axis=MRS concentration results). Grade 2: n=10; grade 3: n=9.

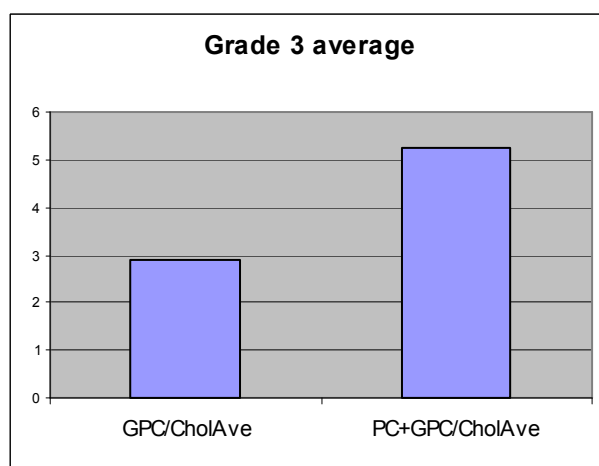


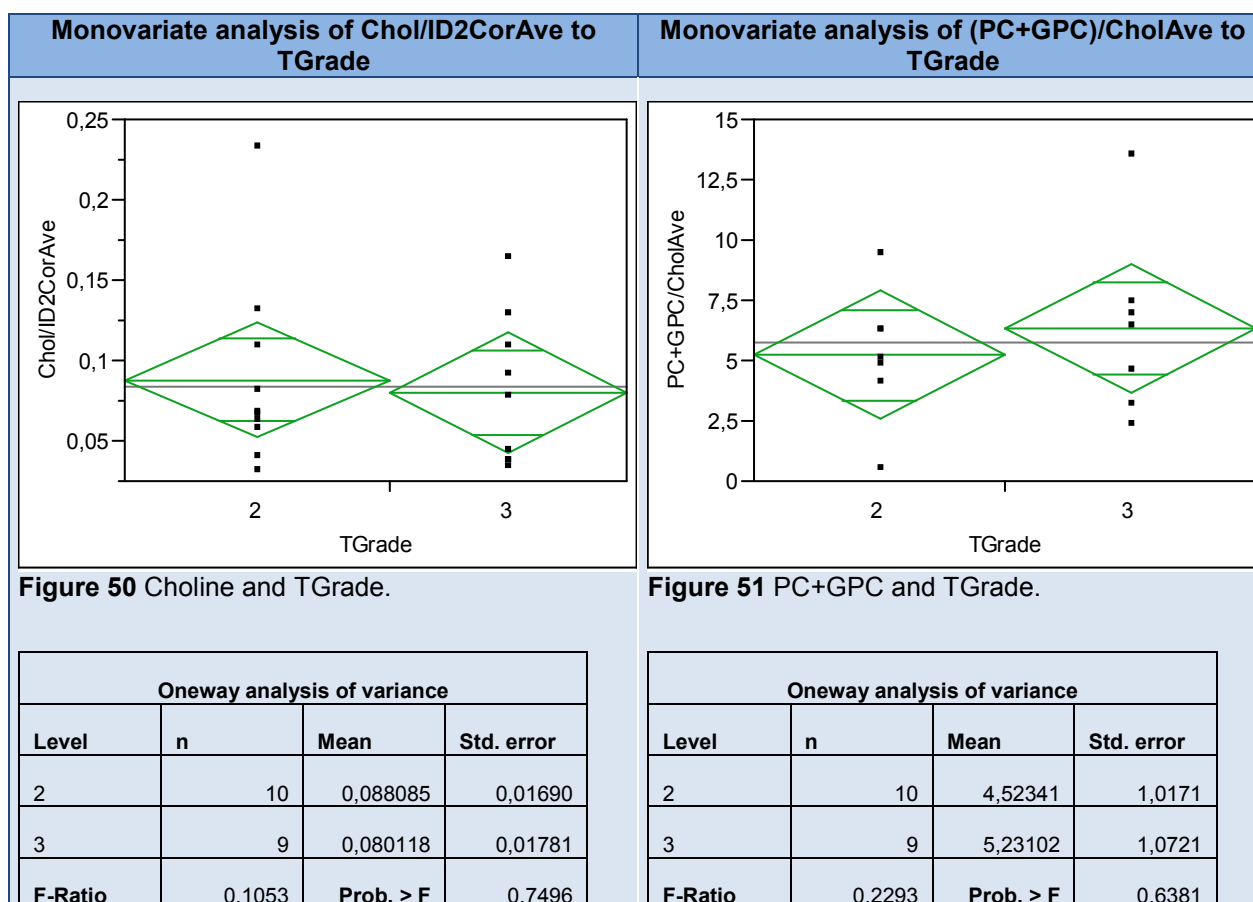
Figure 49 Average concentration ratios measured by MRS (y-axis=MRS concentration results). Grade 2 n=10; grade 3: n=9.

As shown in tables 48-49, we also found the GPC to PC switch described by Ackerstaff. In grade 3, the GPC/CholAve ratio falls by app. 20 %, whereas the (PC+GPC)/CholAve ratio rises by appr.16 % (fig. 24).

	Grade	GPC/CholAve	(PC+GPC)/CholAve
Average; n=10	2	3,59352474	4,52340698
Average; n=9	3	2,88163635	5,23102228
% change		-19,81%	15,64%

Table 24 Comparison of GPC and PC concentration across grades 2 and 3.

This increase can be explained as follows: GPC concentration by itself decreases in grade 3 as opposed to grade 2. Therefore, the increase in combined (PC+GPC)/CholAve ratio can only be explained by either an increase in PC or a decrease of the total choline concentration. For the change in choline concentration, Chol/ID2CorAve ratios are shown for both grades (fig. 50). We find that average tCho concentration in grade 3 is slightly lower than the one in grade 2. Thus, the increase in the (PC+GPC)/CholAve ratio observed in grade 3 can partly be attributed to an increase in tCho concentration. This does not rule out the possibility of a simultaneous increase in PC concentration (due to the limitations of MRS on PC detection, this statement can only be made indirectly through the analysis of changes in the GPC concentration).



In contrast to tCho concentration, PC+GPC/CholAve ratio seems to be rising with increased tumour grade (fig. 51). Once more, this apparent correlation lacks statistical significance with a $p=0,64$.

10.8 General development of genes of interest

Fig. 52 gives an overview over all eight enzymes and their $2^{-\Delta Ct}$ (adj)-values for both grades investigated in the study. For this graph, outliers of every enzyme were identified and subsequently excluded.

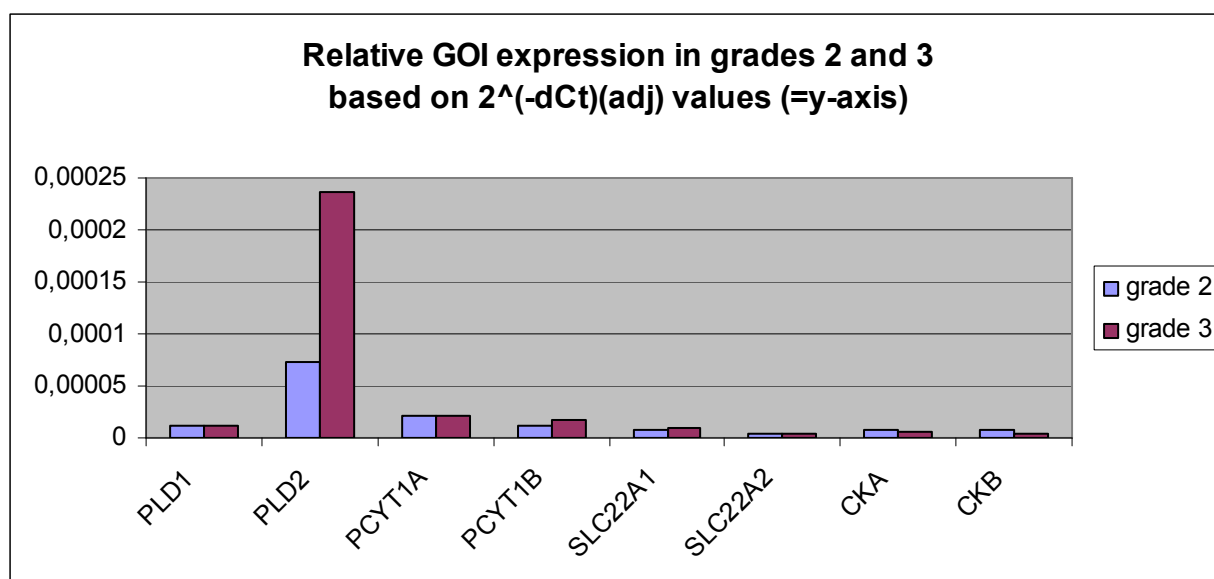


Figure 52 Comparison of GOI concentrations. ($2^{-\Delta Ct}$ (adj)) in both grades w/o outliers.

Tabel 25 gives an overview of the number of samples used in fig. 52. The greatest increase in concentration can be observed for PLD2. Within this group of enzymes of the Kennedy cycle, the smallest difference in concentration in between grades can be observed for PLD1.

Enzyme	Outlier		n	
	Grade 2	Grade 3	Grade 2	Grade 3
ChoK α	11	-	9	9
ChoK β	11	-	9	9
PLD1	22	12	9	8
PLD2	4	5	9	8
PCYT1A	10	12	9	8
PCYT1B	4	12	9	8
SLC22A1	4	12	9	8
SLC22A2	-	12	9	8

Table 25 Overview of sample size and outliers per enzyme.

For an improved frame of reference, fig. 53 uses the same data, but omits PLD2 because of its excessive concentration changes, in order to see ratios more clearly.

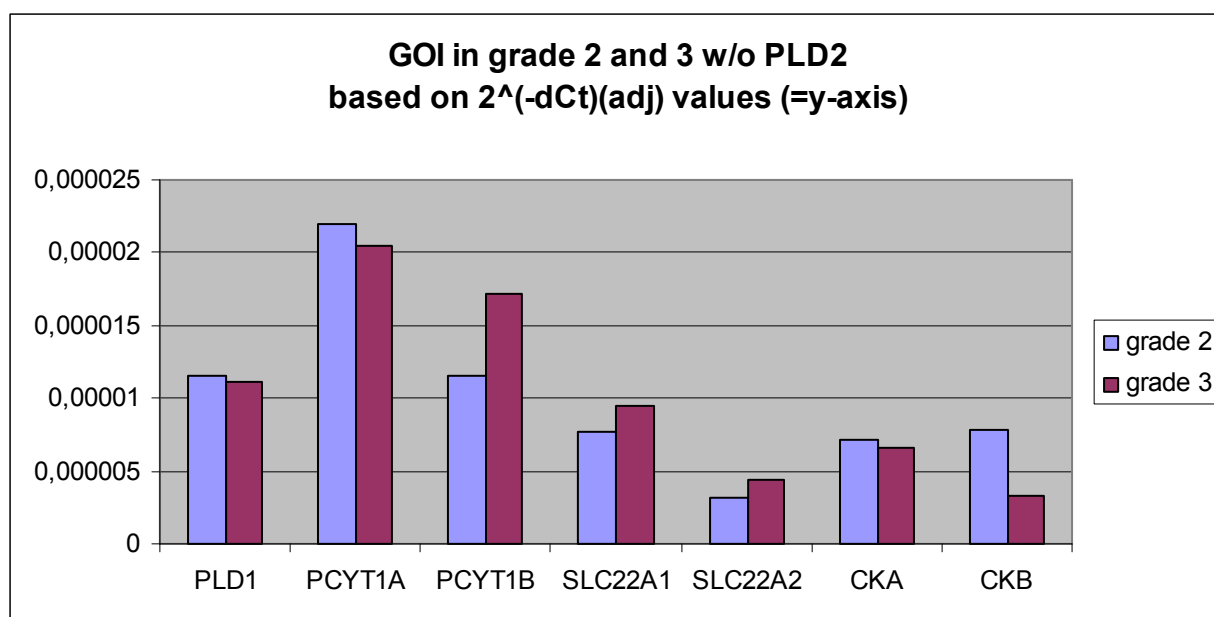


Figure 53 GOI average 2^{-dCt}(adj) in grade 2 and 3 w/o PLD2.

Along with PCYT1A, ChoK α and β decrease in their concentration with higher tumour grade. After PLD2, concentration in general is highest for PCYT1A and B in both tumour grades.

Enzyme	Average 2 ^{-dCt} (adj)		% difference between grades
	Grade 2	Grade 3	
PLD1	1,15E-05	1,11E-05	96,48%
PLD2	7,32E-05	0,00023695	323,79%
PCYT1A	2,20E-05	2,05E-05	93,26%
PCYT1B	1,15E-05	1,72E-05	149,29%
SLC22A1	7,66E-06	9,52E-06	124,28%
SLC22A2	3,19E-06	4,45E-06	139,65%
ChKA	7,12E-06	6,64E-06	93,30%
ChKB	7,80E-06	3,34E-06	42,88%

Table 26 Concentration differences per enzyme and tumour grade w/o outliers.

Once those data are analysed using JMP, there is no statistically significant correlation between the enzyme concentrations and the tumour grade. The p-values for any of the above mentioned enzymes in relation to the tumour grade remain higher than $p = 0,05$.

11 Discussion of results

This chapter will narrow down and interpret the findings, put the results into perspective with the research done so far on the topic and give an outlook on future possible research approaches.

11.1 Existing study approaches and theories on metabolite increase

As outlined in the background chapter, no single biochemical reaction could thus far be ultimately assigned to be at the base of the total choline metabolite increase measured in malign tissue and malign cell populations. Studies and theories differ in their findings and range widely in their explanation for the choline increase: from an upregulation of intracellular pathways rather than increased choline influx via transmembraneous transporters by Hernando [132] over a focus on just these transporters [11] to the targeting of a single enzyme: Michel et. al state that the Kennedy pathway is not considered to be regulated by any other step than CCT, nor by the rate of choline transport [85] through the cell membrane; Ramirez de Molina et al. have focussed their research mainly on ChoK, but have recently included upstream regulatory influences such as GTPA-families [53]; Bañez-Coronel et al. were able to report promising results for therapeutical use by inhibition of ChoK α and short-hairpin-RNA (shRNA).

Overall, it seems to be safe to say that mechanisms leading up to the changes in choline metabolite levels are highly complex and interconnected.

11.2 Main findings of the study

Based on the data raised in this study, H₀ has to be rejected.

In the following, only the statistically significant findings (as suggested by their p-value $\leq 0,05$) will be listed. In addition, statistically non-significant findings will be discussed in the following part.

- a) ChoK β concentration is negatively correlated with grade (i.e. ChoK β concentration falls in grade 3) (Mann-Whitney-U test p-value = 0,0458)
- b) ChoK α and total choline levels are positively correlated
- c) ChoK α/β levels in grades 2 and 3 are negatively correlated with the (PC+GPC)/choline ratio
- d) GPC and ChoK α concentrations are negatively correlated in grade 2

e) GPC/choline ratio and PCYT1A are negatively correlated in grade 3.

11.2.1 ChoK

Overall, the above mentioned correlations suggest an increase in tCho concentration with rising ChoK levels, possibly linked to a GPC to PC switch, as higher levels of ChoK α are accompanied by lower PC+GPC levels.

In general, the data presented suggest that with increasing ChoK (both α and β) concentration, both GPC and PC+GPC concentration decrease significantly. 25% of the variance of (PC+GPC)/choline can be explained by a rise in ChoK α concentration in grade 2 and 3.

The data for GPC are intuitive and go along with what was to be expected based on the research done so far in the field: since GPC is a part of the total intracellular choline pool and thus one of ChoK's substrate, rising levels of ChoK and falling concentrations of GPC logically go together.

The increase of ChoK α and simultaneous decrease of PC+GPC concentration is counterintuitive. Referring back to fig. 3 in the background chapter (schematic overview of the Kennedy cycle), one would expect a fall in GPC and increase in PC with rising ChoK α concentration, since GPC is a substrate, PC a product of ChoK α . Since ^1H MRS cannot readily distinguish between PC and GPC, the elevated concentration of the compound PC+GPC figure is harder to analyse. It has to be kept in mind that the compound figure of PC+GPC cannot be regarded as an exact PC concentration measure.

In 2008, Plathow and Weber showed that ChoK activity and PC levels were generally not well correlated with proliferation rates, suggesting that activation of ChoK cannot be explained alone through net PC synthesis by proliferating cells [133]. Possibly, there are other factors playing on the ChoK concentration as well as on PC and probably also GPC levels.

However, the data raised for ChoK are surprising. Glunde [72] found that both ChoK concentration and choline levels increase simultaneously in malignant cell lines as opposed to benign cells. Eliyahu (2007) also observed increasing choline transport rates with rising ChoK α concentration. Our results do not concur with these findings. We found a negative correlation between ChoK β and a higher tumour grade ($p = 0,03$). As suggested by Aoyama [47], the ChoK homo- and hetero-dimer isoforms exist in different

ratios, depending on the malignancy of the tissue. Therefore, it is of interest to look for potential correlations between the two isoforms in this study. One possible explanation for our results could thus be a downregulation of the less active β -isoform of the dimer in favour of synthesis of the more active α -isoform in tissues undergoing carcinogenesis, according to Aoyama. This theory however cannot be backed up by statistically significant findings of our study regarding ChoK α differences from grade 2 to 3.

Statistically, our strongest data are those on ChoK β , but we are lacking strong statistical results on ChoK α . In this context, Aoyama's results are particularly interesting: he found that the activity of ChoK in a given cell type must be regulated not merely by the level of each isoform in the cell but also by the combination of each isoform subunit (α_1 , α_2 and β) to generate active dimer complexes (α_1/α_1 , α_1/α_2 , α_2/α_2 , α_1/β , α_2/β , and β/β). As shown in fig. 6 in the Background chapter (Configuration of the active ChoK enzyme), in benign cells there are more hetero-dimers. In malign cells, a shift towards oligo- α -dimers takes place and simultaneously an assumed loss of activity, since the α/α form appears to be less active than the α/β form [47].

As none of the studies so far have looked in detail at the different isoforms of ChoK α and β , data on this particular issue are lacking. This is disappointing, since the findings on ChoK α and β are the statistically strongest and most significant ones of this study. For prospective approaches, it would be very interesting to see more investigation on the characteristics of the two major isoforms of ChoK.

Those findings strongly suggests that the molecular mechanism of regulation of ChoK activity in the cell is much more complicated than was expected and should be considered in future study setups. It will be interesting to reassess the data raised in this study once more research will have been conducted on the role of the different isoforms of ChoK. Also, it will be interesting to see if there is any post-translational regulation for mammalian ChoK, as has already been shown for yeast ChoK. In the bacterial system, phosphorylation by PKA was found to cause a stimulation of ChoK activity [47]. Recent studies have looked at alternative potential upstream regulators of ChoK. As mentioned in the Background chapter, both ChoK and PLD have been found to be under strong influence of Rho and ras families of GTPases. A possible alternative approach to explain the changes in the choline metabolite changes in malignant tissue could be the quantification of those GTPase-families. Possibly, the reason for a choline upregulation can be found at an earlier stage than the one studied here. So far, none of

the identified potential regulatory influences could be proven to be at the base of the ChoK increase in malignant cells. Very likely, there is more than just one metabolic pathway or feedback loop involved:

- in addition to ras, several oncogenes such as src, raf and mos could also increase the endogenous ChoK activity and PCho level when expressed in mouse fibroblasts [51, 134];
- ChoK could also play an important role as second messenger, in malignant as well as in benign cells.

Although in the literature CCT is mostly recognized as the regulatory enzyme in the Kennedy pathway, ample evidence suggests a rate-limiting role for ChoK as well under particular circumstances [46, 48, 82, 135-141]. Thus, we cannot completely dismiss the possibility of ChoK playing a role in the regulation of the choline metabolism.

11.2.2 PCYT

- In grade 3, there is a strong negative correlation between PCYT1A and GPC/choline concentration.

This finding suggests that increasing levels of PCYT are correlated with a fall in GPC, but a rise in PC+GPC. This could be explained through the interdependencies of the Kennedy cycle: when there is more PLD which breaks down PtdCho directly to intracellular choline, less PtdCho can be processed by PLA, which delivers GPC as its product. Thus, an increase in PLD should lead to a decrease in GPC, but an increase in intracellular choline metabolites. This is reflected in our results.

PCYT (coding for CCT) and GPC are involved in two opposite mechanisms: PCYT is involved in the first metabolic step of an anabolic process that results in the production of Ptd-Cho; GPC is the breakdown product of Ptd-Cho, a reaction catalyzed by PLA. Thus, a decrease in PCYT concentration and a simultaneous increase in GPC appear logical: in a catabolic state, production of Ptd-Cho is slowed down its breakdown increases. In this context, it would be interesting to compare data on PLA, the enzyme catalyzing the breakdown of Ptd-Cho to GPC and also the different fractions of total choline.

PCYT1B seems to be the enzyme the least affected by the advancing malignancy. It is not possible to say if this indicates a minor role of this enzyme in the metabolomic changes within tissue undergoing malign restructuring, or if it is to the contrary the most

resistant enzyme, withstanding cell-mechanism altering influences. However, the cell proliferation ensued by malignity results in a doubling of the cellular membrane content prior to each cell division [142]. This requires a significant increase in cellular membrane phospholipid biosynthesis. Therefore, every cell proliferation theoretically needs to be accompanied by an increase in enzymes that provide phospholipids, such as CCT. In our study, we did not see such an increase in PCYT1 concentration in higher tumour grades, assumedly going along with higher proliferation rates. A recent study on CCT activity in proliferating B-cells possibly offers one explanation to this antilogy: the study published by Fagone et al. on B-cells suggests that another source of PtdCho is available that circumvents a requirement for CCT α [143]. If future research finds alternative ways for phospholipid synthesis other than PCYT1, as suggested by our data, it would be crucial to analyse its expression in cancerous breast tissue.

As mentioned in the Background chapter, nuclear CCT α (coded for by PCYT1A) is thought of as a reserve for a prompt response to an extranuclear PtdCho requirement, such as the membrane synthesis associated with mitogenic stimulation of the cell [83]. This would be underlined by an increase in CCT α concentration in tissue of elevated tumour grades. However, the data raised in this study found a (statistically insignificant) decrease in PCYT1A in grade 3 as opposed to its concentration in grade 2.

When looking at the theories regarding the changes in intracellular metabolic pathways taking place in cells undergoing carcinogenesis, it becomes clear that – although coherent within themselves – theories often contradict one another. In the case of CCT, it is not clear which influence on its regulation is the stronger one: a prompt response and thus upregulation of its activity in response to a mitogenic stimulation such as malign transformation, or a downregulation, that could serve as one possible explanation for the increase of PC in malignant tissue.

The increased PC-levels mentioned in recent research papers led us to expectations of lower CCT levels in higher tumour grades, slowing down the metabolization of PC to CDP-Choline and thus leading to a higher PC concentration. However, none of our results on tumour grade and PCYT1-concentration are statistically significant.

For PCYT1A there is an apparent negative correlation between tumour grade and enzyme concentration. Our apparent results support the latter theory on CCT expression, i.e. a decrease of concentration in higher tumour grades.

It will be interesting to reconsider the results of this study once more research on the different isoforms of CCT has been performed.

11.3 Additional findings

Many of the results on PLD, SLC22A and OCT lack statistical significance. Depicting a trend, they nevertheless provide an indication of possible correlations between enzymes of the Kennedy pathway and the choline metabolism. In the following paragraphs these results are shortly pointed out and put into perspective with research done so far on the topic.

11.3.1 PLD

PLD concentration seems to be closely linked to cellular changes undergone during carcinogenesis:

- PLD2 significantly rises with histological grade (highest concentration of any of the enzymes measured in grade 3;p-value = 0,18)
- PLD2 is positively correlated with the (PC+GPC)/choline ratio (in grade 2)

A trend towards overall positive correlation between PLD and the (PC+GPC)/choline ratio can be observed. Due to the already mentioned difficulties concerning the PC spectra, an exact analysis of this ratio is complicated. In the Kennedy pathway, PLD is only indirectly linked to the PC level. PLD breaks down membraneous choline, which leads to an increase of the intracellular choline level, acting as a substrate for ChoK, which in turn catalyzes the formation of this intracellular choline to PC. Thus, the data on PLD would support the theory of the important role of membraneous PtdCho breakdown as one explanation for increased intracellular choline concentration.

Since the two enzymes are so closely connected by their products / respective substrates, Ramirez de Molina et. al. studied the activation of PLD and ChoK to see if they are activated sequentially or in an independent manner. They found that activation of PLD does not influence ChoK activity. Rather, ChoK activity appeared to be susceptible to specific regulation by oncogenic ras [48]. This, again, suggests the important role of upstream regulation.

11.3.2 SLC22A

Glunde found membraneous choline metabolites to be the source for the increased intracellular choline concentration, indicating a higher metabolic flux from membrane PtdCho to choline and PC in breast cancer cells (rather than an increase in influx from

extracellular choline, requiring an increase in transmembraneous transporters). This goes against our (statistically insignificant) findings of slightly increased SLC22A-concentration in higher tumour grades (SLC22A1 increased by 24 %, SLC22A2 by 40 % in grade 3). Our findings are however supported by recent studies that suggest choline transport rather than choline phosphorylation as the key factor for choline increase in cancer cells [144]. Those studies found that a large fraction of the intracellular choline represents still non-metabolized choline [144], suggesting that choline transport and not phosphorylation is the key factor for choline uptake of cancer cells.

Although none of our analyses regarding SLC22 were statistically significant, we can see a certain tendency towards a SLC22 increase in grade 3 as opposed to grade 2 ($p = 0,29$). As the family of SLC22 transporters functions as uniporters with substrate transport in either direction in or outside the cell, it remains unclear if the possible increase in SLC22 transporters is a reaction to elevated intracellular choline levels or a contributing factor. As the driving force for substrate transport is supplied solely by the electrochemical gradient of the transported organic cation, the transporter should stop working once a certain level of choline concentration is reached within the cell. It can be assumed that the influx of choline facilitated by SLC22 stops automatically once equilibrium is reached. It could then be determined if expression of the transporter increases with higher tumour grade, i.e. choline metabolite concentration as a counter-regulatory reaction to the rising intracellular concentration.

Regarding the very low levels of concentration for SLC22A found in the study at hand, it has to be mentioned that other studies have been faced with similar problems: Eliyahu [15] and Morse [145] both report quantities of OCT 1 and 2 too small to be measured. The very low concentrations of SLC22A might require different measurement techniques than those used in the study at hand.

In general, it is difficult to relate the contribution of the OCT transporters to the overall kinetics of transport, as their choline affinities vary extensively in their K_m -values (30-100 μmol). As the OCT1/2 transporters only display a relatively low affinity to their substrate choline, it can be assumed that their transport rates rely to a higher extent on the chemical gradient than on their intrinsic affinity to choline. Thus, their contribution to the overall transport kinetics assumedly increases with higher choline concentration, both within and outside of the cell. However, as mentioned in the Background chapter,

choline transport via OCT1/2 is saturable by a sufficiently high concentration of choline. This threshold has so far not been defined.

In addition to intracellular/extracellular concentration gradients, certain enzymes such as PKC, PKA, tyrosinkinase (stimulation) and cGMP (inhibition) have been found to possess a regulatory influence on SLC22A expression (see Background chapter). Since those potential regulatory entities were not included in this study, we cannot evaluate their influence on SLC22A expression. It is very likely that more than one biochemical pathway is involved in the regulation of their activity rate.

11.3.3 GPC to PC switch

Consistent with recent publications on the subject [24], we found a GPC to PC switch in the composition of the choline peak in grade 3 as compared to grade 2. Referring to the Kennedy cycle pathways, this could be attributed to either:

- an increase in PLC activity
- an increase in ChoK activity
- a decrease in CCT activity.

Our data analyses on PCYT1 back up the third of those possible explanations, indicating an increase in both PCYT1 isoforms in grade 3 and a positive correlation of PCYT1B and PC+GPC levels.

Bhakoo also found the PC/GPC ratio to be a reliable indicator for the malignant transformation process of cellular entities [146]. In the context of overall choline metabolite increase observed in malignant cells, these results provide a promising lead as to where exactly the changes in the metabolic pathway take place. The GPC to PC switch supports the theory of a rise in ChoK and PLC concentrations, relating the increase in choline metabolites either to an increased influx of extracellular choline or to the catabolic processing of membraneous PtdCho by PLC (for graphic illustration please refer to schematic overview of the Kennedy cycle in the Background chapter). However, as the sequence of PtdCho-specific PLC has so far not been determined, mRNA quantification of this enzyme is not yet possible. Based on the PC and GPC data, the role of PLA in PtdCho breakdown to PC in the rise of choline metabolites can quite safely be dismissed, since it would at a first time lead to an increase in GPC concentration, which is contradicted by the data raised here and seen in other publications.

Underlining this theory is the fact that PC is a precursor as well as a breakdown product of the major membrane component PtdCho, whereas GPC is solely a membrane breakdown product.

A different thought necessary to be taken into consideration is the observation made by Lacal (2001), who suggests that PC could serve as a second messenger or mediator in the mitogenic signaling cascade [44]. This would mean that PC levels are under an additional, potentially very strong influence within cells undergoing malign transformation. Also, transfection with erbB2 oncogene has been reported to cause a significant increase in PC levels in human mammary epithelial cells [14]. Therefore, a possible correlation of any enzyme with the PC (or for that matter, any choline metabolite) level requires a very strong statistical power to be reliable, since there are a vast amount of potential regulators. Unfortunately, most of our results do not exhibit this high level of statistical power (e.g. p-value < 0,001).

11.3.4 Enzymatic changes between tumour grades

When looking solely at the concentration of all enzymes measured in this study w/o outliers:

- the lowest concentrations were measured for SLC22A2
- an increase in concentration with higher tumour grade can be described for
 - PLD1/2
 - PCYT1B
 - SLC22A/B
- a decrease in concentration with higher tumour grade can be described for
 - ChoK α/β
 - PCYT1A

Applying the above mentioned findings to the schematic Kennedy cycle, these enzymatic changes could potentially result in:

- an elevated catabolic activity of PLD2 in grade 3 tissue breaking down membraneous PtdChol;
- a lower ChoK activity in grade 3 tissue, leading to lower PC concentrations from the ChoK-catalysed phosphorylation reaction;
- less turnover of PC to CDP-Cho through the decrease in CCT;

- an increase of extracellular choline influx into cells of higher tumour grade tissue due to the increase of transport molecules such as OCT1/2.

As mentioned before, none of the changes in enzymatic concentration are statistically significant.

11.4 Correlation of the histological grade with MRS

However distinctive the changes may be that we found on the enzymatic level, they do not express themselves in spectral changes of the corresponding metabolites. For example, one would expect an increase in total choline in grade 3 when compared to grade 2, and the increase in PLD1 could serve as one possible explanation for this. We were not able to show an overall increase of tCho when comparing tCho levels in grade 2 to grade 3 tissue. Although contrary to the findings of Glunde or Eliyahu, there have also been studies consistent with our results (i.e. Ackerstaff [24], Bolan [25], Jacobs [147]). Also, Qihong et. al found that tumours with intermingled micronecrosis and cells of high neoplastic potential show low or no choline signal [21].

We found a certain MRS pattern for choline metabolites and enzymes of the Kennedy pathway that can be correlated with malignancy in breast tissue. It is characterised by the above mentioned features, mainly a negative correlation of PC+GPC levels and ChoK α in both grades (p -value = 0,033) and a positive correlation of ChoK α and tCho levels (p -value = 0,056) in grade 2 and 3. As MRS does not measure membranous choline metabolites, these findings imply a conversion of membranous PtdCho through intracellular choline to PC, thus leading to increased tCho levels. However, only 21 % of tCho increase can be explained by the increase in ChoK α concentration (see fig. 22), so that additional factors for the increase in tCho need to be researched.

11.5 Discrepancies to other studies

The results of this study differ in several ways from previous research done in the field.

There are several explanations for these incongruities:

- use of breast cancer tissue instead of multiple cell lines
- stable confluence (confluence +1 day) vs. variable tissue states
- defect in contact inhibition
- differences in experimental design

- differences in methodologies used to determine expression
- differences in the modes of normalisation

Most of these discrepancies can possibly be explained by the general differences between work performed on cell lines and tissue samples. As the regulatory influences on the enzymes of the Kennedy pathway are not yet fully understood, results gained from in vitro studies are prone to systemic errors. It is highly likely that an important part of regulation is of extracellular nature. Measurements of in vitro enzyme activity in cell lysates may not reflect its activity in intact cells because of the regulation imposed by the membrane lipid composition, the availability of metabolic intermediates, and the action of degrading pathways [82].

11.6 Results of this study in context with current research

In vivo results are not always recapitulated in vitro. For example, Morse et al. found the PC concentration to be quantifiably higher in metastatic cell lines in vitro but not significantly different from tumourigenic cell lines in vivo. Morse suggests that this discrepancy could partly be explained by the partial-volume effect, having a lower proportion of viable cancer cells in the whole tumour volume compared with tumourigenic cell lines, since tumour xenografts are more necrotic than comparable cell lines [148].

Both of the studies by Glunde (2004) and Eliyahu (2007) - the results of which served in part as a basis for this study - worked with cell lines and not with real tissue samples. It is maybe herein that lays the explanation for some of the differing results of our study.

11.7 Possible confounders of the study

Apart from the human error which is inherent in all types of physical and mental work, several other factors were identified which could have had a biasing impact on the results of this study.

11.7.1 Unknown interdependencies of enzymes

All enzymes measured in this study could not only be part of just one particular metabolic pathway, but very likely are involved in a number of biochemical reactions,

e.g. as second messengers. Therefore, they are most probably subject not only to one source of regulation but to multiple feedback loops and regulatory mechanisms. More work on the nature of these interdependencies needs to be conducted before specific causal connections can be appointed.

11.7.2 Limitations of MRS

When performed on solid tumour tissue, ^1H MRS produces an unresolved signal of overlapping PC, GPC and free choline resonances. Due to skimming, packing of the tissue in the probe and differences within the magnetic field, ^1H MRS produces an unresolved signal of overlapping PC and GPC curves, which are in consequence not readily distinguishable. Therefore, the ratio of combined PC and GPC over average total choline $((\text{PC}+\text{GPC})/\text{tCho})$ is used. On one hand, this procedure allows considering choline and a combined PC+GPC figure; on the other hand, this combined PC+GPC approach unfortunately adds an additional obstacle towards drawing conclusions as to where the change in the system takes place.

The limited MRS specificity also does not allow for distinction between intra- and extracellular choline levels. Due to the nature of biopsies, samples always include a large part of interstitial material. We do not know in which way the extracellular compartment may confound the spectroscopic measurements.

The limitations of MRS are also due to low tissue concentrations of metabolites and proteins as well as the severe overlapping of these molecules.

In addition, relaxation rates may differ at various field strengths. Gadolinium-based contrast agents can also affect relaxation rates.

11.7.3 Implications of the Kennedy pathway

The Kennedy pathway is an open system. Extracellular choline may enter the cycle at any given moment through carrier molecules within the cell wall. Likewise, choline may be integrated into the cell wall as PtdCho. As mentioned before, ^1H MRS is not capable of differentiating choline, PtdCho and extra- and intracellular choline (it does not measure membrane choline). Furthermore, correct functioning of the enzymes involved in the Kennedy cycle depends on the supply of molecules such as ATP, CTP and DAG.

Any change – which cannot be ruled out - in their supply would ultimately affect the proper working of the choline metabolism.

11.7.4 Challenges of the rt-q-PCR technique

Due to the minimal amounts and thus high cycle differences of the proteins measured, an alternative approach for concentration determination (e.g. microarrays, enzyme activity, etc.) might deliver more specific results.

As demonstrated in the Results chapter, cycle differences for some of the tested enzymes were minimal. This was to be expected, as we were not comparing malign with benign tissue, but histological grade 2 with grade 3 cancerous tissue. As we had to deal with very small cycle differences which led to difficulties in the data processing, it may be interesting to determine which cycle differences can truly be attributed to the expression of the gene and which ones to the experimental setup. When dealing with very small numbers, errors are inevitably more likely to occur. This is a systematic risk which is hard to avoid when dealing with molecular material.

As can be observed in studies using different techniques for evaluating gene expression in cancerous tissue to test for expression levels of specific proteins, rt-q-PCR reacts least sensitively to changes in concentration: in their work on PLD1 expression levels in cancerous and normal breast tissue, Noh et al. used rt-q-PCR, immunoblotting and a PLD-activity assay [29]. The ratio of cancerous/normal PLD1 expression levels is elevated in all three methods, but lowest in rt-q-PCR. This indicates that methods other than rt-q-PCR are possibly better suited in the search for enzyme concentration differences.

11.7.5 Limitations of statistical analysis

The number of samples analysed in this study is $n = 19$. Statistical analysis of the data gathered includes ANOVA, correlation coefficients, p-values and confidence intervals. Analysis of variance is normally used for sample sizes with a minimal of $n = 20$. An $n < 20$ bears the inherent danger of overlooking certain effects in the statistical analysis. As the sample size for some enzymes was limited to only 16 samples, many of the possible correlations lack statistical significance. Possibly, a type II error has been committed because of the small sample size or high variability.

The main problem of the study is the relatively small number of samples. This fact also explains the large impact of so-called outsiders. Based on the data raised, we cannot decide if these seemingly extreme values are genuine outliers or simply part of the “normal” range of values appearing in the measured context.

11.7.6 Posttranslational regulation

The main focus of this study was the translation rate of certain enzymes involved in the Kennedy cycle. We did not look at post-translational modifications. A growing amount of research indicates that posttranslational changes are essential to many regulatory processes on the cellular level. Therefore, further research needs to be conducted which include the posttranslational phase.

11.8 Alternative experimental approaches

If the study was to be redone, it could be considered to:

- measure enzymes with enzyme activity assays and Northern/Western blot analyses rather than with rt-q-PCR
- increase sample size n
- match benign with malign tissue from the same patient
- include data on posttranslational modification.

11.9 Conclusion

No common pathway has so far been identified to be at the base of the complex changes in cell growth regulatory systems taking place in malign cells. As the change in the choline phospholipid metabolism has been found across various types of cancer, it displays high potential for being just this kind of pathway at the base of many cancer cell multiplication systems.

The study at hand provides first-hand human breast cancer data that correlate the observed concentrations of choline metabolites with their biosynthetic origins. In particular, this study looked at the differences in enzymatic expression patterns between histologically staged grade 2 and 3 breast cancer tissue. Ultimately, the aim was to understand which enzymes contribute to the overall increase of choline-containing

metabolites in cancerous tissue. Analysis of the MRS-spectra aimed at determining recurring characteristic features in the tissue samples that may allow recognizing a common pattern in malign breast lesions. This knowledge could be used to assist the design of more efficient MRS imaging paradigms that utilise the sensitivity of these choline metabolites.

We were not able to identify one particular enzyme of the Kennedy pathway as being the sole cause for the changes in the metabolite makeup of a cell undergoing carcinogenesis. We did find significant differences in enzyme concentrations between the two histological groups. The fact that the concentration of some of the analysed enzymes varied substantially between grades indicates their close relationship to malignant transformation undergone by malignant tissue. In particular, our results suggest an important role of the two isoforms of ChoK in this process. In future studies, the isoforms will need to be treated as separate entities, as they seem to react differently in the course of malignant transformation.

Regarding the reason for intracellular choline concentration changes, we found supporting data for both increased transporter and catabolic membrane activity. TCho concentration measured in the course of this study was not elevated in higher graded breast cancer tissue.

The important role of choline metabolites in the process of carcinogenesis is underlined by the successful therapeutical lowering of choline concentration in cancer patients. To improve the targeting of these drugs, additional work on the enzymes of the Kennedy pathway is vital. The rise in concentration levels in the majority of the enzymes presented in this study indicates their strong involvement in the metabolic changes undergone by a cell during carcinogenesis. Today's therapies aimed at decreasing choline synthesis are purely empirical. Choline levels are lowered *ex post*, without knowledge of the underlying mechanism that increased the level in the first place. Further research will clarify if those enzymes are merely passively reacting or actively contributing to malignant transformation, and in the latter case be effective targets for future cancer drugs.

Results of this study are consistent with previous studies, which concluded that increased choline uptake and increased phospholipase-mediated turnover of PtdCho contribute to the observed increase in PC in breast cancer.

11.9.1 Possible clinical use of the findings

As in vivo and routine clinical use of 14T spectroscopy is unrealistic at this time, the practical implications of this study can only aim at an improved linkage of available data. For a successful clinical application of the techniques at hand, an integrative approach is necessary. If different data such as spectroscopy, histopathology and patient statistics are to be linked efficiently, pattern recognition methods and multi-stage statistical classification strategies need to be further refined in order to deal with the large amount of data. Provided the existence of sufficient datasets, the efficient linkage of the available information could make additional surgical interventions after a biopsy or FNAB unnecessary: one biopsy specimen would then be sufficient to estimate the risk of lymphatic spread, vascular invasion and grading of the tumour.

In general – even at lower field strengths – MRS has the potential to increase specificity of the otherwise sensitivity-strong MRI technique: incorporated into MRI analysis, a minimum signal-to-noise ratio of the MRS choline resonance peak could serve as an indicator for malignancy in suspicious lesions found in MRI. A routine conduction of MRS on suspicious MRI findings could give an indication as to their classification (e.g., consistent increase in choline in infiltrating ductal carcinoma, low choline concentration for in-situ lesions). As pointed out in the introduction, early detection is crucial for successful treatment of breast cancer. Apart from the diagnostic and economic advantages, this integrative approach could lead to improved reliability of screening results and thus ultimately to higher survival rates.

12 Summary

This study analysed invasive ductal carcinoma grade II and III with the use of two different analytical techniques: ^1H MRS at 14T and real-time PCR. The results were matched and monitored for specific patterns.

Simultaneous analysis of the datasets led to rejection of the null-hypothesis: there was a statistically significant correlation between histological grade, the concentration of certain enzymes of the Kennedy pathway and metabolites measured by ^1H MRS in malignant breast cancer tissue. The following significant differences in enzyme concentration within the two histological groups were found: a negative correlation between ChoK β and higher pathological grade; a positive correlation between ChoK α and total choline concentration in both grades. In both grades, there was a negative correlation between ChoK α/β and the (PC+GPC)/choline ratio, as well as between ChoK α and the GPC level in grade 2. Apart from ChoK, there was one statistically significant finding for another enzyme involved in the Kennedy cycle: PCYT1A concentration and GPC/choline ratio were negatively correlated in grade 3.

These results underline the notion that there is a specific spectral pattern that allows differentiation between different breast tissue lesions. The study discusses several possible explanations for the results and puts them into perspective with work done so far in the field.

Provided a sufficiently large dataset, the integration of MRS with MRI data could lead to higher quality and reliability of diagnostic procedures. A comprehensive histopathologic, clinical and biochemical classification of breast lesions could allow for less repetitive surgical interventions and ultimately higher survival rates of breast cancer patients.

13 Selbständigkeitserklärung

„Ich, Hannah Maria Schäfer, erkläre, dass ich die vorgelegte Dissertation mit dem Thema:

*Assessment of the choline metabolism in human breast cancer by High Resolution
Magic Angle Spinning ^1H Magnetic Resonance Spectroscopy and quantitative
Polymerase Chain Reaction*

selbst verfasst und keine anderen als die angegebenen Quellen und Hilfsmittel benutzt, ohne die (unzulässige) Hilfe Dritter verfasst und auch in Teilen keine Kopien anderer Arbeiten dargestellt habe.“

Datum

Unterschrift

14 Acknowledgements

- Prof. Leo Cheng: Without his constant scientific, organisational and personal support, this work would not have been possible.
- PD Dr. Matthias Taupitz: His invaluable scientific input and thorough knowledge of the field was crucial to the design and completion of this work.
- Florian Sturm: His presence, scientific skill and motivational spirit helped to overcome all dead ends.
- Sévérine Jungmann: For her presence even after her departure.

15 Bibliography

1. Jemal, A., et al., *Cancer Statistics, 2009*. CA Cancer J Clin, 2009. **59**(4): p. 225-249.
2. Nover, A.B., et al., *Modern Breast Cancer Detection: A Technological Review*. International Journal of Biomedical Imaging, 2009. **2009**: p. 1-14.
3. Orel, S.G. and M.D. Schnall, *MR imaging of the breast for the detection, diagnosis, and staging of breast cancer*. Radiology, 2001. **220**(1): p. 13-30.
4. Hata, T., H. Takahashi, and K. Watanabe, *Magnetic resonance imaging for preoperative evaluation of breast cancer: a comparative study with mammography and ultrasonography*. Journal of the American College of Surgeons, 2004. **198**(2): p. 190-197.
5. Kriege, M., C.T.M. Brekelmans, and C. Boetes, *Efficacy of MRI and mammography for breast-cancer screening in women with a familial or genetic predisposition*. The New England Journal of Medicine, 2004. **351**(5): p. 427-437.
6. Kuhl, C.K., *The "Coming of Age" of Nonmammographic Screening for Breast Cancer*. Journal of the American Medical Association, 2008. **299**(18): p. 2203-2205.
7. Heywang-Köbrunner, S.H., et al., *International investigation of breast MRI: results of a multicentre study (11 sites) concerning diagnostic parameters for contrast-enhanced MRI based on 519 histopathologically correlated lesions*. European Radiology, 2001. **11**(4): p. 531-546.
8. Bluemke, D.A., C.A. Gatsonis, and M.H. Chen, *Magnetic resonance imaging of the breast prior to biopsy*. Journal of the American Medical Association, 2004. **292**(22): p. 2735-2742.
9. Baltzer, P.A.T., et al., *False-Positive Findings at Contrast-Enhanced Breast MRI: A BI-RADS Descriptor Study*. Am. J. Roentgenol. **194**(6): p. 1658-1663.
10. Kuerer, H.M., et al., *Ductal Carcinoma in Situ: State of the Science and Roadmap to Advance the Field*. J Clin Oncol, 2009. **27**(2): p. 279-288.
11. Glunde, K., C. Jie, and Z.M. Bhujwala, *Molecular Causes of the Aberrant Choline Phospholipid Metabolism in Breast Cancer*. Cancer Res, 2004. **64**(12): p. 4270-4276.
12. Singer, S., K. Souza, and W.G. Thilly, *Pyruvate Utilization, Phosphocholine and Adenosine Triphosphate (ATP) Are Markers of Human Breast Tumor Progression: A ³¹P- and ¹³C-Nuclear Magnetic Resonance (NMR) Spectroscopy Study*. Cancer Res, 1995. **55**(22): p. 5140-5145.
13. Ting, Y., D. Sherr, and H. Degani, *Variations in energy and phospholipid metabolism in normal and cancer human mammary epithelial cells*. Anticancer Res, 1996. **16**: p. 1381-1388.
14. Aboagye, E.O. and Z.M. Bhujwala, *Malignant Transformation Alters Membrane Choline Phospholipid Metabolism of Human Mammary Epithelial Cells*. Cancer Res, 1999. **59**(1): p. 80-84.
15. Eliyahu, G., T. Kreizman, and H. Degani, *Phosphocholine as a biomarker of breast cancer: Molecular and biochemical studies*. International Journal of Cancer, 2007. **120**(8): p. 1721-1730.
16. Al-Saffar, N.M.S., et al., *Noninvasive Magnetic Resonance Spectroscopic Pharmacodynamic Markers of the Choline Kinase Inhibitor MN58b in Human Carcinoma Models*. Cancer Res, 2006. **66**(1): p. 427-434.
17. Mori, N., et al., *Choline Kinase Down-regulation Increases the Effect of 5-Fluorouracil in Breast Cancer Cells*. Cancer Res, 2007. **67**(23): p. 11284-11290.

18. Nelson, S.J., et al., *In vivo molecular imaging for planning radiation therapy of gliomas: An application of 1H MRSI*. Journal of Magnetic Resonance Imaging, 2002. **16**(4): p. 464-476.
19. Meisamy, S., et al., *Adding in vivo quantitative 1H MR spectroscopy to improve diagnostic accuracy of breast MR imaging: preliminary results of observer performance study at 4.0 T* Radiology 2005. **236**: p. 465–75.
20. Warburg, O., F. Wind, and E. Negelein, *The metabolism of tumors in the body*. The Journal of General Physiology, 1927. **8**(6): p. 519-530.
21. QiuHong, H., et al., *Magnetic resonance spectroscopic imaging of tumor metabolic markers for cancer diagnosis, metabolic phenotyping, and characterization of tumor microenvironment*. Disease Markers, 2003. **19**(2/3): p. 69-94.
22. Beckonert, O., et al., *Visualizing metabolic changes in breast-cancer tissue using 1H-NMR spectroscopy and self-organizing maps*. NMR in Biomedicine, 2003. **16**(1): p. 1-11.
23. Merchant, T.E., et al., *31P Magnetic Resonance Spectroscopic Profiles of Neoplastic Human Breast Tissues*. Cancer Res, 1988. **48**(18): p. 5112-5118.
24. Ackerstaff, E., K. Glunde, and Z.M. Bhujwalla, *Choline phospholipid metabolism: A target in cancer cells?* Journal of Cellular Biochemistry, 2003. **90**(3): p. 525-533.
25. Bolan, P.J., et al., *In vivo quantification of choline compounds in the breast with 1H MR spectroscopy*. Magnetic Resonance in Medicine, 2003. **50**(6): p. 1134-1143.
26. Rozic, J., C. Chakraborty, and P. Lala, *Cyclooxygenase inhibitors retard murine mammary tumor progression by reducing tumor cell migration, invasiveness, and angiogenesis*. International Journal of Cancer, 2001(93): p. 497-506.
27. Ramírez de Molina, A., et al., *Increased choline kinase activity in human breast carcinomas: clinical evidence for a potential novel antitumor strategy*. Oncogene, 2002(21): p. 4317-4322.
28. Katz-Brull, R. and H. Degani, *Kinetics of choline transport and phosphorylation in human breast cancer cells*. Anticancer Res, 1996(16): p. 1375-1380.
29. Noh, D.-Y., et al., *Overexpression of phospholipase D1 in human breast cancer tissues*. Cancer Letters, 2000. **161**(2): p. 207-214.
30. Guthridge, C., et al., *Phospholipases A2 in ras-transformed and immortalized human mammary epithelial cells*. Cancer Letters, 1994(86): p. 11-21.
31. Blusztajn, J.K., *Choline, a vital amine*. Science, 1998. **281**(5378): p. 794.
32. Cai, H., et al., *Hydrolysis of phosphatidylcholine couples Ras to activation of Raf protein kinase during mitogenic signal transduction*. Mol. Cell. Biol., 1993. **13**(12): p. 7645-7651.
33. Cuadrado, A., et al., *Phosphorylcholine: a novel second messenger essential for mitogenic activity of growth factors*. Oncogene, 1993(8): p. 2959-2968.
34. BioCarta, *The salvage pathway from serine to phosphatidylcholine*. 2009.
35. Löffler, G., P.E. Petrides, and P.C. Heinrich, *Biochemie und Pathobiochemie*. 8 ed. 2007: Springer.
36. Vance, D., *Biochemistry of lipids, lipoproteins and membranes*, ed. D. Vance and J. Vance. 2002: Elsevier Science B.V. 205-232.
37. Kennedy, E.P. and S.B. Weiss, *The Function of Cytidine Coenzymes in the Biosynthesis of Phospholipides*. J. Biol. Chem., 1956. **222**: p. 193-214.

38. Borkenhagen, L.F. and E.P. Kennedy, *The enzymatic synthesis of cytidine diphosphate choline*. J. Biol. Chem., 1957. **227**: p. 951-962.
39. Glunde, K., et al., *Real-time changes in ¹H and ³¹P NMR spectra of malignant human mammary epithelial cells during treatment with the anti-inflammatory agent indomethacin*. Magnetic Resonance in Medicine, 2002. **48**(5): p. 819-825.
40. Mori, N., et al., *Choline Phospholipid Metabolites of Human Vascular Endothelial Cells Altered by Cyclooxygenase Inhibition, Growth Factor Depletion, and Paracrine Factors Secreted by Cancer Cells*. Molecular Imaging, 2003. **2**(2): p. 124-130.
41. Inglese, M., et al., *Diffusely elevated cerebral choline and creatine in relapsing-remitting multiple sclerosis*. Magnetic Resonance in Medicine, 2003. **50**(1): p. 190-195.
42. Bodennec, J., et al., *Phosphatidylcholine synthesis is elevated in neuronal models of Gaucher disease due to direct activation of CTP:phosphocholine cytidyltransferase by glucosylceramide*. FASEB J., 2002: p. 02-0149fje.
43. Pettegrew, J., et al., *Magnetic resonance spectroscopic changes in Alzheimer's disease*. Annals of the New York Academy of Sciences, 1997. **826**: p. 282-306.
44. Lacal, J.C., *Choline kinase: a novel target for antitumor drugs*. IDrugs, 2001. **4**(4): p. 419-426.
45. Smith, T.A.D., et al., *Phospholipid metabolites, prognosis and proliferation in human breast carcinoma*. NMR in Biomedicine, 1993. **6**(5): p. 318-323.
46. Kent, C., *Regulatory enzymes of phosphatidylcholine biosynthesis: a personal perspective*. Biochimica et Biophysica Acta (BBA) - Molecular and Cell Biology of Lipids, 2005. **1733**(1): p. 53-66.
47. Aoyama, C., H. Liao, and K. Ishidate, *Structure and function of choline kinase isoforms in mammalian cells*. Progress in Lipid Research, 2004. **43**(3): p. 266-281.
48. Ramírez de Molina, A., et al., *Regulation of choline kinase activity by Ras proteins involves Ral-GDS and PI3K*. Oncogene, 2002(21): p. 937-946.
49. Ramírez de Molina, A., et al., *Inhibition of ChoK is an efficient antitumor strategy for Harvey-, Kirsten-, and N-ras transformed cells*. Biochem Biophys Res Commun, 2001(285): p. 873-879.
50. Ratnam, S. and C. Kent, *Early increase in choline kinase activity upon induction of the H-ras oncogene in mouse fibroblast cell lines*. Arch Biochem Biophys, 1999(323): p. 313-322.
51. Hernandez-Alcoceba, R., et al., *Choline kinase inhibitors as a novel approach for antiproliferative drug design*. Oncogene, 1997(15): p. 2289-2301.
52. Ramirez de Molina, A., et al., *Increased choline kinase activity in human breast carcinomas: clinical evidence for a potential novel antitumor strategy*. Oncogene, 2002(21): p. 4317-4322.
53. Ramírez de Molina, A., et al., *Choline Kinase Is a Novel Oncogene that Potentiates RhoA-Induced Carcinogenesis*. Cancer Res, 2005. **65**(13): p. 5647-5653.
54. Ishidate, K., M. Tsuruoka, and Y. Nakazawa, Biochem Biophys Res Commun, 1980(96): p. 946-952.
55. Aoyama, C., et al., *Induction of choline kinase alpha by carbon tetrachloride (CCl₄) occurs via increased binding of c-jun to an AP-1 element*. Biochimica et Biophysica Acta (BBA) - Molecular and Cell Biology of Lipids, 2007. **1771**(9): p. 1148-1155.

56. Martin, T.W. and K. Michaelis, *P2-purinergic agonists stimulate phosphodiesteratic cleavage of phosphatidylcholine in endothelial cells. Evidence for activation of phospholipase D*. J. Biol. Chem., 1989. **264**(15): p. 8847-8856.
57. Huang, D., et al., *Identification of phosphatidylcholine-selective and phosphatidylinositol-selective phospholipases D in Madin-Darby canine kidney cells*. J. Biol. Chem., 1992. **267**: p. 16859-65.
58. Siddiqui, R.A. and J.H. Exton, *Phospholipid base exchange activity in rat liver plasma membranes. Evidence for regulation by G-protein and P2y-purinergic receptor*. J. Biol. Chem., 1992. **267**: p. 5755-61.
59. Brown, H.A., et al., *ADP-ribosylation factor, a small GTP-dependent regulatory protein, stimulates phospholipase D activity*. Cell, 1993. **75**: p. 1137-44.
60. Kanfer, J.M. and D. McCartney, *Phospholipase D activity of isolated rat brain plasma membranes*. FEBS Lett., 1994. **337**: p. 251-54.
61. Gustavsson, L., et al., *The role of cytosolic Ca²⁺, protein kinase C, and protein kinase A in hormonal stimulation of phospholipase D in rat hepatocytes*. J. Biol. Chem., 1994. **269**: p. 849-859.
62. Exton, J.H., *Phosphatidylcholine breakdown and signal transduction*. Biochem. Biophys. Acta 1994. **1212**: p. 26-42.
63. Billah, M.M. and J.C. Anthes, *The regulation and cellular functions of phosphatidylcholine hydrolysis*. Biochem. J., 1990. **269**: p. 289-291.
64. Chalifa, V., H. Mohn, and M. Liscovitch, *A neural phospholipase D activity from rat brain synaptic plasma membranes. Identification and partial characterization*. J. Biol. Chem., 1990. **265**: p. 17512-17519.
65. Uings, I.J., et al., *Tyrosine phosphorylation is involved in receptor coupling to phospholipase D but not phospholipase C in the human neutrophil*. Biochem. J., 1992. **281**: p. 597-00.
66. Cockcroft, S., et al., *Phospholipase D: a downstream effector of ARF in granulocytes*. Science, 1994. **263**: p. 523-526.
67. Kiss, Z. and W.H. Anderson, *Selective down-regulation of protein kinase c-epsilon by carcinogens does not prevent stimulation of phospholipase D by phorbol ester and platelet-derived growth factor*. Biochem. J. , 1994. **300**: p. 751-756.
68. Massenburg, D., et al., *Activation of rat brain phospholipase D by ADP-ribosylation factors 1,5, and 6: separation of ADP-ribosylation factor-dependent and oleate-dependent enzymes*. Proc. Natl. Acad. Sci. USA, 1994. **91**: p. 11718-11722.
69. Mohn, H., V. Chalifa, and M. Liscovitch, *Substrate specificity of neutral phospholipase D from rat brain studied by selective labeling of endogenous synaptic membrane phospholipids in vitro*. J. Biol. Chem. , 1994. **267**: p. 11131-11136.
70. Rodríguez-González, A., et al., *Phospholipase D and choline kinase: their role in cancer development and their potential as drug targets*. Prog Cell Cycle Res, 2003(5): p. 191-201.
71. Friesen, J.A., H.A. Campbell, and C. Kent, J. Biol. Chem., 1999. **274**: p. 13384–13389.
72. Xie, M., Smith, J. L., Ding, Z., Zhang, D., and Cornell, R. B. (2004) J. Biol. and Chem. 279, J. Biol. Chem., 2004. **279**: p. 28817–28825.
73. Nishida, I., et al., *Cloning of Brassica napus CTP:phosphocholine cytidylyltransferase cDNAs by complementation in a yeast cct mutant*. Plant Mol. Biol., 1996. **31**(2): p. 205–211.

74. Cornell, R.B. and I.C. Northwood, *Regulation of CTP:phosphocholine cytidyltransferase by amphitropism and relocalization*. Trends in Biochemical Sciences, 2000. **25**(9): p. 441-447.
75. Stern, W., C. Kovac, and P.A. Weinhold, *Activity and properties of CTP: choline phosphate cytidyltransferase in adult and fetal rat lung*. Biochim. Biophys. Acta, 1976. **441**: p. 280-293.
76. Tang, W., G.A. Keesler, and I. Tabas, J. Biol. Chem. , 1997. **272**: p. 13146–13151.
77. Karim, M.A., Jackson, P., and Jackowski, S. (2003) Biochim. Biophys. Acta and 1633, Biochim. Biophys. Acta, 2003. **1633**: p. 1–12.
78. Lykidis, A., I. Baburina, and S. Jackowski, J. Biol. Chem., 1999. **274**: p. 26992–27001.
79. Lykidis, A., K.G. Murti, and S. Jackowski, J. Biol. Chem., 1998. **273**: p. 14022–14029.
80. Kent, C., *CTP:phosphocholine cytidyltransferase*. Biochimica et biophysica acta, 1997. **1348**(1-2): p. 79-90.
81. Sleight, R. and C. Kent, *Regulation of phosphatidylcholine biosynthesis in cultured chick embryonic muscle treated with phospholipase C*. J. Biol. Chem., 1980. **255**: p. 10644–10650.
82. Jackowski, S. and P. Fagone, *CTP:Phosphocholine Cytidyltransferase: Paving the Way from Gene to Membrane*. J. Biol. Chem., 2005. **280**(2): p. 853-856.
83. Northwood, I.C., et al., J. Biol. Chem. , 1999. **274**: p. 26240–26248.
84. Lagace, T.A., J.R. Miller, and N.D. Ridgway, Mol. Cell. Biol., 2002. **22**: p. 4851–4862.
85. Michel, V., et al., *Choline Transport for Phospholipid Synthesis*. Experimental Biology and Medicine, 2006. **231**(5): p. 490-504.
86. Sleight, R. and C. Kent, *Regulation of phosphatidylcholine biosynthesis in mammalian cells: II. Effects of phospholipase C treatment on the activity and subcellular distribution of CTP: phosphocholine cytidyltransferase in Chinese hamster ovary and LM cell lines*. J. Biol.Chem. , 1983. **258**: p. 831-835.
87. Sleight, R. and C. Kent, *Regulation of phosphatidylcholine biosynthesis in mammalian cells: III. Effects of alterations in the phospholipid compositions of Chinese hamster ovary and M cells on the activity and distribution of CTP: phosphocholine cytidyltransferase*. J. Biol.Chem. , 1983. **258**: p. 836-839.
88. Lockman, P.R. and D.D. Allen, *The Transport of Choline*. Drug Development & Industrial Pharmacy, 2002. **28**(7): p. 749-771.
89. Lerner, J., *Choline Transport Specificity in Animal Cells and Tissues*. Comp. Biochem. Physiol., 1989. **93**(1): p. 1-9.
90. Bansal, A., et al., *Biodisposition and metabolism of [18F]fluorocholine in 9L glioma cells and 9L glioma-bearing fisher rats*. European Journal of Nuclear Medicine and Molecular Imaging, 2008. **35**(6): p. 1192-1203.
91. Koepsell, H. and H. Endou, *The SLC22 drug transporter family*. Pflugers Arch - Eur J Physiol 2004. **447**: p. 666–676.
92. Koepsell, H., K. Lips, and C. Volk, *Polyspecific Organic Cation Transporters: Structure, Function, Physiological Roles, and Biopharmaceutical Implications*. Pharmaceutical Research, 2007. **24**(7): p. 1227-1251.
93. Sweet, D.H., D.S. Miller, and J.B. Pritchard, *Ventricular Choline Transport. A role for organic cation transporter 2 expressed in choroid plexus*. J. Biol. Chem., 2001. **276**(45): p. 41611-41619.

94. Zhang, L., et al., *Cloning and functional expression of a human liver organic cation transporter*. Mol Pharmacol, 1997. **51**: p. 913-921.
95. Mehrens, T., et al., *The affinity of the organic cation transporter rOCT1 is increased by protein kinase C-dependent phosphorylation*. J Am Soc Nephrol, 2000. **11**: p. 1216-1224.
96. Schlatter, E., et al., *The organic cation transporters rOCT1 and hOCT2 are inhibited by cGMP*. J Membr Biol 2002. **189**: p. 237-244.
97. Bogin, L. and H. Degani, *Hormonal Regulation of VEGF in Orthotopic MCF7 Human Breast Cancer*. Cancer Res, 2002. **62**(7): p. 1948-1951.
98. Ronen, S.M., et al., *Magnetic resonance detects changes in phosphocholine associated with Ras activation and inhibition in NIH 3T3 cells*. Br J Cancer, 2001. **84**(5): p. 691-696.
99. Kiss, Z., K.S. Crillya, and W.H. Anderson, *Carcinogens stimulate phosphorylation of ethanolamine derived from increased hydrolysis of phosphatidylethanolamine in C3H/101/2 fibroblasts*. FEBS Lett., 1993. **336**: p. 115-118.
100. Ramírez de Molina, A., et al., *Choline Kinase Activation Is a Critical Requirement for the Proliferation of Primary Human Mammary Epithelial Cells and Breast Tumor Progression*. Cancer Res, 2004. **64**(18): p. 6732-6739.
101. Claudino, W.M., et al., *Metabolomics: Available Results, Current Research Projects in Breast Cancer, and Future Applications*. Journal of clinical oncology, 2007. **25**: p. 2840-2846.
102. Jordan, K. and L. Cheng, *NMR-based metabolomics approach to target biomarkers for human prostate cancer*. Future Drugs, 2007. **4**: p. 389-400.
103. Chapman, D., et al., *NMR of gel and liquid crystalline phospholipids spinning at the "magic angle"*. FEBS Letters, 1972. **25**(2): p. 261-264.
104. Emory, www.emory.edu/NMR/web_swu/HRMAS/. Emory University NMR Research Center Website excerpt dating from Jan. 23rd, 2010.
105. Cheng, L.L., et al., *Quantification of microheterogeneity in glioblastoma multiforme with ex vivo high-resolution magic-angle spinning (HRMAS) proton magnetic resonance spectroscopy*. Neuro-oncol, 2000. **2**(2): p. 87-95.
106. Cheng, L.L., et al., *Evaluating Human Breast Ductal Carcinomas with High-Resolution Magic-Angle Spinning Proton Magnetic Resonance Spectroscopy*. Journal of Magnetic Resonance, 1998. **135**(1): p. 194-202.
107. Podo, F., *Tumour phospholipid metabolism*. NMR Biomed, 1999(12): p. 413-439.
108. Gribbestad, I., et al., *Metabolite composition in breast tumors examined by proton nuclear magnetic resonance spectroscopy*. Anticancer Res, 1999(19): p. 1737-1746.
109. Bell, J. and K. Bhakoo, *Metabolic changes underlying 31P MR spectral alterations in human hepatic tumours*. NMR Biomed, 1998(11): p. 354-359.
110. Li, X., et al., *Analysis of the spatial characteristics of metabolic abnormalities in newly diagnosed glioma patients*. J Magn Reson Imaging 2002(16): p. 229-237.
111. Negendank, W., *Studies of human tumors by MRS: A review*. NMR Biomed, 1992(5): p. 303-324.
112. Kurhanewicz, J., D. Vigneron, and S. Nelson, *Threedimensional magnetic resonance spectroscopic imaging of brain and prostate cancer*. Neoplasia, 2000(2): p. 166-189.
113. Swindle, P., et al., *Pathologic characterization of human prostate tissue with proton MR spectroscopy*. Radiology, 2003(228): p. 144-151.
114. Bhakoo, K., et al., *Immortalization and transformation are associated with specific alterations in choline metabolism*. Cancer Res, 1996(56): p. 4630-4635.

115. Ackerstaff, E., et al., *Detection of increased choline compounds with proton nuclear magnetic resonance spectroscopy subsequent to malignant transformation of human prostatic epithelial cells*. *Cancer Res*, 2001(61): p. 3599-3603.
116. Bogin, L., et al., *TNF-induced modulations of phospholipid metabolism in human breast cancer cells*. *Biochim Biophys Acta.*, 1998(1392): p. 217-232.
117. Xiaojuan, L., et al., *Analysis of the spatial characteristics of metabolic abnormalities in newly diagnosed glioma patients*. *Journal of Magnetic Resonance Imaging*, 2002. **16**(3): p. 229-237.
118. Ramírez de Molina, A., et al., *Expression of choline kinase alpha to predict outcome in patients with early-stage non-small-cell lung cancer: a retrospective study*. *Lancet Oncol* 2007, 2007. **8**: p. 889–897.
119. Kiss, Z., *Regulation of Mitogenesis by Water-Soluble Phospholipid Intermediates*. *Cellular Signalling*, 1999. **11**(3): p. 149-157.
120. Bañez-Coronel, M., et al., *Choline Kinase Alpha Depletion Selectively Kills Tumoral Cells*. *Current Cancer Drug Targets*, 2008. **8**(8): p. 709-719.
121. Hernandez-Alcoceba, R., F. Fernandez, and J.C. Lacal, *In Vivo Antitumor Activity of Choline Kinase Inhibitors: A Novel Target for Anticancer Drug Discovery*. *Cancer Res*, 1999. **59**(13): p. 3112-3118.
122. Livak, K.J. and T.D. Schmittgen, *Analysis of Relative Gene Expression Data Using Real-Time Quantitative PCR and the 2- $[\Delta\Delta]_{CT}$ Method*. *Methods*, 2001. **25**(4): p. 402-408.
123. Watzinger, F. and T. Lion, *Multiplex PCR for quality control of template RNA/cDNA in RT-PCR assays*. *Leukemia*, 1998. **12**(12): p. 1983.
124. Ullmanová, V. and C. Haškovec, *The Use of Housekeeping Genes (HKG) as an Internal Control for the Detection of Gene Expression by Quantitative Real-Time RT-PCR*. *Folia Biologica (Praha)*, 2003. **49**: p. 211-216.
125. Zhu, L.J. and S.W. Altmann, *mRNA and 18S-RNA coapplication-reverse transcription for quantitative gene expression analysis*. *Analytical Biochemistry*, 2005. **345**(1): p. 102-109.
126. Heid, C., et al., *Real time quantitative PCR*. *Genome Res*, 1996(6): p. 986-994.
127. Yuan, J., et al., *Statistical analysis of real-time PCR data*. *BMC Bioinformatics*, 2006. **7**(1): p. 85.
128. Yuan, J.S., D. Wang, and C.N. Stewart Jr., *Statistical methods for efficiency adjusted real-time PCR quantification*. *Biotechnol. J.*, 2008. **3**: p. 112–123.
129. Qiagen.com, *Critical factors for successful real-time PCR*. 2006: p. 1-48. (Accessed September 21, 2009, at <http://www1.qiagen.com/literature/render.aspx?id=23490>.)
130. Schmittgen, T., et al., *Quantitative reverse transcription-polymerase chain reaction to study mRNA decay: comparison of endpoint and real-time methods*. *Anal Biochem.*, 2000(285): p. 194-204.
131. Winer, J., et al., *Development and Validation of Real-Time Quantitative Reverse Transcriptase-Polymerase Chain Reaction for Monitoring Gene Expression in Cardiac Myocytes in Vitro*. *Analytical Biochemistry*, 1999. **270**(1): p. 41-49.
132. Hernando, E., et al., *A critical role for choline kinase-[alpha] in the aggressiveness of bladder carcinomas*. *Oncogene*, 2009. **28**(26): p. 2425-2435.
133. Plathow, C. and W.A. Weber, *Tumor Cell Metabolism Imaging*. *J Nucl Med*, 2008. **49**(Suppl_2): p. 43S-63.

134. Ratnam, S. and C. Kent, *Early Increase in Choline Kinase Activity upon Induction of the H-rasOncogene in Mouse Fibroblast Cell Lines*. Archives of Biochemistry and Biophysics, 1995. **323**(2): p. 313-322.
135. Yu, Y., et al., *Phosphorylation of Saccharomyces cerevisiae choline kinase on Ser30 and Ser85 by protein kinase A regulates phosphatidylcholine synthesis by the CDP–choline pathway*. J. Biol. Chem., 2002: p. 34978–34986.
136. McMaster, C.R. and R.M. Bell, *Phosphatidylcholine biosynthesis via the CDP–choline pathway in Saccharomyces cerevisiae. Multiple mechanisms of regulation*. J. Biol. Chem., 1994. **269**: p. 14776-14783.
137. Vigo, C. and D.E. Vance, *Effect of diethylstilboestrol on phosphatidylcholine biosynthesis and choline metabolism in the liver of roosters*. Biochem. J., 1981. **200**: p. 321-326.
138. Nishijima, M., et al., *Regulation of phosphatidylcholine metabolism in mammalian cells, isolation and characterization of a Chinese hamster ovary cell pleiotropic mutant defective in both choline kinase and cholineexchange reaction activities*. J. Biol. Chem., 1984. **259**: p. 7101-7108.
139. Infante, J.P., *Rate-limiting steps in the cytidine pathway for the synthesis of phosphatidylcholine and phosphatidylethanolamine*. Biochem. J., 1977. **167**: p. 847-849.
140. Infante, J.P. and J.E. Kinsella, *Evidence from essential-fatty acid-deficient rats*. Biochem. J. , 1978: p. 631-633.
141. Aoyama, C., H. Liao, and K. Ishidate, *Structure and function of choline kinase isoforms in mammalian cells*. Prog Lipid Res, 2004. **43**: p. 266-281.
142. Jackowski, S., *Cell Cycle Regulation of Membrane Phospholipid Metabolism*. Journal of Biological Chemistry, 1996. **271**(34): p. 20219-20222.
143. Fagone, P., et al., *CTP:Phosphocholine cytidyltransferase alpha is required for B-Cell proliferation and class switch recombination*. J. Biol. Chem., 2009: p. M807338200.
144. Bansal, A., et al., *Biodisposition and metabolism of [18F]fluorocholine in 9L glioma cells and 9L glioma-bearing fisher rats*. Eur J Nucl Med Mol Imaging, 2008(35): p. 1192-1203.
145. Morse, D.L., et al., *Characterization of breast cancers and therapy response by MRS and quantitative gene expression profiling in the choline pathway*. NMR in Biomedicine, 2009. **22**(1): p. 114-127.
146. Bhakoo, K.K., et al., *Immortalization and Transformation Are Associated with Specific Alterations in Choline Metabolism*. Cancer Res, 1996. **56**(20): p. 4630-4635.
147. Jacobs, M.A., et al., *Proton magnetic resonance spectroscopic imaging of human breast cancer: a preliminary study*. J. Magn Reson Imaging, 2004. **19**: p. 68-75.
148. Morse, D.L., et al., *MRI-measured water mobility increases in response to chemotherapy via multiple cell-death mechanisms*. NMR in Biomedicine, 2007. **20**(6): p. 602-614.